CHAPTER 13

Mixing and Chemical Reactions

GARY K. PATTERSON
University of Missouri–Rolla

EDWARD L. PAUL
Merck and Co., Inc.

SUZANNE M. KRESTA
University of Alberta

ARTHUR W. ETCHELLS III
The DuPont Company (retired)

13-1 INTRODUCTION

Mixing and chemical reaction are intimately entwined. The method of bringing together reactants that are to undergo reaction can have a significant impact on the course of the reaction. If the reaction can result in only one product, the mixing and mass transfer can influence only the reaction rate. If more than one product is possible, contacting can influence the product distribution as well. These considerations apply to both homogeneous and heterogeneous reaction systems. This issue was identified qualitatively by Danckwerts (1958) and Levenspiel (1962) and demonstrated experimentally by Paul and Treybal (1971). An early theoretical paper by Corrsin (1964) established the framework for modeling turbulent mixing in chemical reactors. Brodkey and co-workers (McKelvey et al., 1975) achieved experimental verification of the Corrsin theory. This topic was then expanded with development of test reaction systems and modeling by Bourne and co-workers as summarized in the comprehensive treatise by Baldyga and Bourne (1999). Many workers in this field have made valuable contributions, not all of which can be discussed in this chapter.

Handbook of Industrial Mixing: Science and Practice, Edited by Edward L. Paul, Victor A. Atiemo-Obeng, and Suzanne M. Kresta
ISBN 0-471-26919-0

In this chapter we address the key conditions that determine whether mixing is important. The main objectives of the chapter are to answer the following questions:

- When are mixing effects important?
- What are the criteria for quantifying mixing and reaction?
- What mixing design will optimize yield and selectivity?

Our current understanding of these issues is discussed in the context of industrial applications.

To determine what conditions are required for mixing processes to affect reaction processes, we will use a number of concepts. *Most important is the comparison of time constants of the various processes*. The processes of interest are blending, mixing, mass transfer between phases, and chemical reaction. Some typical time constants are the blend time and reaction half-life. For simple exponential processes (first-order reactions), rates and characteristic times, such as reaction half-lifes, are related. The first-order rate equation is

$$\frac{dC_A}{dt} = -k_R C_A \tag{13-1}$$

where k_R is the reaction rate constant and $1/k_R$ is a characteristic reaction time for a first-order reaction. We can also find the reaction half-life by integrating the rate expression to give

$$\frac{C_A}{C_{A_o}} = e^{-k_R t} \tag{13-2}$$

giving the time when C_A has dropped to half of C_{A_o}:

$$t_{1/2} = \frac{-\ln(0.5)}{k_R} \tag{13-3}$$

Even for more complicated reactions, the linear half-life expression is a good approximation for short times. Second-order reactions have a characteristic time of 1/kC, and a general time constant for higher-order reactions can be defined: $1/kC^{n-1}$. The concepts of rate and characteristic time are used interchangeably throughout the chapter.

Mixing effects in chemical reactions are complicated in that the easily formulated global time constants, such as blend time, are not the ones of interest, but rather, time constants based on local conditions in the reactor, such as local mixing time or local mass transfer rate. When the rates of reaction, mixing, and mass transfer approach one another, mixing will affect the outcome of the process. At the lab scale, mixing effects change the apparent kinetics of the reaction so that the measured kinetics are limited by the rate of mixing rather than by the rate of reaction.

13-1.1 How Mixing Can Cause Problems

Consider two beakers of reactive reagents. They are low viscosity miscible liquids that will react when combined. However, no reaction will take place until the liquids are brought into intimate contact by being mixed on the smallest scales. Thus, the processes of mixing and chemical reaction are linked; they operate in series initially, then in parallel. Now consider the case where the chemical reaction is slow, with a half-life of several minutes. If the mixing takes place quickly, say within seconds, the mixing is essentially finished before significant chemical reaction takes place. There is no effect of mixing on the slow chemical reaction, and the ideal mixed batch reactor analysis may be used. Now consider a very fast chemical reaction: for example, an acid–base neutralization with a half-life of 0.001 s. If the mixing again takes place in seconds, as before, the rate of the chemical reaction depends on the rate of the mixing, which is much slower. If the reaction rate were measured, the result would be the mixing rate, not the molecular chemical reaction rate. The result is the "apparent" reaction rate.

The rate of mixing for fast reactions can often be mistaken for the rate of chemical reaction. Tests in which the rate of mixing is varied (say, by varying mixer speed) must be used to determine the true reaction kinetics. The information presented in this chapter is aimed at solving the problem of fast chemical reactions where the mixing rate and the reaction rates are intertwined. When reactions are fast relative to the mixing rate, not only are the reaction rates affected but the entire time and temperature history of the reactions is affected, yielding different selectivities and yields depending on the intensity of the mixing. This leads to the scale-up problem, where yields of desirable products in a plant scale reactor are not as good as in the small scale reactor in the laboratory or the pilot plant. If the yield is poorer in the plant scale reactor, there is a mixing problem, assuming that other important variables are held constant, such as temperature, pressure, and composition.

The competition between reaction and mixing is well represented by a mixing Damkoehler number, Da_M, which is the ratio between the reaction rate and the local mixing rate, or conversely, the ratio of the characteristic mixing time, τ_M, and the reaction time, τ_R:

$$Da_M = \frac{\tau_M}{\tau_R} \tag{13-4}$$

A smaller Da_M indicates less effect of mixing; a larger Da_M indicates that mixing will be a concern. Estimates of mixing rates and mass transfer rates can be made from existing information for several reactor configurations for both homogeneous and heterogeneous reactions. These estimates combined with an estimate of the magnitude of the reaction rate can give a rough but useful approximation of the conditions under which mixing effects may be critical to the course of a reaction system and in scale-up. This chapter is focused on the determination of those conditions. Several examples are included to illustrate reactor design problems and solutions for the major types of reacting systems. Example 13.1 shows how mixing affects selectivity in various reactor configurations.

Example 13-1: How Mixing Conditions Affect Selectivity to a Desired Product. A comparison of the selectivity of a competitive-consecutive chemical reaction under various mixing conditions is made (see Section 13-1.4 for a definition of selectivity). The chemical reactions are as follows:

$$A + B \rightarrow R \qquad k_{R1} = 35\ m^3/kmol \cdot s \qquad C_{Ao} = 0.2\ kmol/m^3$$

$$R + B \rightarrow S \qquad k_{R2} = 3.8\ m^3/kmol \cdot s \qquad C_{Bo} = 0.2\ kmol/m^3$$

R and S are not present in the feed solutions. The solutions containing A and B must mix in order for the reaction to proceed. The reactions are allowed to go to completion to obtain the final yield of R. Table 13-1 shows the selectivity for various reaction conditions. The nonideal results are taken from simulations discussed in Section 13-5.

From this example of a fast, competitive consecutive reaction scheme we can see that nonideal mixing can cause a decrease in selectivity in both continuous and semibatch reactors. Residence time distribution issues can cause a reduction in yield and selectivity for both slow and fast reactions (see Chapter 1), but for fast reactions, the decrease in selectivity and yield due to inefficient local mixing can be greater than that caused by RTD issues alone. In semibatch reactors, poor bulk mixing can also cause these reductions (see Example 13-3).

13-1.2 Reaction Schemes of Interest

Mixing effects on product distribution are of importance in multiple reactions because the impact on design and economics can be profound. In such reactions the desired product is one of two or more possible products. Economics are directly affected by yield of desired product, and both design and economics are affected by downstream separation requirements.

The effects of mixing on selectivity have been most carefully investigated for a competitive-consecutive reaction of the type

$$A + B \xrightarrow{k_{R1}} R$$

$$R + B \xrightarrow{k_{R2}} S$$

Table 13-1 Selectivity for Ideal and Imperfectly Mixed Reactions

Type of Reactor	Selectivity of $R = R/(A_o - A_{final})$
Ideal plug flow with perfectly mixed feed	0.861
Ideal CSTR	0.731
Imperfect tubular reactor	0.571 with turbulence parameters: $k = 0.008\ m^2/s^2$, $\varepsilon = 0.03\ m^2/s^3$, 10 s residence time
Imperfect stirred tank	0.652 for 6280 L, Rushton turbine with N = 24.4 rpm, feed at impeller discharge

B is added to A in the semibatch case. A and B are mixed continuously in the tubular reactor case. R is considered to be the desired product. The objective is to determine how mixing conditions can affect the yield of R. We are concerned with the time period from when the reactants are first contacted until they are completely mixed to a molecular scale. During this time, zones of local B concentration can vary from an upper limit equal to the feed concentration to a lower limit of essentially zero. This critical stage is depicted schematically in Figure 13-1, where B is added to A and B is the limiting reagent. The reaction of A with B to form the desired product, R, is occurring along with the normally undesired reaction of R with B to form S. In the first case, the mixing takes place before reaction occurs. A and B are intimately mixed and very little unwanted material S is formed. In the other case, there is a boundary between A and B. Although a lot of desirable product R is formed, it quickly reacts with high concentrations of B to form undesirable product S. While this reaction system has received the most attention, the course of any reaction that is influenced by concentration has the potential to be influenced by mixing. The effect can be on the reaction rate, the product distribution, or both (see Examples 13-3 and 13-4).

Competitive-parallel reactions can also be subject to mixing effects, as shown by Baldyga and Bourne (1990) and Paul et al. (1992). Many variations are possible, but the basic reactions of these systems are as follows:

$$A + B \xrightarrow{k_{R1}} R$$

$$A + C \xrightarrow{k_{R2}} U$$

where the first reaction is the desired one and the second is a simultaneous decomposition of A to undesired U (see Example 13-8a).

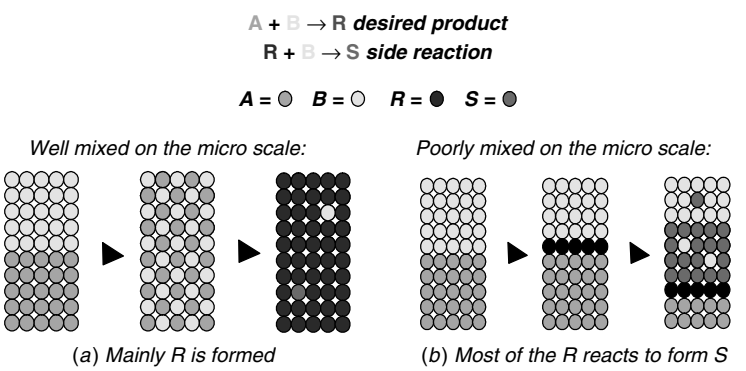

Figure 13-1 Diffusion and chemical reaction at an A–B mixing surface. In this competitive-consecutive reaction, the first reaction, which forms the desired product (R), is fast, and the consecutive reaction step, forming the undesired by-product (S), is slower. Local mixing conditions at the molecular scale determine the amount of undesired by-product (S) formed.

A very significant variation on this basic system is the decomposition of a product during pH adjustment as follows:

$$\text{acid} + \text{base} \rightarrow \text{salt}$$

When base is added to acid,

$$A + \text{base} \rightarrow U$$

When acid is added to base,

$$A + \text{acid} \rightarrow U$$

(Both A and the desired product, R, could be decomposed in this way.)

Although the acid–base neutralization is normally orders of magnitude faster than the decomposition of A, areas of extreme pH resulting from inadequate mixing can exist and a significant loss of A during seemingly straightforward pH adjustment operations can result in loss of product. This effect is particularly important on scale-up to large vessels, including fermenters, and provision must be made for adequate mixing (see Example 13-8b).

Returning to the basic competitive-consecutive reaction system, consider a semibatch operation. Reagent B is added over time and is instantaneously mixed to a molecular level with the vessel contents. The maximum selectivity for the desired product, R, is a function of the rate constants k_{R1} and k_{R2}, the overall molar charge ratio of A to B, and the degree of conversion of A. The degree of conversion of A can depend on the charge ratio and the residence time. The discussion that follows is limited to the case of sufficient residence time such that all of the B charged will react, provided that B is not charged in excess of what is required for complete conversion of A to S. The maximum selectivity for R, in the absence of mixing effects, then becomes a function only of k_{R1}/k_{R2} and the molar charge ratio. If we now fix k_{R1}/k_{R2} and the molar charge ratio, the selectivity is fixed, as are the yield and the degree of conversion of A.

The term *expected (ideal) yield*, Y_{exp}, is used to denote the yield that would be obtained for a competitive-consecutive reaction under conditions of perfect mixing and complete conversion of the limiting reactant, as presented by Levenspiel (1972):

$$Y_{exp} = \frac{R}{A_o} = \frac{1}{1-\kappa}\left[\left(\frac{A}{A_o}\right)^{\kappa} - \frac{A}{A_o}\right] \tag{13-5}$$

where $\kappa = k_{R2}/k_{R1}$ and capital letters denote molar concentrations. This equation applies to both batch and semibatch operations, provided that both reaction rates depend on B in the same way (e.g., second order) and provided that B is added to A in the semibatch case and B is consumed completely. This equation is often used in flowsheeting programs to solve for A given a specified yield. There is

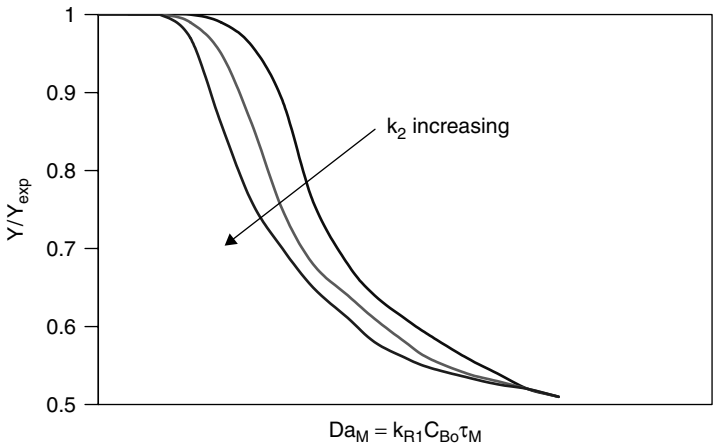

Figure 13-2 Normalized yield, Y/Y_{exp}, as a function of Damkoehler number based on k_1. This is a qualitative conceptualization of the interaction between mixing rate as expressed by a local mixing time, τ_M, reaction rate, k_1C_{Bo}, and reaction yield. As the mixing improves (smaller Da_M), the yield increases. As the second reaction gets faster (increasing k_2), the mixing time must also drop, to maintain yield.

no guarantee that the desired yield, Y_{exp}, and A will be obtained—unless the equipment is carefully designed for good mixing conditions.

A useful way of visualizing the relationship between the magnitude of the primary reaction rate constant and its potential to affect yield is illustrated in Figure 13-2, in which normalized yield, Y/Y_{exp}, is plotted against a mixing Damkoehler number based on k_{R1} [Y_{exp} is the maximum yield as calculated using eq. (13-5)]. For low values of k_{R1} the yield equals that expected from the chemical kinetics. As k_{R1} increases, yield decreases because of mixing effects. The decline accelerates with increasing values of k_{R2}, as shown in Figure 13-2. These relationships can also be expressed as shown in Figure 13-3, where (Sharratt, 1997) X_S is used to represent the amount of S formed where $X_S = 2S/(2S + R)$ and k_{R2} to represent the undesired reaction kinetics.

Mixing effects for homogeneous reactions can only reduce yield below the expected (ideal) as calculated by eq. (13-5). The primary concern is the magnitude of the yield reduction attributable to deviation from instantaneous perfect mixing to the molecular level.

13-1.3 Relating Mixing and Reaction Time Scales: The Mixing Damkoehler Number

The final phase of mixing during which chemical reactions can occur and before complete molecular homogeneity is achieved may be visualized as the molecular diffusion-controlled mixing of the smallest eddies in the turbulence energy dissipation spectrum. The smallest eddy size can vary over several orders of

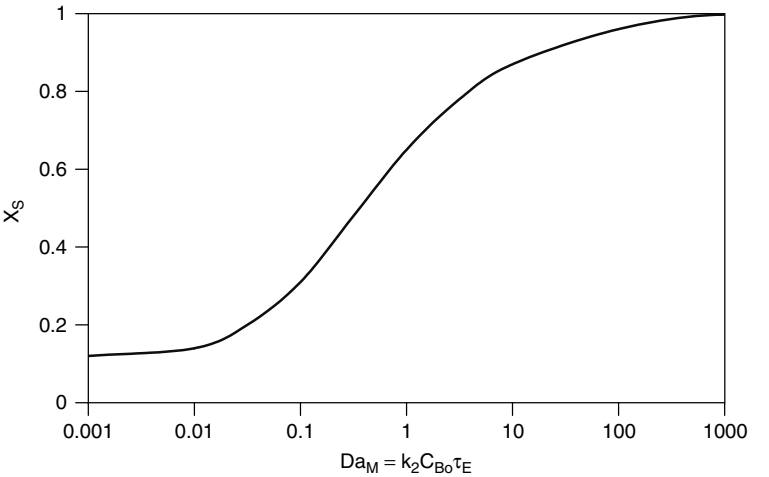

Figure 13-3 By-product selectivity, X_s, as a function of Damkoehler number based on k_2. These data of Bourne in Sharratt (1997) show the increased by-product formation with increasing mixing time based on the engulfment model, τ_E. As the reaction rate for the second reaction, $k_2 C_B$, increases, the mixing time must decrease to maintain yield.

magnitude, from $\sim$1 μm in intense jet mixing to $>$100 μm in stirred tanks with low-shear impellers. The reader is referred to Chapter 2 for a discussion of the time and length scales of turbulence and small scale diffusion.

When fluids mix, the elements of the two fluids are stretched into striations or lamellae. In laminar flow, the average lamellar thickness, δ, can be used to generate a mixing time, τ_L, based on the molecular diffusivity, D_{AB}. This gives

$$\tau_L = \frac{\delta^2}{D_{AB}} \tag{13-6}$$

The final stage of diffusion in turbulent flow, although conceptually identical to this model, is more complicated, and we defer definition of turbulent mixing time scales to Section 13-2.1.3. In the case of consecutive-competitive chemical reactions [$A + B \rightarrow R$; $R + B \rightarrow S$] product R must mix with reactant B for the second chemical reaction to proceed. At any location in the vessel and at any instant in time, local concentration gradients normal to stretching fluid lamella may appear as shown in Figure 13-4. This concentration pattern is repeated layer upon layer throughout the mixing fluid as the two mixing fluids diffuse together. The lamellae or striations are not flat: they twist, roll up, and are stretched thinner and thinner by the turbulent vortices in the flow.

The magnitude of yield reduction due to imperfect mixing is determined by the following major factors:

1. *Local mixing time:* a measure of the time from initial contact of the reactants to final homogeneity on a molecular scale at a given point. Any

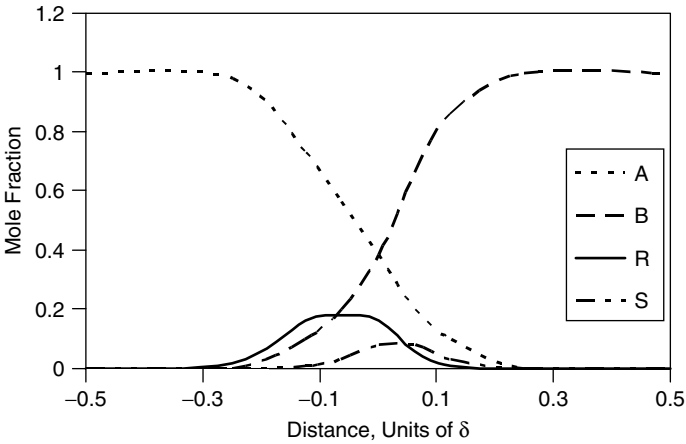

Figure 13-4 Mole fraction profiles across a lamella or striation. The lamellar thickness is $\delta = 1.0$. At one edge, the mole fraction of A is 1.0; at the other edge the mole fraction of B is 1.0. The components diffuse across the layer, reacting to A and B. While Figure 13-1 showed the molecular scale at the interface, this figure shows the mole fraction across a full striation. Figure 13-12 shows the same phenomenon at the surface of a bubble or a drop.

overreaction of R to S must occur during this time because once the reactants are molecularly mixed, the relative amounts of R and S obtained are fixed by k_{R1}/k_{R2} and the molar charge ratio A_0 to B_0 according to eq. (13-5) and the dependence of A on B_0. Estimating the local mixing time at a given point in a reactor is not easy and will be strongly affected by both the reactor configuration and the way the reagent is fed into the reactor. There are a number of models: Corrsin, Baldyga, and Bourne's micromixing, Baldyga and Bourne's engulfment, and Villermaux's interchange models. All of these try to predict how the reaction conditions at the addition point are affected by local mixing and by the subsequent history of the feed as it is dispersed throughout the mixing vessel. All the models depend on local turbulence conditions as measured by local energy dissipation per unit volume. Depending on the model, a scale of turbulence is often required. This will be an eddy scale ranging from the Corrsin integral length scale to the Kolmogorov scale. In some cases physical properties such as viscosity and molecular diffusivity are required. See Section 13-2.1 for further discussion.

2. *Chemical kinetics:* the absolute values of k_{R1} and k_{R2}. The magnitude of the rate constant, k_{R1}, will determine how much A can be converted during the time required to achieve molecular mixing. The extent of the conversion will determine the amount of R that is subject to excess B concentration and hence overreaction to S as determined by k_{R2}. In some cases the kinetics can be determined by use of a stopped-flow reactor or similar device. For

the results to be valid, the response of the device must be much faster than the fastest reaction.

3. *The mixing Damkoehler number:* the ratio of rates of the first or second reaction and the local mixing rate.

R is converted to S, depending on the probability of a molecule of R reacting with a molecule of B. In a B-rich zone this probability is greater than in the perfectly mixed zone and the extent to which it occurs will depend on the rate at which R can diffuse out of the B-rich zone relative to the rate at which it reacts with B. For reactor design purposes, the key issues are (1) methods of determining and/or predicting which reactions are mixing sensitive, and (2) reactor design guidelines to minimize yield loss on scale-up in which the information discussed above is used to predict and describe mixing considerations in industrial reactors. These issues are considered further later in the chapter.

13-1.4 Definitions

To assure accurate and consistent interpretation of theories, models, and results, precise definitions of important terms must be established. The most important definitions used in this chapter are as follows:

- *Conversion:* ratio of moles of a key reactant reacted to moles charged, $(A_0 - A)/A_0$
- *Yield:* ratio of moles of the desired product to moles of a key reactant charged, $Y = R/A_0$
- *Selectivity:* ratio of moles of the desired reaction product to moles of key reactant consumed, $S = R/(A_0 - A)$

Note: *Some texts, including Levenspiel (1962), Fogler (1999), and Baldyga and Bourne (1999), use alternative definitions:*

- *Yield* (alternative)*:* $R/(A_0 - A)$ (same as selectivity above)
- *Selectivity* (alternative)*:* R/U, where U is an undesired product
- *Selectivity* (alternative)*:* selectivity as used by Baldyga and Bourne for the competitive-consecutive reaction scheme described in Section 13-1.2, $X_S = 2S/(2S + R)$

The definitions for yield and selectivity used throughout this book are the first definitions since in many industrial reaction systems, the amounts of individual undesired reaction by-products may not be known. When another definition is used, it will be noted explicitly.

- *Blending rate:* the rate that concentration differences are reduced by large scale circulation and convective flow down to a selected level of variation everywhere in the whole vessel.

- *Blend time:* the reciprocal of the blending rate, typically the blending time constant, τ_B, for reduction of concentration fluctuations by 95% according to eqs. (13-8) and (13-9).
- *Local mixing rate:* the reciprocal of the local mixing time defined below.
- *Local mixing time:* the time constant for local mixing to molecular scale, which depends on geometry, local shear rates, and physical properties (see Section 13-2).
- *Mixing Damkoehler number:* the ratio of mixing time to reaction time, $Da_M = \tau_M/\tau_R$. The mixing Damkoehler number may be referred to simply as the Damkoehler number. (Note that the traditional Damkoehler number is the vessel residence time divided by the reaction time.)
- *Reaction time:* the time constant for chemical reaction based on the molecular reaction rate constant as follows:

$$\tau_R = \begin{cases} 1/k & \text{for first-order reactions} \\ 1/kC & \text{for second-order reactions} \\ 1/kC^{n-1} & \text{for higher-order reactions} \end{cases}$$

- *Scale of segregation:* a measure of the large scale breakup process (bulk and eddy diffusivity) without the action of diffusion. It is the size of the packets of B that can be distinguished from the surrounding fluid A. See the discussion in Chapters 2 and 3.
- *Segregation:* a measure of the difference in concentration between the purest concentration of B and the purest concentration of A in the surrounding fluid. Molecular diffusion is needed to reduce the segregation, as even the smallest turbulent eddies have a very large diameter relative to the size of a molecule. Segregation can be defined mathematically as $s = \overline{c_i^2}$, where c_i is the fluctuating concentration of component i, given by $c_i = C_i - \overline{C_i}$, and $\overline{C_i}$ is the average concentration. Intensity of segregation is the segregation divided by the product of the average concentrations of A and B.
- *Micromixing:* mixing at the scale of the smallest turbulent eddies and concentration striations (see Figure 13-5*a*).
- *Macromixing:* another term for blending to a degree of homogeneity throughout a vessel. For the blend time correlation, this degree is 95%. This is the largest scale reduction of concentration fluctuations (see Figure 13-5*b*).
- *Mesomixing:* all intermediate scales of mixing. Mesomixing effects most typically occur when the feed rate is greater than the local mixing rate, allowing a plume of higher concentration to spread from the feed point (see Figure 13-5*c*).

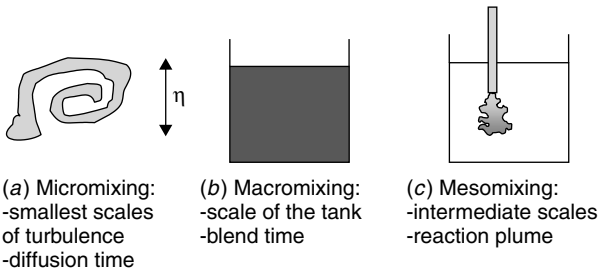

Figure 13-5 (*a*) Micromixing at the smallest scales; (*b*) macromixing at the largest scale; and (*c*) mesomixing at intermediate scales.

13-2 PRINCIPLES OF REACTOR DESIGN FOR MIXING-SENSITIVE SYSTEMS

The rate at which reactants are brought together is very important in many reactions. For very fast acid–base reactions, the time it takes to mix is the apparent reaction time. Reaction cannot take place before mixing, so the processes take place essentially in series. A reduction in apparent reaction rate is often not critical to the process result. However, with fast reactions, slower mixing results in high local reactant concentrations, which can allow an undesired consecutive or parallel reaction to proceed to a greater extent than predicted by the rate constant ratio, thereby decreasing selectivity. Mixing rates are frequently important in determining the yields of desired products in semibatch reactors, since the reaction rates may be fast relative to mixing rates. Scale-up from bench scale to commercial production scale can result in yield reductions of more than 10%, unless the mixing requirements are recognized in development and provided for on scale-up.

13-2.1 Mixing Time Scales: Calculation of the Damkoehler Number

There are several mixing or blending times that can be measured and observed in an agitated vessel. The bulk blending time is the time it takes to get all points in the tank within some arbitrary range of all other points. Local mixing time is the measure of how fast material at a given point losses its identity. Thus, the local mixing time varies with position, while the bulk blending time may vary with position of addition but not position of measurement. Bulk blending time is usually based on the longest time or the slowest rate of mixing in the vessel. Local mixing times depend on the local turbulence.

The Damkoehler number requires characteristic time scales for both mixing and reaction. Calculation of the reaction time scale is relatively straightforward, although the necessary data may be difficult to obtain. Many choices for the mixing time have been proposed, and data are available for many common semibatch geometries.

13-2.1.1 Characteristic Reaction Time. As shown in Example 13-1, mixing can affect the selectivity of a reaction, not just the rate. Reactions that show selectivity are usually two-step reactions which are either consecutive or parallel. One reaction is usually so fast that it is mixing controlled. The second reaction has a characteristic time constant of the order of the local mixing time. The reaction time is usually given by

$$\tau_R = \frac{1}{k_{R2} C_{Bo}} \tag{13-7}$$

where k_{R2} is the rate constant of the second undesirable reaction and C_{Bo} is the initial concentration of B in the feed—*not* the well-mixed concentration. The component A is usually present in large excess, so its concentration is essentially constant and does not appear in the equation. The reaction half-life $[\tau_R = -\ln(0.5)/k_R]$ as given in eq. (13-3) is another characteristic reaction time, but it does not account for the effect of concentration. Use of the feed concentration, C_{Bo} rather than the well mixed concentration gives the reaction time at the end of the feed pipe. This is the worst condition in the reactor and is the location where mixing must overcome kinetics in order to avoid the formation of undesirable by-products.

13-2.1.2 Blend Times. Even though it is known that local mixing time is more relevant to yield effects for mixing rate-controlled reactions, blend times are a more common way to compare mixing and reaction time constants. The blend time is the time it takes after an input change to a stirred vessel for spatial variation of average concentration to drop to 5% of the original variation. Typically, changes in conductivity are used to make measurements of degree of blending (see Grenville, 1992; Nienow, 1997). The Grenville correlations for blend times are used extensively for design and scale-up. They are dependent on the Reynolds number range as follows:

$$N\tau_B = \begin{cases} \dfrac{5.4}{N_p^{1/3}} \left(\dfrac{T}{D}\right)^2 & \text{for } Re > 6400 \quad (13\text{-}8) \\ \dfrac{1}{Re} \dfrac{184.2}{N_p^{2/3}} \left(\dfrac{T}{D}\right)^2 & \text{for } 500 < Re < 6400 \quad (13\text{-}9) \end{cases}$$

Vessel blend times are typically about 2 s in a 1 L vessel and about 20 s in a 20 000 L vessel for low viscosity liquids.

Other blend time correlations were presented by Penney (1971), Khang and Levenspiel (1976), and Fasano and Penney (1991). Use of these correlation equations allows the estimation of blending times, which can be compared to molecular reaction times for all the reactions in the reactor. Even though local mixing time is the critical time for determining apparent reaction rate, blend time can be used in an approximate manner. If the characteristic molecular reaction time (e.g., the half-life) is much greater than the characteristic blend time

(typically, 100 times), the chemical reactions occur under well-mixed conditions. If, on the other hand, the characteristic blend time is very long compared to the characteristic reaction time, there will be regions rich in some reactants that could lead to unwanted by-products and reduced yield of the desired products. The study of such yield effects as affected by mixing rate is frequently called *micromixing* because it deals with small characteristic times and small (local) scales of concentration fluctuation. It must be emphasized that the use of blend time is only approximate because it is the spectrum of local mixing times that actually determines how the mixing rate affects the yield. The reader is referred to Chapter 9 for more details on blending in tanks and to Chapter 7 for in-line blending.

13-2.1.3 Local Mixing Time Scales. In dealing with mixing effects on reaction two topics are of interest. The first is the size of the additive blob or feed stream. The second is its rate of disappearance or the inverse local mixing time. For low viscosity liquids, very rapid mixing with local mixing time constants, τ_M, as short as 0.01 s is easily obtained in liter-sized reactors, but due to mechanical limitations, local mixing times on the order of 0.1 s or longer typically occur in reactors of 10 000 or more liters. The size of the blob together with the local mixing time determines the amount of undesirable product that can be formed. There are many formulations for these two effects.

The discussion of local mixing time scales must begin with a definition of the turbulent scales which underlie many of the mixing time formulations. These scales are developed in Chapter 2, so only a brief summary is provided here. The range of turbulent length scales starts at the largest integral scales of motion, which is a dimension close to the blade width or the feed pipe diameter. The eddies cascade energy down through smaller and smaller scales until the turbulent energy is dissipated by viscosity at the smallest scales of motion. The Kolmogorov length scale is the size of the smallest turbulent eddy:

$$\eta = \left(\frac{\nu^3}{\varepsilon}\right)^{1/4} \tag{13-10}$$

At the Kolmogorov scale, the following statements apply:

$$\varepsilon \propto \frac{u_\eta'^3}{\eta}$$

where ε is the rate of dissipation of turbulent kinetic energy per unit mass.

$$\mathrm{Re}_\eta = 1.0 = \frac{\eta u_\eta'}{\nu}$$

where Re_η is the local Reynolds number at the Kolmogorov scale. Thus,

$$u_\eta' = \frac{\nu}{\eta} = (\nu\varepsilon)^{1/4}$$

so the time that it takes to dissipate a Kolmogorov sized eddy is

$$\tau_K = \frac{u_\eta'^2}{\varepsilon} = \frac{u_\eta'^2 \eta}{u_\eta'^3} = \frac{1}{(\nu\varepsilon)^{1/4}} \left(\frac{\nu^3}{\varepsilon}\right)^{1/4}$$
$$= \left(\frac{\nu}{\varepsilon}\right)^{1/2} \tag{13-11}$$

This the Kolmogorov time scale.

Batchelor (1959) developed an expression for the smallest concentration (or temperature) striation based on the argument that for diffusion time scales longer than the Kolmogorov scale, turbulence would continue to deform and stretch the blobs to smaller and smaller lamellae. Only once the lamellae could diffuse at the same rate as the viscous dissipation scale would the concentration striations disappear. The Batchelor length scale is the size of the smallest blob that can diffuse by molecular diffusion in one Kolmogorov time scale. Using the lamellar diffusion time from eq. (13-6) gives

$$\tau_B = \frac{\lambda_B^2}{D_{AB}}$$

If the Batchelor and Kolmogorov times are equal, $\tau_B = \tau_K$, the Batchelor length scale is

$$\lambda_B = \left(\frac{\nu D_{AB}^2}{\varepsilon}\right)^{1/4} = \left(\frac{D_{AB}}{\nu}\right)^{1/2} \left(\frac{\nu^3}{\varepsilon}\right)^{1/4} = \frac{\eta}{\sqrt{Sc}} \tag{13-12}$$

where $Sc = \nu/D_{AB}$ is the Schmidt number. Because the Batchelor and Kolmogorov time scales are equal, mixing times proportional to τ_K are referred to as Batchelor scale mixing (see Table 2-3 and related text). For liquids with Schmidt numbers much larger than 1, the smallest striation thicknesses are given by the Batchelor scale. For large Sc, say 1000, the Batchelor length scale can be 30 times smaller than the Kolmogorov length scale.

Corrsin Mixing Time. One of the first theoretical formulations of mixing time is due to Corrsin (1964). For isotropic homogeneous turbulence, he determined the time required for a reduction of scale from the largest scales of concentration fluctuations, L_s, through the full range of the inertial convective scales of turbulence to the Kolmogorov scale, η, and then through the viscous scales to the Batchelor scale, λ_B, by integrating the scalar (concentration) and turbulence spectra. This gives

$$\tau_M = \begin{cases} 2\left(\dfrac{L_s^2}{\varepsilon}\right)^{1/3} + \dfrac{1}{2}\left(\dfrac{\nu}{\varepsilon}\right)^{1/2} \ln(Sc) & \text{for liquids where } Sc \gg 1 \quad (13\text{-}13) \\ 1.36\left(\dfrac{L_s^2}{\varepsilon}\right)^{1/3} & \text{for gases where Sc is about 1.0} \quad (13\text{-}14) \end{cases}$$

L_S is the local scale of segregation or the average size of unmixed regions and ε is the local rate of energy dissipation. The first term arises from describing the large inertial scales which contain most of the turbulent energy. The second term gives the time scales at the smallest scales of mixing. This is the time required to reduce the blob from the Kolmogorov length scale [eq. (13-10)] to the Batchelor length scale [eq. (13-12)] for large Sc, where molecular diffusion is much slower than the diffusion of momentum. Baldyga and Bourne have restated the second term in eq. (13-13) as asinh(0.05Sc) using a somewhat more rigorous derivation than Corrsin's. In both cases, this term will be vanishingly small most of the time.

Micromixing. Alternative ways of expressing the local mixing time constant have been developed by Bourne and co-workers, and they have dubbed this approach *micromixing*. In the micromixing analysis it is assumed that the amount added and the rate of addition are very small and that the scale of interest is set by the local turbulence. The earliest approach was to assume that added material did not do anything until the Kolmogorov scale was reached and the subsequent mixing took place by molecular diffusion. Using eqs. (13-6) and (13-10) yields

$$\tau_M = \frac{\eta^2}{D_{AB}} = \left(\frac{\nu^3}{\varepsilon D_{AB}^2}\right)^{1/2} = Sc\left(\frac{\nu}{\varepsilon}\right)^{1/2} \tag{13-15}$$

This concept was replaced by the engulfment model, which is a more realistic way of treating the breakup of the added reactant. Here the engulfment rate is

$$E = 0.06\left(\frac{\varepsilon}{\nu}\right)^{1/2}$$

and thus

$$\tau_E = \frac{1}{E} = 17\left(\frac{\nu}{\varepsilon}\right)^{1/2} \tag{13-16}$$

The differences in the approaches are small. Both include local energy dissipation, and both include the viscosity. The molecular diffusivity is important only when the viscosity is high (see Section 13-2.1.5). The similarity between τ_E and the last term in the Corrsin development is not surprising, but the implication of the much larger coefficient (17 instead of 0.5) is that viscosity may play a role at scales significantly larger than the Kolmogorov scale, and the effective micromixing rate for reactions must include these scales.

Mesomixing. This term is used to describe a set of phenomena between macromixing, which involves the whole vessel, and micromixing, which involves a small volume at the smallest eddy scales. Although the term *mesomixing* was first used by Bourne and co-workers, the first group to describe the phenomenon was that of Villermaux. His group was doing experiments similar to those of Bourne, but in their experiments with colored materials and precipitating materials they

observed a plume near the point of addition. The size and rate of disappearance of this plume in semibatch experiments did not fit any of the models that Bourne and others had proposed. Villermaux and Devillon (1972) and Villermaux and David (1987) developed a semiempirical model called *IEM* (interaction by exchange with the mean) to describe the volume and the rate of exchange between the plume volume and the bulk. They assumed that the plume was at or near the composition of the inlet and that the bulk was well mixed. Turbulent mass transfer occurred across the boundary by turbulent interchange. Empirical relations were developed for the size of the plume and the rate of mixing. Thus, effects of inlet geometry velocity and flow rates were taken into account. Thoma (1989), Bourne and Thoma (1991), and Thoma et al. (1991) looked at the time of addition in semibatch operation and observed that when the addition time was very short there was an additional undesirable selectivity change. This effect is shown for a sample reaction system in Figure 13-6. It appeared that higher rates of addition were sufficient to overcome the local ability to take material away, and micromixing by turbulence of small packets was overwhelmed. They called this phenomenon *mesomixing*. It now seems that what Villermaux's group observed was very similar. A plume exists when the feed is added faster than the fine scale micromixing turbulence can take it away. This plume is clearly shown in concentration isoplots of mixing-reaction simulations. The processes governing mesomixing are not as well worked out as those for micromixing, but many useful thoughts come from understanding the concepts. Thoma et al. (1991) discussed the relationship of micromixing to macromixing in detail.

In terms of the Corrsin development, for mesomixing the initial scale is set by the inlet conditions (e.g., feed pipe diameter), not by the local turbulence. The first term of eq. (13-13) accounts for the mesomixing effect, and the second term is related to the micromixing effect: large values of the first term occur when an unmixed plume is evident.

Bourne and Thoma (1991) found that the critical addition time was inversely proportional to impeller speed. When running below the critical addition time, scale-up could be affected by absolute impeller speed in addition to local energy dissipation. For addition times longer than the critical mixing time, local turbulent energy dissipation alone governed selectivity. Mesomixing occurs mainly at intermediate scales of turbulence, which are not affected by viscosity. Micromixing occurs at scales smaller than the Kolmogorov scale, η, where there is a definite viscosity effect, as shown above. Bourne and Hilber (1990) showed that the number of addition points affected the critical feed time so that the following expression could be developed:

$$\tau_{crit} \mathrm{Nn} = \text{constant} \tag{13-17}$$

The constant is a function of local turbulence and chemistry, as shown in Figure 13-6. Attempts have also been made to define the mesomixing parameters from basic turbulence theory. For example, Baldyga and Bourne (1999) suggest

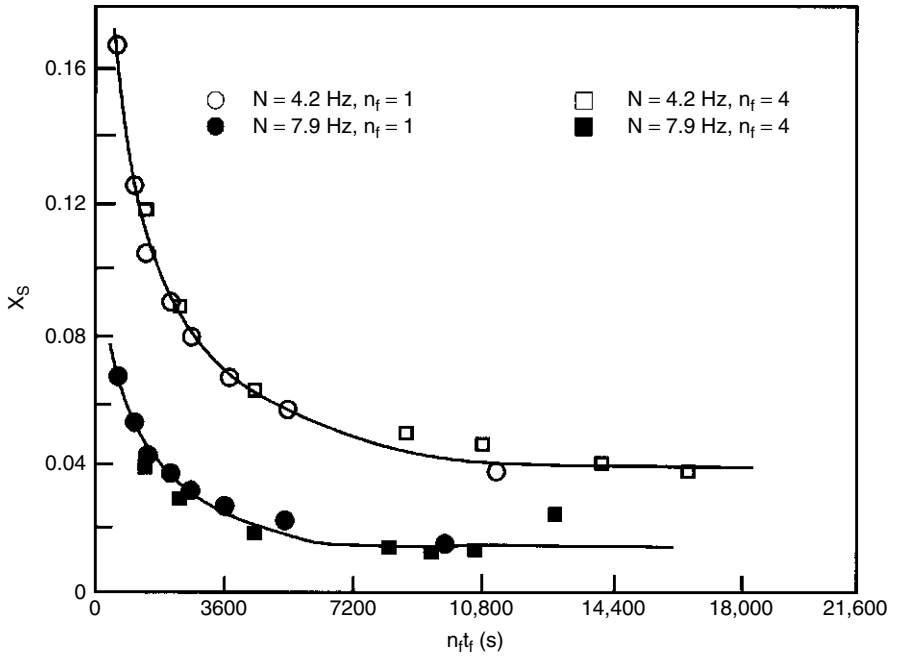

Figure 13-6 Effect of addition time on selectivity in semibatch operation. Number of nozzles and feed time ($n_f t_f$) determine selectivity at constant N. If N decreases on scale-up, the minimum critical addition time ($n_f t_f$) must increase to achieve the same selectivity. Feed nozzles are in the impeller discharge region. (Data from Bourne and Hilber, 1990.)

that the mesomixing time is given either by

$$\tau_D = \frac{Q_B}{UD_t} \tag{13-18}$$

where τ_D is the mesomixing time for dispersion of feed, Q_B the volumetric feed rate of B, U the local velocity in surrounding fluid at the feed point, and D_t the local turbulent diffusivity ($D_t = 0.1k^2/\varepsilon$) in the surrounding fluid; or by Corrsin's form for the mesomixing time scale:

$$\tau_S = A\left(\frac{L_S^2}{\varepsilon}\right)^{1/3} \propto \left(\frac{Q_B}{U_B\varepsilon}\right)^{1/3} \tag{13-19}$$

where τ_S is the mesomixing time for disintegration of large eddies, A is a constant between 1 and 2, L_S is the concentration macroscale, and ε is the local turbulent energy dissipation rate.

However, these expressions work to only a limited extent. For example, an inlet jet can be designed to develop a high local energy dissipation at the inlet and rapid mixing. Current theories cannot incorporate this effect. A simple ordering

argument would suggest that if the energy dissipation from the jet given by the velocity cubed divided by the jet diameter is larger than the surrounding local energy dissipation per unit mass, that is the energy to use and the pipe diameter is the dimension. More detail on the experimental and theoretical foundation of these concepts is given in Baldyga and Bourne (1999, Chap. 12). Cases for jet mixers and motionless mixers are discussed.

An interesting sidelight of these mixing effects is the increasing importance of mixing on scale-up, as illustrated in Example 13-2.

Example 13-2: Scale Effects on Mixing in Stirred Vessels. Determine whether the fast reaction from Example 13-1 will be affected by mixing on scale-up if the feed point is close to the impeller. Compute the values of the Corrsin mixing time, τ_M, at the impeller tip and the blend time, τ_B, for (a) 1 L and (b) 20 000 L vessels stirred by a disk turbine ($N_P = 6$) at power per unit volume of 0.36 kW/m^3. Use properties of water: $\rho = 1000$ kg/m^3; $\nu = 10^{-6}$ m^2/s; Sc = 2000 for a typical solute.

SOLUTION: The reaction time scale is taken from the first reaction in Example 13.1: $\tau_{R1} = 1/k_{R1}C_{A0} = 0.14$ s. The Corrsin equation (Section 13-2.1.3) is

$$\tau_M = 2\left(\frac{L_S^2}{\varepsilon}\right)^{1/3} + \frac{1}{2}\left(\frac{\nu}{\varepsilon}\right)^{1/2}\ln(Sc)$$

where L_s is the largest length scale of the scalar, often taken to be the feed pipe diameter. If this length scale is not known, Zipp and Patterson (1998) suggest using $L_S = 0.39L_T$, where L_T is the largest eddy size, proportional to $k^{3/2}/\varepsilon$. This gives a modified Corrsin equation based on k and ε:

$$\tau_M = 1.1\left(\frac{k}{\varepsilon}\right) + \frac{1}{2}\left(\frac{\nu}{\varepsilon}\right)^{1/2}\ln(Sc) \tag{13-20}$$

From Wu and Patterson (1989) we know that the energy dissipation per unit mass at the impeller tip is 20 times the average for the tank and that the random turbulence energy per unit mass, k, is approximately $0.06U_{tip}^2$. Our objective is to compare the mixing time scales with the reaction time scale for both the small and the large vessel. As long as the mixing time scales are shorter than the reaction time scale, the reaction will not be limited by mixing.

(a) For the 1 L vessel:

$$T = 0.108 \text{ m}$$

$$D = 0.036 \text{ m}$$

$$P = (360 \text{ W/m}^3)(0.001 \text{ m}^3)$$

$$= N_p\rho N^3D^5 = (6)(1000 \text{ kg/m}^3)(N^3)(0.036 \text{ m})^5$$

$$N = 9.97\ s^{-1} \text{ or } 598\ rpm$$
$$U_{tip} = \pi ND = (\pi)(9.97\ s^{-1})(0.036\ m) = 1.13\ m/s$$

For this geometry, the random turbulence energy, k, is about $0.06U_{tip}^2$, so

$$k = 0.06(1.13\ m/s)^2 = 0.0766\ m^2/s^2 \text{ at the tip of the impeller}$$
$$\varepsilon = 20(P/V)/\rho = 20(360\ W/m^3)/(1000\ kg/m^3) = 7.2\ m^2/s^3$$

Therefore, for $\tau_M = 0.5[2.2\ k/\varepsilon + (\nu/\varepsilon)^{1/2} \ln(Sc)]$:

$$\tau_M = 0.5\{2.2(0.0766\ m^2/s^2)/(7.2\ m^2/s^3) + [(10^{-6}\ m^2/s)/(7.2\ m^2/s^3)]^{1/2} \ln(2000)\}$$
$$= 0.0117\ s + 0.0014\ s = 0.0131\ s$$

The inertial mixing (first term) is controlling since its time constant is about eight times the time constant of the Batchelor scale mixing. The Corrsin scale mixing is much faster than the reaction time constant.

$$Re = ND^2\rho/\mu = (9.97\ s^{-1})(0.036\ m)^2(1000\ kg/m^3)/(0.001\ kg/m \cdot s)$$
$$= 12\ 921$$

Therefore,

$$N\tau_B = 5.4/N_p^{0.333}/(D/T)^2 \quad \text{for } Re > 6400$$
$$\tau_B = 5.4/6^{0.333}/(1/3)^2/9.97\ s^{-1} = 2.7\ s$$

about 206 times the local mixing time at the impeller tip, or 230 times the inertial term in the Corrsin equation. Bulk blend time is much slower than the reaction time, so it is important to feed into the zone of maximum dissipation, close to the tip of the impeller blades.

(b) For the 20 000 L vessel:

$$T = 2.94\ m$$
$$D = 0.98\ m$$
$$P = (360\ W/m^3)(20\ m^3) = 7200\ W$$
$$= N_p\rho N^3 D^5 = (6)(1000\ kg/m^3)(N^3)(0.98\ m)^5$$

so $N = 1.1\ s^{-1}$ or 66 rpm.

$$U_{tip} = \pi ND = (\pi)(1.1\ s^{-1})(0.98\ m) = 3.39\ m/s$$
$$k \approx 0.06(3.39^2) = 0.688\ m^2/s^2$$

at the tip of the impeller, assuming that k/U_{tip}^2 remains constant during scale-up.

$$\varepsilon = 20(P/V)/\rho = 20(360\ W/m^3)/(1000\ kg/m^3) = 7.2\ m^2/s^3$$

assuming that $\varepsilon/\varepsilon_{avg}$ remains constant during scale-up. Therefore, for $\tau_M = 0.5[2.2k/\varepsilon + (\nu/\varepsilon)^{1/2} \ln(Sc)]$,

$$\begin{aligned}\tau_M &= 0.5\{2.2(0.688\ m^2/s^2)/(7.2\ m^2/s^3) \\ &\quad + [(10^{-6}\ m^2/s)/(7.2\ m^2/s^3)]^{1/2} \ln(2000)\} \\ &= 0.1051\ s + 0.0014\ s = 0.1065\ s\end{aligned}$$

The inertial mixing (first term) is controlling since its time constant is about 75 times the time constant of the Batchelor scale mixing. The contribution due to the Batchelor scale mixing is negligible when the vessel is scaled up. At the large scale, the Corrsin time scale is similar to the reaction time scale (0.14 s). This very fast reaction may be limited by mixing on scale-up, allowing the second reaction to produce additional undesired by-product.

$$\begin{aligned}Re &= ND^2\rho/\mu = (0.98\ m)^2(1.1\ s^{-1})(1000\ kg/m^3)/(0.001\ kg/m \cdot s) \\ &= 1\ 056\ 440\end{aligned}$$

Therefore,

$$N\tau_B = 5.4/N_p^{0.333}/(D/T)^2 \qquad \text{for } Re > 6400$$

$$\tau_B = 5.4/6^{0.333}/(1/3)^2/1.1\ s^{-1} = 24.3\ s$$

about 228 times the local mixing time at the impeller tip. Again, it is important to feed into the zone of maximum dissipation, close to the tip of the impeller blades.

Message: From the comparisons above, it is clear that τ_M and τ_B scale-up in the same way. It turns out that each is proportional to 1/N as long as geometry and the power per unit volume remain constant and the contribution due to the Batchelor scale mixing can be neglected. The key time scales for this problem are summarized in Table 13-2. Chemical reactions and their rates are scale-independent phenomena while the local mixing time is both scale and position dependent. Mixing effects get worse on scale-up.

Summary of Key Time Constants

- Reaction: $\tau_R = \dfrac{1}{k_{R2}C_{Bo}}$ (13-7)
- Lamellar diffusion: $\tau_L = \dfrac{\delta^2}{D_{AB}}$ (13-6)

Table 13-2 Summary of Time Scales in Example 13-2

Time	Small Scale	Large Scale
Reaction τ_R	0.14 s	Same
Corrsin–Batchelor micromixing term	0.0014 s	Same
Corrsin mesomixing term	0.0117 s	0.105 s
Corrsin mixing time τ_M	0.013 s	0.107 s
Blend time τ_B	2.7 s	24.3 s
Bourne engulfment τ_E	0.006 s	Same
N	9.97 rps	1.1 rps

- Kolmogorov or Batchelor time scale: $\tau_K = \left(\frac{\nu}{\varepsilon}\right)^{1/2}$ (13-11)
- Bourne engulfment time scale for micromixing: $\tau_E = 17\left(\frac{\nu}{\varepsilon}\right)^{1/2}$ (13-16)
- Baldyga and Bourne mesomixing time for dispersion of feed:

$$\tau_D = \frac{Q_B}{UD_t} \tag{13-18}$$

- Corrsin mesomixing time for disintegration of large eddies:

$$\tau_M = 2\left(\frac{L_s^2}{\varepsilon}\right)^{1/3} + \frac{1}{2}\left(\frac{\nu}{\varepsilon}\right)^{1/2} \ln(Sc) \tag{13-13}$$

13-2.1.4 Laminar Micromixing. Looking at the simple case of laminar mixing the initial feed of reactant appears as a blob which is then stretched by the laminar mixing action. The blob is still at its inlet concentration. Molecular diffusivity starts to spread the reactant out and reaction takes place at the interface. With progressive mixing the interface stretches increasing transfer area and reducing diffusion distance. There may also be an interchange of streamlines if a mixer is present. The growth and redistribution of streamlines is discussed in Chapter 3 on laminar flow and in the work of Ottino (1980). The process continues until all the controlling reactant is used up. A good example of this technique applied to a copolymerization is the work of Tosun (1997).

13-2.1.5 Turbulent Micromixing: Effect of High Viscosity. In a turbulent field a similar phenomenon happens when a blob of one reactant is distorted and diffusion and chemical reaction take place. The initial model of Bourne pictured a blob of reactant fluid that rapidly broke down to the smallest eddy size without much diffusion and reaction. The smallest eddy size is the Kolmogorov size, and at that size diffusion takes place via molecular diffusion [see eq. (13-15)]. Later, Bourne abandoned that model and went to an engulfment model based on

a concept of stretching lamellae and is believed to more accurately represent the turbulent process [eq. (13-16)].

Higher viscosity generally reduces the mixing rate at the same turbulence energy dissipation rate or power per unit mass. The mixing theory of Corrsin (1964) accounts for the effects of viscosity and molecular diffusivity on the time constant for local mixing, although the viscosity appears in the smaller term. The second term in his time constant equation is frequently an order of magnitude smaller that the first term. For instance, if viscosity is increased by a factor of 100, the impeller stream mixing time constant would be almost doubled for the 1 L vessel but would be little affected in the 20 000 L vessel, since in the latter, inertial mixing dominates completely.

A similar estimate of the effect of viscosity on local mixing rate can be obtained from the "engulfment" model of Baldyga and Bourne (1989). Their time constant, τ_E, for the final step of mixing, engulfment of unmixed fluid, $\tau_E = 17(\mu/\rho\varepsilon)^{1/2}$, shows that the mixing time constant increases in proportion to the square root of viscosity if turbulence energy dissipation rate and density are constant and engulfment rate (Batchelor scale mixing) is controlling.

From these time scales, it is clear that both the viscosity and the diffusivity affect mixing at the smallest scales. The Schmidt number,

$$\mathrm{Sc} = \frac{\mu}{\rho D_{AB}} = \frac{\nu}{D_{AB}} = \frac{\text{momentum diffusivity}}{\text{molecular diffusivity}} \tag{13-21}$$

defines limits for the different mechanisms as discussed in Chapter 2. For Schmidt numbers smaller than 4000, the turbulent engulfment model works (see Baldyga and Bourne, 1999, p. 576), while for larger numbers the mixing is by viscous stretching. Note that for low viscosity liquids such as water, the Schmidt number is on the order of 1000; for gases it is on the order of 1; and for viscous liquids or feeds at 1000 mPa · s it is on the order of 10^6. A large Sc value means that the smallest eddy dissipated by viscosity (the Kolmogorov scale eddies) will be much larger than the smallest concentration striations, which are dissipated by molecular diffusivity (the Batchelor scale striations).

13-2.1.6 Summary: Da_M. Given an estimate of reaction time and an estimate of the appropriate local mixing time constant, one can calculate Da_M and use Figure 13-2 and/or Figure 13-3 for an estimate of yield and selectivity. This is, however, based on the assumption that the local mixing time is constant as the initial blob moves away from the inlet position. In fact, there is a wide distribution of values of local mixing time constants, and the entering material moves through many different zones of varying energy dissipation. The distribution of energy dissipation in a reactor is thus very important. This explains the interest in laser Doppler anemometry and computational fluid dynamics.

This distribution of energy dissipation complicates any mathematical analysis immensely. It also explains why many modelers have gone to zone model analyses to predict the path of the reactants more accurately. In such models the

vessel is divided into a number of zones of different energy intensity where local mixing varies. An example of such a model developed by Patterson (1975) is discussed in Section 13-5. Other examples of contributions in this area are the papers by Bourne and Yu (1994) and Baldyga et al. (1995).

Often, a full analysis is not possible because of the lack of full kinetic data for all the steps. In such cases the scale-up protocols in Section 13-4.3 can be very useful. Running small scale experiments in which key parts of the local mixing rate are varied, including position, number of feed points, and rate of addition, can greatly aid in understanding any choice of final reactor design. In some cases the final reactor design is known, and then the local mixing time for the large scale can be estimated and experiments under similar time scales run on the small scale. This process is often called *scaling down*.

13-2.2 How Mixing Affects Reaction in Common Reactor Geometries

Although there are many reactor geometries in practice, discussion here is limited to four geometries where mixing is of particular interest: the pipe, Tee mixer, static mixer, and stirred tank. Figure 13-7 illustrates these geometries. The full range of stirred tank geometries and impellers is the subject of Chapter 6. A brief description of each geometry and the mixing issues particular to each is given below.

13-2.2.1 Pipes. The simplest mixed chemical reactor is a pipe with reactant injectors at one end. The reactants mix as they flow toward the outlet, forming a *tubular reactor*. There are two measures of mixing in a pipe: (1) the degree of uniformity of the average concentration in the radial direction, and (2) the mean square of the level of concentration fluctuations (referred to as *segregation*) at various locations across the pipe.

The perfect reactor analysis assumes that there is no radial distribution of concentration and the reaction occurs with time along a length with no radial effect. This reduces the analysis to a simple differential equation with time or, at constant velocity, with length. This is the ideal plug flow assumption. When there is only a single reactant, radial concentration gradients are small if the velocity profile is nearly flat, as in high Reynolds number turbulent flow. For multiple reactants it takes a finite time for them to achieve radial uniformity at the molecular scale where chemical reactions occur, so the ideal plug flow assumption does not hold and mixing rates must be considered.

Pipe reactors can be operated in laminar or turbulent flow. In *laminar flow* radial diffusivity is molecular only, which is very slow, particularly if the viscosity is high. In turbulent flow the radial fluctuating velocity component produces the radial turbulent diffusivity which is much faster than molecular diffusivity. Many devices have been developed to promote fast radial mixing in laminar flow, such as static mixers, which are discussed below and in Chapter 7. Besides static mixers, a number of methods exist to promote faster radial mixing in *turbulent flow*, since even in turbulent flow it takes 50 to 100 pipe diameters to achieve

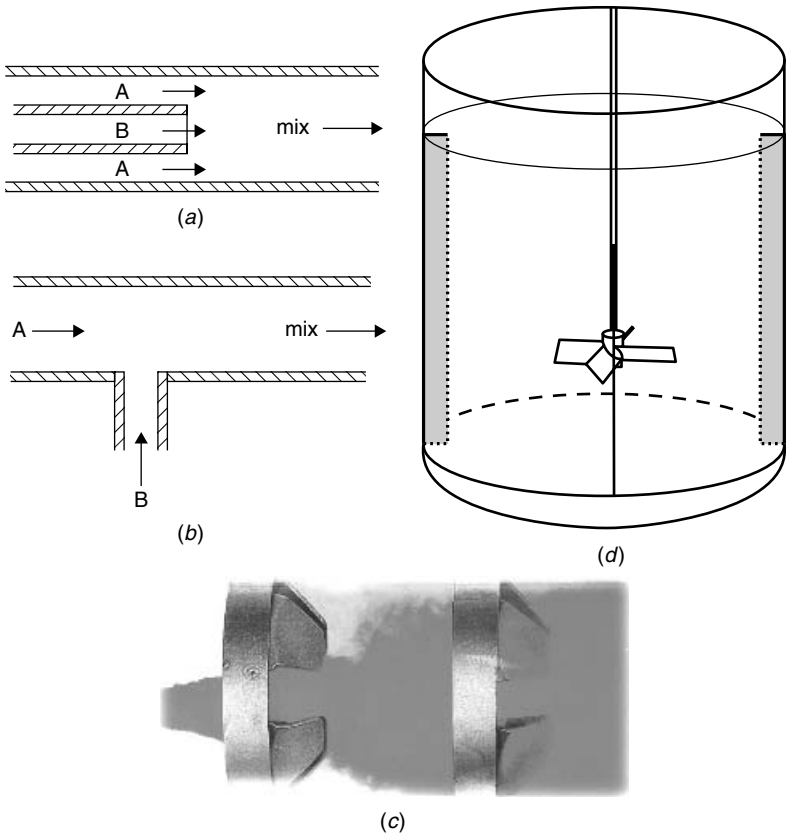

Figure 13-7 Various mixing geometries used for chemical reactors: (*a*) co-axial jet and (*b*) Tee mixing in a pipe, (*c*) static mixer, and (*d*) stirred tank.

mixing to 95% uniformity if one reactant is injected into the centerline of the pipe. Mixing in pipes is discussed in more detail in Chapter 7.

13-2.2.2 Tee Mixers. To shorten the mixing length of a pipe reactor, one variation is the tee mixer. Tee mixers can shorten the length for blending to 95% uniformity to three to five pipe diameters. The tee mixer is a simple version of the pipe reactor in which one reactant is injected into a flow of the other reactant by a side-entering flow. Care must be taken, however, to prevent the injected reactant from staying adjacent to the pipe wall and not mixing with the flowing stream as expected. This is particularly true for laminar flow and high viscosity, as shown by Forney et al. (1996).

Another type of tee mixer involves opposing flows of reactants with outflow through the side exit into a mixing pipe. One example is the impinging jet reactor used in reaction injection molding technology. The Tee mixer, which is frequently used for liquid-phase reactions, is easier to construct and maintain

than the multiport injector or the coaxial flow injector frequently used for rapid gas phase reactions such as combustion. The downstream mixing pipe for a tee mixer is again considered to be a tubular reactor.

13-2.2.3 Static Mixers. Strictly stated, pipe and tee mixers are static mixers since there are no moving parts within them. The term *static mixer*, however, is more frequently associated with pipes containing internal flow diverters and obstacles that promote mixing. Two common types are the twisted-ribbon mixer (Kenics KM) and the structured-packing mixer, one of which makes use of layers of criss-crossed corrugations (Koch-Sulzer SMV). Another structured packing static mixer is the overlapping lattice type (Koch-Sulzer SMX). Details of the construction and operation of various types of static mixers are given in Chapter 7 and additional examples of operation in Examples 13-3, 13-6, and 13-8a below.

13-2.2.4 Stirred Tanks. There is a large variety of stirred-vessel reactor types. They range from laminar regime mixing for bulk polymerization or fermentation to highly turbulent mixing for promotion of high yields in competitive reaction synthesis schemes. They cover batch, semibatch (or fed-batch), and continuous flow reactors. They can be single-phase liquid, liquid with suspended solids (usually catalysts, but sometimes reactants or products), liquid with sparged gas reactants, liquid with vaporizing products (boiling reactors), liquid with immiscible suspended liquid droplets, or three-phase reactors. The stirred-vessel reactors can be nearly isothermal or highly exothermic or endothermic. Stirred-vessel reactors can range in size from 0.004 m^3 to 10 m^3 (a gallon or two to thousands of gallons) may require glass or other special surface treatments to inhibit corrosion, and require a variety of impeller types to achieve success in all the uses above. Mixing issues for all of these types of contacting are discussed in the appropriate chapters of this book and in examples of reactions throughout this chapter. Typical values for the maximum local energy dissipation in selected geometries are given in Table 13-3.

13-2.3 Mixing Issues Associated with Batch, Semibatch, and Continuous Operation

13-2.3.1 Batch Operation. Pure batch operation is actually a rare application since something must trigger a chemical reaction to proceed, usually the addition of a reactant, catalyst, or heat. If the chemical reaction is fast enough to proceed during the addition of a chemical reactant or a catalyst, the mode is actually semibatch, and mixing effects may be present. If the chemical reaction is so slow that the times needed for the addition of reactants and/or catalyst and for mixing are negligible compared to reaction time, mixing rate is not likely to be a factor in chemical yield. If a threshold temperature must be reached through heating, mixing rate is again unlikely to be a controlling factor, because heating is usually much slower than mixing. Pure batch reactors are, therefore, not generally considered to be affected by mixing rate, with the exception of heterogeneous

Table 13-3 Maximum Energy Dissipation in Various Geometries

Stirred Tanks

Impeller[a]	D/T	C/T	2r/D (Axial) or 2z/W (RT)	$\frac{\varepsilon_{max}}{P/\rho V_{tank}}$	$\frac{\varepsilon_{bulk}}{P/\rho V_{tank}}$	Source[b]
RT	0.33	0.5	0.50	21	0.9	1
RT	0.5	0.5	0.0	21	0.5	2
RT	0.33	0.33	0.0	48	0.7	2
PBT-6U	0.33	–	–	37	0.7	3
PBT-4U	0.5	0.5	1.15	18	0.6	2
PBT-4U	0.33	0.33	0.85	37	0.7	2
A310	0.55	0.5	0.68	19	0.4	2
A310	0.35	0.25	0.85	40	0.7	2
HE3	0.5	0.5	0.85	27	0.3	2
HE3	0.33	0.33	0.80	99	0.3	2

Other Geometries

Pipe mixing	$\overline{\varepsilon} = (\Delta P V_S)/\rho L$, where V_S is the superficial velocity. See Chapter 7 for calculation of $\Delta P/L$ for static mixers and other pipeline devices
Gas–liquid devices	See Tables 13-7 and 11-3
Liquid–liquid devices	See Figure 12-11

[a] Fully baffled with four rectangular T/10 baffles, flat-bottomed tanks at fully turbulent Reynolds numbers ($Re > 2 \times 10^4$). Tank diameters are 0.24 m, with traverses taken within 2 mm of the impeller blades. All fluctuations are included unless otherwise noted. Data cited are a small selection of data available in the literature.

[b] 1, Wu and Patterson (1989); blade passage fluctuations removed; 2, Zhou and Kresta (1996); 3, Medek (1980).

reactions, including (1) dissolving solid reactants and (2) two liquid-phase reactions when the reaction rate could be limited by the dissolution rate and the interfacial area, respectively.

13-2.3.2 Semibatch Operation. Semibatch reactors, also referred to as fed-batch, are very common in the specialty chemical and pharmaceutical manufacturing industries. Semibatch operations are typically carried out in a more-or-less standard type of stirred mixing vessel in both homogeneous and heterogeneous applications, although special provision is often required for fast and/or heterogeneous reactions (see examples in Section 13-3). Their use is very flexible in that they can be quickly reconfigured for various types of chemical reactions needed in a series of chemical synthesis steps (see Chapter 17). The key step of blending in semibatch operation is addressed in Chapter 9. Often, by feeding a particularly reactive reagent later or slower and in a region of high energy dissipation, the reactions can be forced along a more desirable path, producing a better yield of desired products. This is particularly true of consecutive-competitive reactions as discussed below.

13-2.3.3 Continuous Flow Operation. Continuous flow mixed reactors are most common in high-capacity processing operations. Continuous flow reactions may be carried out in all the geometries discussed above: pipe and tee mixers, static mixers and other types of in-line mixers, and many types of stirred vessel. Sizes of such reactors range from very small tee mixer reactors on the scale of 1 cm to stirred vessels holding thousands of liters of liquid with impellers in the range of 3 m or more in diameter. Yields for very small continuous reactors may be studied in a pilot unit and applied directly to the plant, but yields for the very large reactors represent a severe design problem if the reactions are very mixing-rate sensitive. These and the semibatch reactors discussed above bring major scale-up problems, even for single-phase chemical reactions. In both continuous flow and semibatch reactors, feed location and local turbulence intensity have a major effect on yield. Multiple-phase chemical reactions cause even more complex scale-up problems, particularly if the mass transfer rate effects are compounded by chemical reaction yield effects in the reaction phase.

Continuous and semicontinuous flow reactors are sometimes used in fine chemical and pharmaceutical applications, primarily because some reactions require the high intensity of mixing that can only be achieved in in-line mixers (see Examples 13-3, 13-7, and 13-8a and discussion in Chapter 17).

An important question for the design of continuous flow systems is: When can the classic perfectly mixed assumption (ideal CSTR) be used in a continuous flow stirred tank reactor? The blend time concept can be used here. If the blend time is small compared to the residence time in the reactor, the reactor can be considered to be well mixed. That is because the residence time is proportional to the characteristic chemical reaction time. A 1 : 10 ratio of blend time to reaction time is often used, but often, larger values result because the mixer must do other jobs, which lead to even smaller blend times. Frequently, residence time distributions are used to determine whether a reactor is well-mixed. It is usually easy to achieve well-mixed conditions in continuous flow, turbulent stirred vessels unless the reactions are very fast, such as acid–base neutralizations. Even in laminar systems the blend time can be made much less than the required residence time for the chemical reaction mainly because required residence times are so long for high viscosity reactants. For discussions of residence time distribution analysis, see Chapter 1, Levenspiel (1972), and Nauman (1982).

In Chapter 9 it is suggested that if the batch blending time is less than one-tenth the residence time and the inlet and outlet are separated in such a way that a line drawn from the inlet to the outlet passes through the impeller, fully back mixed conditions will be achieved. Even in the case of a perfectly backmixed vessel, mixing effects on selectivity must also be checked.

13-2.4 Effects of Feed Point, Feed Injection Velocity, and Diameter

One of the most important concepts that comes from the micromixing theory is the importance of addition position for selectivity in competitive-consecutive homogeneous reactions. In Chapter 2 it was shown that there is a wide range

of turbulent length scales and intensities in a stirred tank. The effect of position on mixing selectivity has been shown by a number of researchers, and several methods have been used to demonstrate this effect. A CFD simulation of this effect is included on the Visual Mixing CD affixed to the back cover of the book.

Nienow and Inoue (1993) gave an interesting set of examples using a small tank and the semibatch barium sulfate method of Villermaux to demonstrate the importance of feed position, as shown in Figure 13-8. In all cases the mixer speed and rate of addition were held constant; only the position of addition was changed. All vessels were at about the same power per unit tank volume. The selectivity given is that of unwanted by-product. High numbers mean that more by-product was formed.

Tank 1 was agitated by a radial turbine. The turbulence levels in the tank vary with position, and so does the local mixing rate leading to different by-product selectivities for different feed locations. At the high intensity region just entering the flow through the impeller or near the impeller tips, the turbulence is high and the by-product formation is low. At the top surface where turbulence levels are very low, the by-product selectivity is very high. Similarly, at the vessel bottom the by-product selectivity is poor. The radial impeller located off bottom delivers little turbulence to the bottom.

In tank 2, an axial down-pumping impeller is used. Again, feed at the surface has the most by-product formation, and feed in the impeller gives the best result. For the axial impeller, the feed position at the bottom of the tank is not bad because the impeller is delivering turbulence at that position in contrast with the radial impeller where the bottom has very high by-product selectivity.

Tank 3 is unbaffled. Near the impeller there is high turbulence and low by-product selectivity results. The surface and throat of the vortex with its rotational motion and poor incorporation have very high by-product formation.

Generally, the fastest, most immediate mixing of feeds or of a feed with resident fluid occurs when the feed is introduced into the region with the shortest local mixing time constant, or the most intense turbulence, whether in a pipe

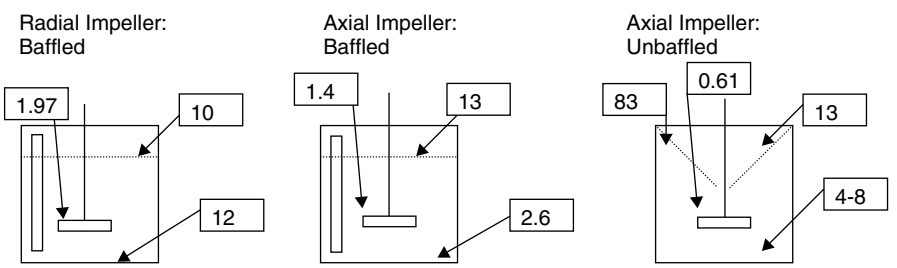

Figure 13-8 Impact of different feed positions on the precipitation of barium sulfate. The selectivity to by-product as percent of reactant is shown for feed into zones of high and low turbulent energy dissipation. The impeller speed and reactant addition time were held constant. More by-product is formed at feed points where the local mixing is slow.

mixer, a static mixer, or a stirred tank. For instance, in a stirred tank the region with the fastest mixing is in or near the impeller discharge flow. The rate of turbulence energy dissipation is greatest and the scale of mixing is smallest in that region. For feed in other regions of a vessel, especially on the top liquid surface, the exposure of high fed reactant B concentrations at reduced mixing intensity can result in the most dramatic reduction in selectivity and increase in by-product formation.

Experimental measurements of yield and selectivity as a function of feed location have borne out the ideas expressed above (see Paul and Treybal, 1971; Bourne et al., 1981; Bourne and Rohani, 1983; Bourne and Dell'Ava, 1987; Baldyga and Bourne, 1990; Bourne and Yu, 1994; Baldyga et al., 1997).

Tipnis et al. (1994) investigated experimentally the scale-up of a competitive-parallel chemical reaction (the third Bourne reaction; see Section 13-2.5) in stirred vessels of 2.15, 20, 178, and 600 L. The vessels were geometrically similar, with two feed positions in each. The impellers were all six-blade disk turbines with $D/T = \frac{1}{3}$. The feed points were at two distances (G/T of 0.33 and 1.33) above the impellers near the impeller shaft. The chemical reaction rates at 298 K were as follows:

$$\mathrm{NaOH + HCl \rightarrow NaCl + H_2O} \qquad k_{R1} = 1.3 \times 10^{11}\ \mathrm{L/g\text{-}mol \cdot s}$$

$$\mathrm{NaOH + CH_2ClCOOC_2H_5 \rightarrow CH_2ClCOONa + C_2H_5OH} \qquad k_{R2} = 700\ \mathrm{L/g\text{-}mol \cdot s}$$

For these conditions they found that equal blend time, which implies equal impeller rotational speed, N, gave nearly equal yields of C_2H_5OH for all scales at each of the two feed locations. Plots of yield versus blend time up to 30 s for all scales gave nearly identical curves with little effect of feed concentration. Feed pipe backmixing (see Section 13-4.1.4) was not an issue since v_f/v_t was relatively high. Both injection locations are in zones of relatively low turbulence, close to the impeller shaft. The implication is that tank blending rate ($\propto N$) is more important than local mixing rate [$\propto (\varepsilon/\nu)^{1/2}$] for these competitive-parallel reactions with a nearly instantaneous first reaction. This is an example of mesomixing (see Section 13-2.1).

Constant blend time scale-up, however, leads to prohibitively high power requirements at large scale. Tipnis et al. (1994) recommended the use of a static mixer in a pump-around loop to reduce the total power requirement for these competitive-parallel reactions. This shows that high-energy intensities for a short time are a better way to distribute the energy than trying to generate a high intensity in a large tank. All the turbulence energy is focused on mixing a small volume in the confined space of the static mixer. See also Example 13-8a, in which essentially no significant yield of product could be achieved in a vessel, whereas the mixing capability of a static mixer resulted in satisfactory performance.

13-2.5 Mixing-Sensitive Homogeneous Reactions

Laboratory studies of mixing-sensitive homogeneous reactions have been done by many investigators using the four reactions that have become known as the *Bourne reactions*, developed through work by Bourne and co-workers (numerous references), and the reaction of iodine with tyrosine, first used by Paul and Treybal (1971). These studies and others fleshed out the previous theoretical predictions and established the experimental grounds for their confirmation. These experimental results have provided input for many modeling studies, some of which are discussed in Section 13-5. The reactions have been used by many investigators to study the mixing characteristics of stirred vessels in various configurations, including scale-up studies, as well as several types of in-line mixers.

The four Bourne reactions are as follows:

1. Diazo coupling between 1-naphthol and diazotized sulfanilic acid
2. Simultaneous diazo coupling between 1- and 2-naphthols and diazotized sulfanilic acid
3. Competitive neutralization of hydrochloric acid and alkaline hydrolysis of monochloroacetate esters with sodium hydroxide
4. Competitive neutralization of sodium hydroxide and acid hydrolysis of 2,2-dimethoxypropane with hydrochloric acid

Some of the key features of these reactions are summarized in Table 13-4. A case study from an industrial application follows.

Example 13-3: Development of a Mixing-Sensitive Homogeneous Reaction. You are a process development engineer with laboratory and pilot plant facilities available for experimentation and gathering data for scale-up to manufacturing. Your current assignment is to develop a manufacturing process for a reaction that is now being run in flasks by chemists. The reaction is known to be competitive-consecutive:

$$A + B \rightarrow R + S1 + S2 + \text{higher MWs}$$

where R is the desired product and S1, S2, and higher MWs are overreaction products that both consume starting material, causing yield loss, and also react in the subsequent step to cause further yield loss. Separation before the subsequent steps is not feasible. The chemistry is shown in Figure 13-9.

Q: What do you want to know from the chemists before starting developmental studies and experiments?

A: Laboratory procedure and apparatus used; yield of R and analysis of other products.

Procedure: The chemists added B to A in a 1 L flask with good mixing with a paddle impeller. They made the addition in 1 min to minimize overreaction to S's. There is no significant exotherm. They obtained a yield to R of 90% using a B/A molar ratio of 1.0. Overreaction products were S1 = 5% and S2 = 2% with higher MWs not measurable. The A remaining was 5%.

Table 13-4 Bourne Reactions

Practical Range of $\tau_{rxn} = 1/k_2C_{Bo}$ from 20 to 35°C, $\alpha = 1$ ms	Practical Range of Energy Dissipation, ε = W/kg	Relative Ease of Use	Reagent Stability	Material Balance Close?	Method of Analysis	Oral Toxicity LD_{50} (g/kg rat)	Reagents per m^3 Solution at 350 ms	Waste Stream
Competitive Consecutive								
First: 1-naphthol with diazotized sulfanilic acid (Bourne et al., 1990)								
65–5000	Up to 400	Difficult	Marginal	No (>95%)	UV multicomponent	2	150	<1 wt % dyes; water
Competitive Consecutive and Competitive								
Second: 1- and 2-naphthol with diazotized sulfanilic acid (Bourne et al., 1992)								
30–5000	Up to 10^5	Difficult	Marginal	No (>95%)	UV multiparameter	2	150	<1 wt % dyes; water
Competitive (Parallel) Reaction								
Third (a): Base hydrolysis of ethylchloroacetate vs. HCl (Bourne and Yu, 1994)								
350–9000	Up to 1	Good	Marginal 4% in 30 min at 32°C and 130 mM starting soln.	Yes (>99%)	G.C. single component	0.2	550	<1% NaCl–acetate; <1% alcohol; salts; water
Third (b): Base hydrolysis of methylchloroacetate vs. HCl (Bourne and Yu, 1994)								
200–5000	Up to 10	Good	Marginal	Yes (>99%)	G.C. single component	0.2	550	<1% NaCl–acetate; <1% alcohol; salts; water
Fourth: Acid hydrolysis of 2,2-dimethoxypropane vs. NaOH (Baldyga et al., 1998)								
1–2000	$1–10^6$	Excellent	Excellent <0.6%/day at 25°C and 200 mM DMP	Yes (>99%)	G.C. single parameter linear regression	1	180	25% EtOH; <5% MeOH–acetone; salts; water

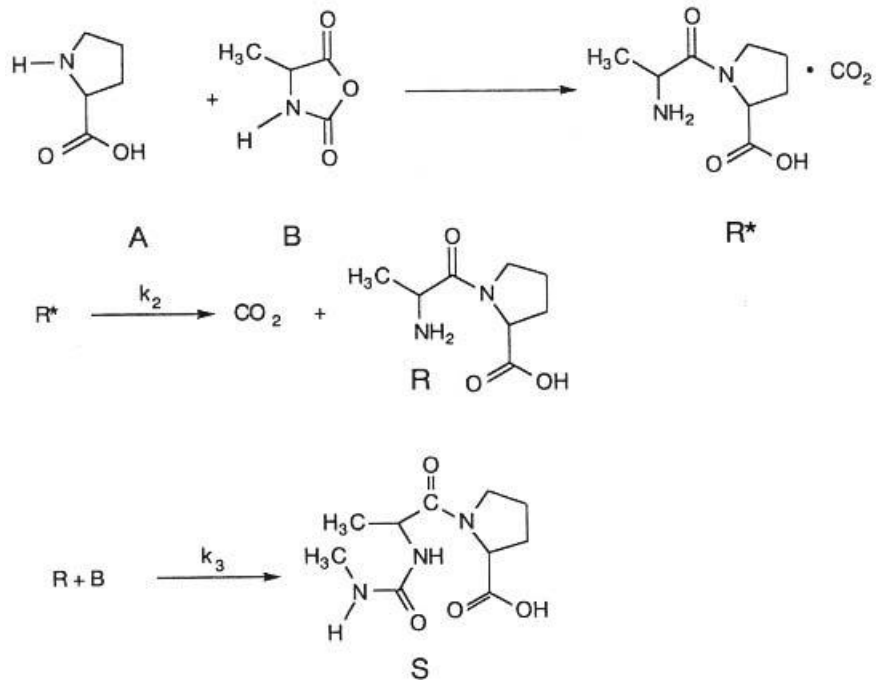

Figure 13-9 Coupling reaction of L-alanyl-L-proline: chemistry of the consecutive-competitive reaction.

Q: What experiments do you run before the pilot plant trials? What were the results?

A: As time and starting material supplies permit, some runs in a 4 L cylindrical vessel with a fully baffled 6 cm. Rushton turbine at two speeds with two addition points and two rates of addition (Table 13-5).

Time did not permit completion of all the experiments. These results indicate mixing sensitivity, as noted by the improved yield at higher speed, matching the chemists' results. At this scale, however, it is noted that the yield differences are not large, so pilot scale operation can be started (material is needed for further studies).

Q: What vessel and mixing system would you select for the pilot pant study? What results were obtained?

Table 13-5

Speed (rpm)	Addition Point	Feed Time (s)	k (m^2/s^2)	ε (m^2/s^3)	$\tau_M = 1.1k/\varepsilon$ (s)	P/V (W/m^3)	R (%)	S (%)
200	Surface	60	0.0052	0.031	0.18	38	82	12
400	Impeller	60	0.021	0.25	0.09	304	90	7

Table 13-6

Speed (rpm)	Addition Point	Feed Time (s)	k (m^2/s^2)	ε (m^2/s^3)	τ_M (s)	P/V (W/m^3)	R (%)	S (%)
100	Surface	1000	0.0172	0.0527	0.347	77	80	15
150	Impeller	60	0.179	3.57	0.075	260	86	10
150	Impeller	1000	0.179	3.57	0.075	260	80	13

A: A fully baffled 200 L vessel with a 22 cm Rushton turbine. Addition points are on the surface and into the impeller discharge stream (Table 13-6).

These results continue to indicate mixing sensitivity, indicating that extreme caution must be taken on scale-up to manufacturing. The effect of addition time is not as expected for a classic consecutive-competitive reaction system, suggesting that the reaction pathway contains a step that requires maintaining short addition time on scale-up.

Note: This kind of unexplained difference in result is not uncommon, and in many cases, time does not permit finding the exact cause as long as the negative effect can be overcome by effective design.

Q: What vessel and mixing system would you specify for manufacturing that would achieve laboratory results?

A: The production requirements for this step of a multistep process require a 10 m^3 (10 000 L) stirred tank. The sensitivity to mixing experienced in the experiments above indicates that scale-up to this size vessel may not be feasible to obtain expected yield. The complication of the unexpected sensitivity to addition time further indicates that an alternative design is indicated.

Alternatives to be considered:

- Multiple injection points in the tank
- Rapid recycle loop on a standard reactor for addition into the high-shear zone
- In-line mixer device in semicontinuous operation

In-line premixing of the reactants with a static mixer was selected since this method of operation was compatible with the overall process design, and the mixing intensity required could be expected at the size and throughput required.

Solution: A static mixer was developed successfully for production scale operation, as shown schematically in Figure 13-10. The mixer chosen was a static mixer with an L/D ratio of 4. The nominal residence time of the combined two-liquid-phase stream was 1 s. The Reynolds number in the mixer was 2000 based on empty tube diameter. The reactant mole ratio was 0.95 to 1.0 mol B/A.

Results for the static mixer in both laboratory scale 0.008 m (0.8 cm) and plant scale 0.0254 m (2.54 cm) operation were excellent. No change in selectivity or product distribution occurred over this scale-up. When there are compelling reasons to use a semibatch reactor instead of a semicontinuous system, the reactor

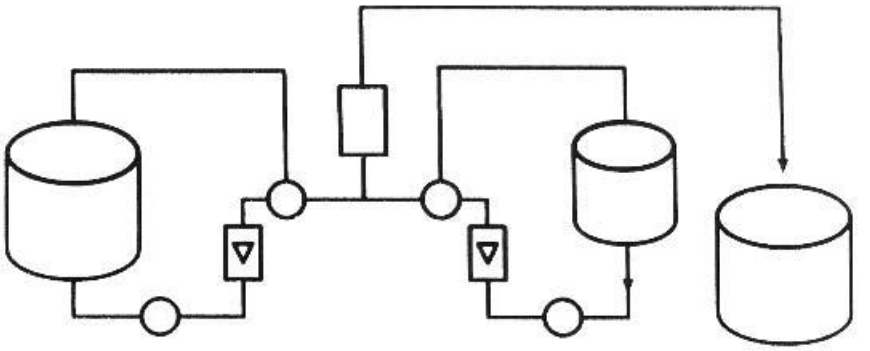

Figure 13-10 In-line mixer for the L-alanyl-L-proline reaction: developed to maintain expected yield on scale-up to full scale. The pilot plant scale showed a drop in yield from the bench scale results. Intense local mixing is required.

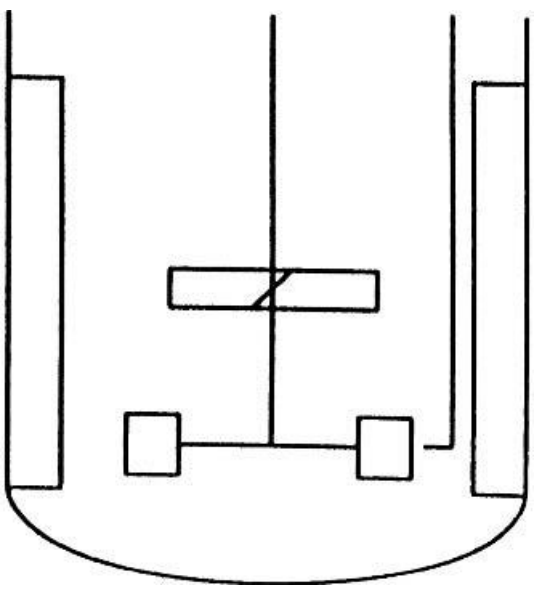

Figure 13-11 Mixing configuration for semibatch reactors for mixing-sensitive reactions when in-line reaction systems are not viable. Note the feed directly into the region of highest turbulence and the second impeller used to maintain turbulence and flow in the top third of the tank.

shown in Figure 13-11 with dual turbines and a properly located subsurface addition line can provide the best scale-up opportunity to achieve expected selectivity for a fast, complex reaction.

Message: This example shows that such a reaction system requires feed addition directly into the fast-mixing zone to achieve maximum selectivity and to

maintain that selectivity upon scale-up. The mixing intensity of a stirred vessel in semibatch operation was believed to be too low to maintain selectivity on scale-up. A static mixer was developed that achieved the required selectivity.

The increased local energy dissipation rate of the static mixer over the impeller region of a stirred tank is the key to this scale-up. Although not measured quantitatively in this system, the mixing literature (see Chapter 7 for static mixers, Chapter 12 and Table 8-1 for liquid–liquid dispersion devices, Table 13-9 for gas–liquid dispersion equipment, and Table 13-3 for stirred tanks) provides information that allows choices to be made. The effectiveness of the equipment can then be verified experimentally.

The change in selectivity on initial scale-up from the laboratory to a pilot plant vessel showed that mixing was a key issue without prior quantitative determination of rate constants, a step that is often not feasible in the time available.

13-2.6 Simple Guidelines

The concepts of micromixing and mesomixing can be reduced to a set of simple guidelines. For fast reactions having time scales of seconds and tens of seconds:

- Always add the ingredients to the point of highest turbulence. Avoid adding to the surface, a point of low turbulence.
- Scale-up and scale-down based on constant power per unit volume or mass. Even then there can be a loss of yield or by-product selectivity on scale-up.
- Consider using smaller reactors with higher energy dissipation rates, such as in-line mixers in recirculation loops.
- Consider diluting the incoming reagents.
- Question the size of the reactor.
- If experiments show a possibility of mixing reaction interactions and the rate of addition is important, consider multiple point injections. The feed time will have to be increased in large scale equipment.

13-3 MIXING AND TRANSPORT EFFECTS IN HETEROGENEOUS CHEMICAL REACTORS

When chemical reactors have more than one phase, the problem increases in complexity because the reaction and mass transfer processes interact. The interaction is governed by the relative rates of the reaction and mass transfer. In some cases, chemical reactions are mass transfer rate controlled (very fast chemical reactions) and in others they are reaction kinetics controlled (very slow chemical reactions); however, in reality very few reactions strictly fit this classification. To understand the complex interactions and the various variables involved, the following simplified discussion and equations may be useful in explaining certain topics of interest and the relations between key variables. Thorough discussions of this

problem are given by Astarita (1967), Cichy and Russell (1969), and Schaftlein and Russell (1968).

For simplicity we assume a single reactant entering in one phase and reacting in the other. Examples are a gaseous reactant passing as bubbles through an agitated liquid in a tank, a solid powdered reactant being added to a liquid, and even two liquid phases, one dispersed in the other. The reactant that is being transferred we will call B. Initially, there is no B in the liquid. A further simplification will be to consider a gas phase as containing the reactant.

The general mass balance on B in the continuous liquid in units of moles per time is

mass transfer rate	reaction rate	flow out	accumulation	
$k_L a' \Phi V(C_B^* - C_B)$	$-rV$	$-Q_L C_B$	$= V\dfrac{dC_B}{dt}$	(13-22)

In a steady-state batch liquid vessel, dC_A/dt and Q_L are zero and the mass transfer rate equals the reaction rate. All other cases are more complicated.

First consider the terms making up the mass transfer rate.

- **k_L** The first term is the overall mass transfer coefficient k_L. This is the reciprocal of the mass transfer resistance. This development is based on the film theory concept of mass transfer and consists of resistances in series: the resistance of the gas film (usually negligible), the resistance of the liquid film (the most important), and the resistance of any contaminant layer between the phases, such as solids or a surfactant. Again for simplicity we assume that all resistance is in the liquid phase. The variable k_L is most dependent on the chemistry of the fluids. It can be estimated from surface renewal theory and related to molecular diffusivity and dispersed phase bubble or drop or particle size. In addition, the liquid film coefficient can be increased due to rapid reactions which effectively thin the diffusion layer. This is discussed below. k_L estimates are often not reliable and are usually obtained by experiment in well-understood geometries.
- **a'** This is the area per unit volume of a bubble. Actually, it is an average of the total surface area over the total bubble volume. Thus, it can be written as 6/d, where d is the average bubble or drop or particle size. In Chapter 11 there are several correlations for this value based on a large variety of experiments. The average drop size is the result of the combination of drop or bubble breakup and coalescence. Breakup is determined by fluid forces and the surface or interfacial tension-resisting force. Coalescence is controlled by various physiochemical effects, such as double layers and the presence of surface-active agents. For example, coalescing systems such as air and water will have a certain bubble size under a given set of agitation conditions. The addition of small amounts of salt will decrease coalescence and make smaller drops, giving larger holdups and increased mass transfer. Addition of surfactants will also reduce bubble size and increase holdup,

but the extra film resistance often balances this effect, leading to no increase in mass transfer rate.

- **Φ** This is the holdup as a volume fraction of fluid in the vessel. It is the volume of dispersed phase (e.g., gas) in the vessel divided by the total volume. This is a variable strongly affected by the mixing conditions. In Chapter 11 there are several correlations for this variable. Holdup (Φ) times a' gives total mass transfer surface area per unit vessel volume, which is often called a. Thus, one often sees correlations of $k_L a$ versus mixing parameters. It should always be remembered that this value contains implicitly the holdup and the bubble size. One way to think of holdup is as the ratio of the superficial gas velocity to the bubble rise velocity. This comes from a simplistic picture of the motion of the gas phase:

$$Q_G = Av_s = A\Phi v_r \tag{13-23}$$

where A is the cross-section of the vessel, v_s is the superficial gas velocity, and v_r is the effective rise velocity of the gas.

The advantage of this concept is that it shows the strong effect to be expected of the gas superficial velocity on mass transfer. This is certainly found experimentally. Assuming a typical rise velocity of gas bubbles of 0.3 m/s, it gives a crude estimate of holdup. As gas volume fraction increases, hindered rising and bubble swarms break down this simple relation. This relation also shows that a decrease in bubble size which leads to more surface area, and slower rise velocity results in more holdup.

Bubble size, holdup, rise velocity, and area per unit volume are all tied together in a complex way.

- **C_B^*** This is the saturated concentration of B in the liquid in equilibrium with the other phase (e.g., the gas phase). This relation is a thermodynamic property (such as a Henry's law coefficient) and is affected only by pressure and temperature, not by fluid dynamics or mixing.
- **C_B** This is the concentration of B in the liquid phase. This is the variable that is most affected by the transport and reaction rates. We return to this below.
- **r** This is the reaction rate and for a simple reaction could be expressed as $k_R C_B$. However, there is no necessity to use such simple forms. In most cases the reaction rate will depend on the concentration of the transferred ingredient in the liquid/continuous phase.
- **Q_L** This is the flow rate of liquid phase from the vessel. It can be zero in semibatch operation.

Now consider the effect of reaction rate. For a given design all the other variables are fixed except C_B. For a fast reaction rate the maximum mass transfer rate will occur when C_B is zero. This condition is sometimes called *mass transfer*

control because the reaction rate is fixed by mass transfer limitations. Such terminology often creates confusion. C_B cannot be zero but only small compared to the saturation concentration C_B^*. It must be finite for there to be any reaction. One can think of the reaction rate being limited by the rate of mass transfer. In this case it is quite likely that the mass transfer rate will be enhanced by the reaction, and the mass transfer rate with reaction will be faster than without reaction.

If the reaction rate is very slow, the concentration difference between C_B^* and C_B grows closer. In the limit, C_B is equal to C_B^* and the maximum reaction rate is obtained at the saturation composition. It almost all cases it is assumed that the continuous or liquid phase is well mixed, so that no gradients exist. This is true in most equipment because the blend time is usually small compared to the mass transfer time. This means that C_B is the same at all places in the vessel.

There is another equation to consider: the reactant balance in the gas (mol/time):

$$Q_G(Y_{Bo} - Y_{Bi})K_H - k_L aV(C_B^* - C_B) = \frac{\Phi V\, d(K_H Y_B)}{dt} \tag{13-24}$$

where Q_G is the volumetric flow rate of the gas (m^3/s), or more generally of the dispersed phase; Y_{Bo}, and Y_{Bi} are the outlet and inlet mole fractions of B in the gas phase; ΦV is the volume of the dispersed phase (e.g., the gas); K_H is the Henry's law constant, relating C_B and Y_B [$(mol/m^3)/(mole\ fraction)$]. Thus, the value of C_B depends on what goes on in the second phase, but this equation shows a problem. With what concentration in the gas phase is C_B^* associated? For a continuous gas flow ($dC_B/dt = 0.0$) there are several choices. If the gas is backmixed so that the volume ΦV is all of the same composition, Y_B is given by the outlet composition Y_{Bo}. If the gas phase is not backmixed and has gradients in it, an average of the inlet and outlet concentrations needs to be used. This can often be a simple average. A log mean concentration difference can be used if the approach is close, as in heat transfer. Now we may need to know something about the residence time distribution of the gas or other second phase, even if it is dispersed.

In many mass transfer operations the effect of gas phase residence time distribution is neglected. In fermentations and in wastewater aeration systems, a 15% consumption of the oxygen from the inlet air is on the high side. This translates to going from 21% oxygen to 18% at the outlet. If the air is backmixed, the gas phase composition in equilibrium with the liquid would be based on 18% oxygen. If a simple plug flow assumption is made instead, the composition only rises to 19.5%. This is a minor effect.

When chemical reactions such as organic oxidations are present, more of the reactant is often removed from the gas phase. In organic oxidations it is not uncommon to have exit oxygen composition as low as 3%. This is because of the fast reactions and also for safety reasons. The well-mixed composition would then be 3% and the plug flow average would be 12%. This leads to a factor of 4 difference when estimating the composition in the liquid. Gas phase residence

time distributions are thus of more interest when reaction and mass transfer interact. This is discussed in Section 13-3.4.

Time Constants. If the transport equation were a bit simpler, one could treat reaction with mass transfer as a process of rates in series, such as heat or mass transfer. One could compare half-times of reaction with inverse mass transfer coefficients and even include mixing times as a rate constant. Although an interesting thought, it is hardly ever done.

Some time constants that have been used are

- $\Phi V/Q_G$ is the gas residence time.
- $(1 - \Phi)V/Q_L$ is the liquid residence time.
- $C_B^* V/r$ is a measure of how long the reactor can coast without mass transfer. It applies when the full liquid volume is saturated, and then the gas is suddenly turned off.

For second phases other than gas, the relations are much simpler. For liquid–liquid and liquid–solid systems both phases are usually considered backmixed. Note that there is still holdup and it may not be the inlet volume fraction that is often assumed.

13-3.1 Classification of Reactivity in Heterogeneous Reactions

Astarita (1967), Levenspiel (1972), and Doraiswamy and Sharma (1984) describe an effective framework in which to evaluate the relative contributions of mass transfer and reaction kinetics in heterogeneous systems. This classification is as follows.

- *Regime 1: very slow reactions*. Reaction rates are much slower than the mass transfer rate, so that reaction follows homogeneous kinetics and the reactions are not affected by the mixing and mass transfer rates. The reactants are supplied to the reacting zone at the expected molar ratio, resulting in no departure in conversion or selectivity from that predicted by the reaction rate constants and their ratio. Mixing would not affect the reaction, assuming that the reagents are blended. Only very poor bulk or macromixing (i.e., solids settled on the bottom or large dispersed phase drop size) could result in slow conversion.
- *Regime 2: slow reactions*. The reaction rate is fast enough that significant reaction occurs in the film between the reactants, but the consecutive or competing reactions are slow relative to the primary reaction. In this case, the conversion rate would be slower than expected, but selectivity would be unaffected.
- *Regimes 3 and 4: fast and very fast reactions*. These regimes are combined for purposes of this simplified discussion, although Doraiswamy and Sharma (1984) treat several subsets within these regimes as a function of relative reaction and mass transfer rates. In all cases in these regimes, both

conversion rate and selectivity are affected by mixing and reactor design. In most cases, selectivity is reduced by a restricted supply of reagents in and through the films between the phases. However, selectivity can be improved significantly by manipulation of the interfacial conditions. Mixing design and scale-up are critical to successful performance in manufacturing for these regimes.

The classification system by Doraiswamy and Sharma was treated quantitatively for gas–liquid systems by Middleton (1992), as summarized in Chapter 11 and Section 13-3.4. Middleton describes five regimes instead of four, but in general the classifications are similar. Deviations in the case of homogeneous reactions are more amenable to quantitative analysis and can therefore be developed more completely. The same local considerations developed in Section 13-2 for homogeneous reactions apply for heterogeneous reactions where expected overall molar ratios between reactants cannot be maintained. In heterogeneous reactions, mass transfer limitations at phase boundaries as well as local mixing limitations may affect the reaction. For simple reactions overall reaction rates may be affected and usually decrease, but yield is unaffected given equal degrees of conversion. For complex reactions, the selectivity may be decreased, but unlike homogeneous systems, may also be increased under certain circumstances (see Example 13-8a).

The other key difference between homogeneous and heterogeneous reactions regarding selectivity is that significant selectivity effects can occur in heterogeneous systems at far lower absolute reaction rates because the mass transfer limitations can be very severe. In addition, these effects can be subject to considerable magnification on scale-up to plant operations. These effects can be visualized as changing the inherent k_{R2}/k_{R1} ratio, as measured by independent determination of the rate constants, to an apparent value caused by mass transfer limitations.

In Section 13-3, examples are used to illustrate the mixing issues that can be significant for various types of heterogeneous systems. The analysis of deviations from ideal behavior in homogeneous systems applies in many of these cases. Homogeneous reactions are more amenable to quantitative analysis and can therefore be developed more completely. The extension of the principles to heterogeneous systems will be more qualitative because of the complexity of these systems.

Heterogeneous systems can in some cases be manipulated to achieve improved yields compared to a homogeneous system with the same reactions. There can, therefore, be a great advantage in running under heterogeneous conditions or in some cases to deliberately creating a heterogeneous system for the purpose of improving selectivity. See Example 13-8a for an illustration.

13-3.2 Homogeneous versus Heterogeneous Selectivity

The discussion of selectivity considerations in homogeneous reactions in Section 13-2 provides an introduction to the far more complex issues involving heterogeneous reactions. The continuity of theoretical and practical considerations between these different types of reacting systems is provided by the obvious

fact that the course of reactions is determined by events at the molecular scale, whether or not the reactive molecules are in the liquid, solid, or gas phase when they enter the reaction zone. As in the case of homogeneous reactions, the course of a complex reaction will be determined by local molar ratios and chemical kinetics. The degree of deviation from expected kinetic behavior is determined by the reaction rate relative to the rates of mass transfer and mixing. The possible chemical interactions in the film around a dissolving reagent particle, a reactive gas bubble, or a dispersed liquid drop are illustrated in Figure 13-12 for a consecutive-competitive reaction. B is added to A, and B is the limiting reagent. The reaction of A with B to form the desired product, R, is occurring along with the normally undesired reaction of R with B to form S. In the heterogeneous case, there is a mass transfer boundary between A and B. Although a lot of desirable product R is formed, it quickly reacts with high concentrations of B to form undesirable product S. Differences in selectivity between the same reaction run under homogeneous conditions and heterogeneous conditions are illustrated in Example 13-4.

Example 13-4: Competitive-Consecutive Reaction—Solid–Liquid Compared with Homogeneous (Homsi et al., 1993)

- *Goal:* development of a solid–liquid competitive-consecutive reaction system

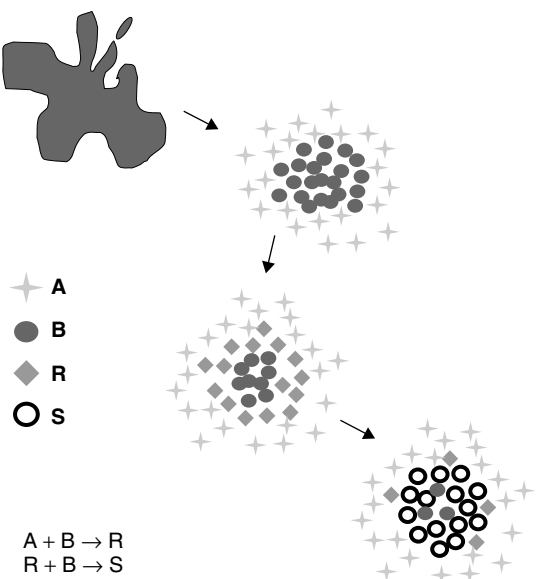

Figure 13-12 Simultaneous mass transfer and reaction in the films around solid particles, gas bubbles, and liquid drops. For a heterogeneous competitive consecutive reaction, mass transfer rates, reaction rates, and mixing rates can all play a role.

- *Issue:* laboratory selectivity not reproducible in the pilot plant
- *Classical bromination:* homogeneous versus heterogeneous selectivity

This example compares a reaction run using reagent addition as a dissolving solid and the same reagent added in solution. The two reactions were run in the same pilot plant equipment with the same mixing conditions. The data for the product distribution in this consecutive-competitive reaction system allow direct comparison of product distributions obtained under homogeneous and heterogeneous conditions.

The reaction shown in Figure 13-13 is a classical competitive-consecutive bromination to mono- and dibromo-substituted products where the mono-substituted product is the desired product. (Both 3- and 5-bromo products are acceptable for the following steps.) Dibromo formation represents a yield loss both in this step and in the reaction steps to follow. The reaction is run in the semibatch mode in all cases. The dissolving reagent is *N*-bromosuccinimide (NBS), and the reaction solvent is acetone. The pilot plant conditions are shown in Table 13-7. The NBS is added over a 6 h period because the reaction is very exothermic. The actual reaction rate is not known, but the addition requires 6 h for heat removal. The impeller is a six-blade Rushton turbine.

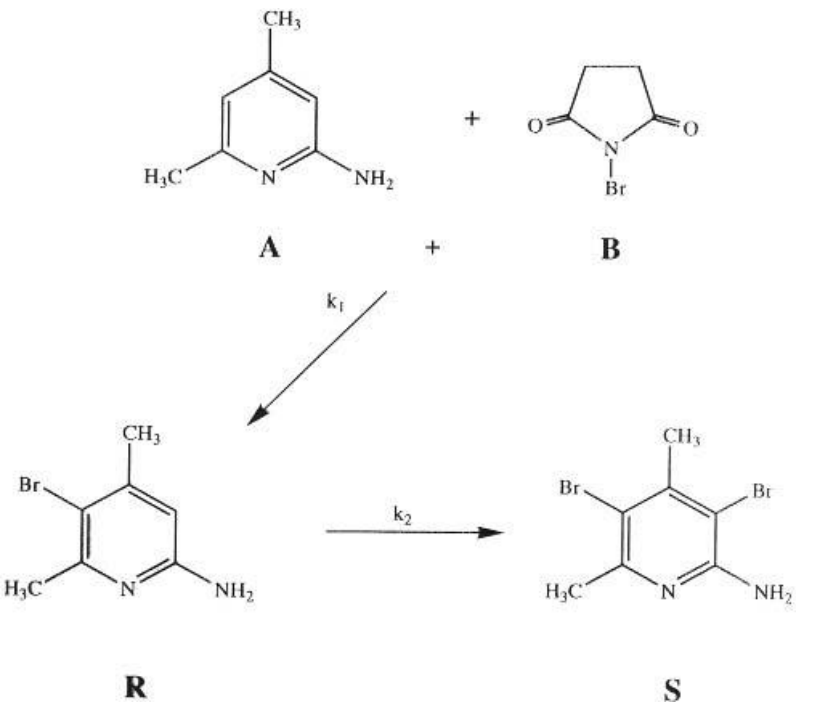

Figure 13-13 Chemistry of a classical consecutive-competitive bromination reaction subject to mixing effects.

Table 13-7 Pilot Plant Conditions for Bromination with *N*-Bromosuccinimide

Variable	Pilot Plant Condition
Vessel volume (m^3)	0.75
Vessel diameter, T (m)	1
Impeller diameter, D (m)	0.4
Impeller speed, N (rpm)	175
Reaction volume H/T	0.5
Power/volume (W/m^3)	117
Local power at point of solution addition (W/m^3)	1170

Results from powder addition of NBS:

- *Laboratory:* 91% monobromo, 2% dibromo. This is an acceptable level of impurity. The relative rates of reaction and mixing are not known or suspected to be a problem. Scale-up to the pilot plant is attempted.
- *Pilot plant:* 83% monobromo, 8% dibromo. This is an unacceptable increase in overreaction to dibromo. The apparent rate constant ratio, k_{R2}/k_{R1}, for the two scales can be calculated from the product distributions [eq. (13-5)]. This apparent ratio increased from 0.02 to 0.08, resulting in a decrease in selectivity.

Mixing effects in the film around the dissolving NBS are the obvious reason—the reaction rate is fast enough to allow significant reaction in the film before the dissolved NBS can be mixed to the molecular level. This indicates that the mass transfer rate is slower than the reaction rate.

Possible solutions:

1. Reduce the particle size of the NBS by milling to reduce dissolution time.
2. Eliminate mass transfer limitations by predissolving NBS in the reaction solvent and running as a homogeneous reaction.

Evaluation of alternative solutions:

1. Reduction in particle size can reduce dissolution time, but its overall effect in reducing reaction in the films around the dissolving particles may not be sufficient. Also, milling of a noxious material such as NBS is not feasible.
2. For a soluble reagent, another alternative is to predissolve it and add it as a solution. The mixing time could be further decreased and could achieve a significant reduction in Da_M.

Solution: Option 2 was run in the laboratory and was shown to reduce dibromo below that obtained with a powder addition (<1%). The same reduction was achieved in the pilot plant under the conditions shown in Table 13-8.

Message: This example indicates that the homogeneous reaction environment is more selective than the film around a dissolving reagent for a consecutive reaction. The result can be represented as an increase in the apparent rate constant ratio, k_{R2}/k_{R1}, for the heterogeneous condition as indicated in Figure 13-14, where the loss in selectivity (increase in X_S) is plotted against k_{R1}.

Table 13-8 Percent Yield of Dissolving Solid and Homogeneous Reactions under Identical Reactor Configurations[a]

Compound	Lab Solid NBS Addition	Batch 1 Solid NBS Addition	Batch 2 Solution Addition
5-Bromo	87	75	82
3-Bromo	4	8	7
Dibromo	2	8.4	<1

[a] *N*-Bromosuccinimide is the reactant and 5- and 3-bromo are the desired products.

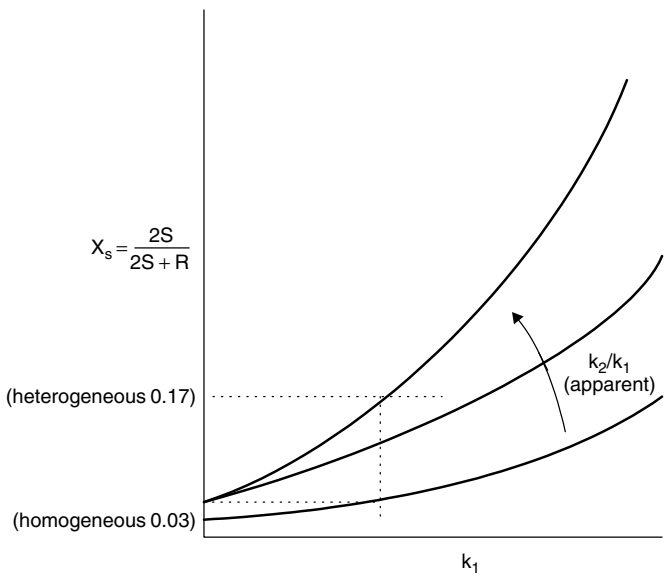

Figure 13-14 Correlation of apparent rate constant ratio with reaction rate and impurity selectivity (Xs); the effect of the mass transfer limitation on a dissolving solid can be shown as an increase in the apparent k_2/k_1 ratio.

As in Example 13-3, time was not available to measure individual rate constants. However, the laboratory and initial poor pilot plant results showing the effect of scale-up on product distribution were sufficient to illustrate the mixing sensitivity of the reaction. The key to solving the problem was not to try to improve mixing but to eliminate the mass transfer and local effects of a dissolving powder by changing the process to use a solution addition. An improvement was realized at both the laboratory and pilot plant scales.

13-3.3 Heterogeneous Reactions with Parallel Homogeneous Reactions

The yield and selectivity of heterogeneous reactions can also be affected by mass transfer in extending the time for completion of a reaction during which a parallel reaction—possibly decomposition of A, B, or R—can be occurring in the bulk phase as well as in the films around the dispersed phase (or in the dispersed phase for liquid–liquid reactions). This problem can develop when the desired reaction rate can only be achieved at a temperature at which the starting materials, any intermediate, or the product can react or decompose during the reaction time. This reaction time can be longer than expected on scale-up if the mass transfer rates do not duplicate those in the laboratory or in piloting. Shorter overall reaction times can also be realized on scale-up when mass transfer rates are increased by improved mixing (e.g., for liquid–liquid or gas–liquid dispersion). Reasons for slower mass transfer and extended reaction time for each type of contact are as follows:

- *Gas–liquid:* lower k_La because of insufficient gas dispersion–holdup and surface area
- *Solid–liquid:* slower dissolution time because of variation in reagent particle size and mass transfer
- *Liquid–liquid:* larger dispersed phase drop size and higher coalescence rates than expected

All of these factors are mixing dependent and can contribute to scale-up difficulty if mass transfer rates are not reproduced successfully.

13-3.4 Gas Sparged Reactors

Gas sparged chemical reactors are designed and used in many different geometries. These reactors are usually continuous in gas, and batch or continuous in liquid. Some of the geometries in use are bubble columns, pipe and static mixer reactors, stirred vessels, packed columns, tray columns, spray columns, jet loop reactors, and venturi ejector reactors. Design equations for each geometry are based on correlations and simplifying assumptions, such as uniform k_La in the stirred vessel. Other gas–liquid reactors include spray columns and spray combustors.

Table 13-9 Comparison of Different Gas–Liquid Contacting Devices[a]

Device	k_La (s^{-1})	V (m^3)	k_LaV (m^3/s)	a' (m^2/m^3)	$1-\Phi$	Liquid Flow	Gas Flow	P/V (kW/m^3)
Baffled agitated tank	0.02–0.2	0.002–100	10^{-4}–20	~200	0.9	~Backmixed	Both	0.5–10
Bubble column	0.005–0.01	0.002–300	10^{-5}–3	~20	0.95	~Plug	Plug	0.01–1
Packed tower	0.005–0.02	0.005–300	10^{-5}–6	~200	0.05	Plug	~Plug	0.01–0.2
Plate tower	0.01–0.05	0.005–300	10^{-5}–15	~150	0.15	Both	~Plug	0.01–0.2
Static mixer	0.1–2	0.001–10	1–20	~1000	0.5	~Plug	Plug	10–500

[a] Approximate values for typical cases; not to be used for design of specific processes. Middleton (see Table 11-3) and Lee and Tsui (1990) found similar characteristics. Note that the characteristic mass transfer time is given by $1/k_La$.

Typical performance values such as k_La, a', Φ, and P/V for each geometry are given in Table 13-9. Of interest is that k_L ranges from 0.0001 m/s for the packed, spray, and tray columns to 0.001 m/s for the stirred vessel and jet loop reactors. The pipe and static mixer reactors and the bubble columns are intermediate. The result of this observation is that for a given reactor, such as the stirred vessel, the local mass transfer rate is probably approximately proportional to the mass transfer area per unit volume, a, since the k_L values are not very sensitive to hydrodynamics. Of course, fluid properties can also affect k_L values, and they must be taken into account.

Reactions most commonly occur in the liquid phase in gas–liquid reactors. The most likely exception to this is spray combustors in which the reactions occur in the gas phase after or as the liquid droplets vaporize. Usually, in chemical reactors one reactant is transferred from the gas phase to the liquid phase, where the chemical reactions occur, as in chlorinations, oxidations, and hydrogenations.

If the time scale of a chemical reaction is short compared to the time scale of mass transfer, the mass transfer slows the chemical reaction but can also cause the concentration in the liquid-side mass transfer film to be decreased, resulting in an increased driving force and an enhanced mass transfer rate. Levenspiel (1999) and Middleton (1992) present diagrams for the interface concentration profiles likely to happen at the various reaction rates relative to the mass transfer rate. Those are shown in Table 13-10 along with estimates of the ranges of variables for the various regimes [similar to those of Doraiswamy and Sharma (1984)] and important variables for design and scale-up.

Levenspiel (1999) has estimated the effect of liquid-phase chemical reaction on the mass transfer coefficient, k_L. The modified coefficient is given here as k_L^*. For Middleton's regime V, where the chemical reaction is so fast that the reaction front is within the mass transfer film, the modified mass transfer coefficient for the gas phase component of the reaction is

$$k_L^* = k_L\left(1 + \frac{D_{AL}C_A}{D_{BL}C_B^*}\right) \tag{13-25}$$

Table 13-10 Various Gas–Liquid Reaction Regimes and Parameters of Importance

Regime	Conditions	Important Variables	Concentration Profile
I. Kinetic control, slow reaction	$(t_D/t_R)^{1/2} < 0.02$	Rate $\propto \theta_L$ $\propto K_R C_{AL} C_{BL}$ Independent of a Independent of K_L	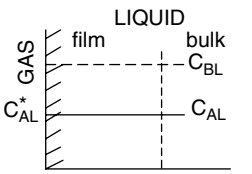
II. Diffusional control moderately fast reaction in bulk of liquid, $C_{AL} \approx 0$	$0.02 < (t_D/t_R)^{1/2} < 2$ Design so that $\Phi_L/a > 100 D_{AL}/K_L$	Rate $\propto$ a $\propto K_L$ $\propto C_{AL}$ Independent of K_R Independent of Φ_L if Φ_L is adequate	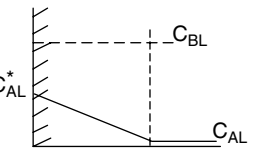
III. Fast reaction in film $C_{AL} \approx 0$ (pseudo first-order in A)	$2 < (t_D/t_R)^{1/2}$ $< C_{BL}/qC^*_{AL}$ $C_{BL} \gg C^*_{AL}$	Rate $\propto$ a $\propto K_R^{1/2}$ $\propto (C^*_{AL})^{(n+1)/2}$ Independent of K_L Independent of Φ_L	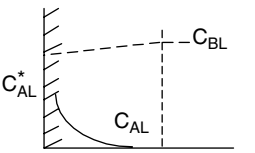
IV. Very fast reaction, general case for regime III	$2 < (t_D/t_R)^{1/2}$ $C_{BL} \approx C^*_{AL}$	Rate $\propto$ a depends on K_L, K_R, C^*_{AL}, C_{BL} Independent of Φ_L	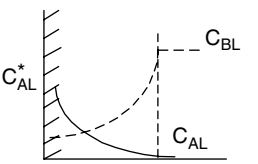
V. Instantaneous reaction at interface, controlled by transfer of B to interface from bulk, J α K_La	$(t_D/t_R)^{1/2} \gg C_{BL}/qC^*_{AL}$	Rate $\propto$ a $\propto K_L$ Independent of C^*_{AL} Independent of K_R Independent of Φ_L	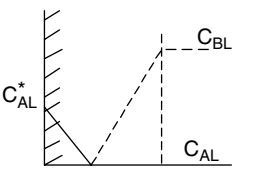

where C_A is the bulk concentration of the liquid-phase reactant and C^*_B is the concentration of the gas phase reactant in the liquid at the interface (the equilibrium concentration). For Middleton's regime IV, the very fast reaction regime, the modified mass transfer coefficient is

$$k^*_L = (D_{BL} k_R C_A)^{1/2} \tag{13-26}$$

For both eqs. (13-25) and (13-26), the chemical reactions are for stoichiometric coefficients and kinetic rate exponents of one for both components. Middleton and Levenspiel give equations for general coefficients, but such cases are not common for fast reactions, since more than one reaction is usually involved in

such cases. Note also that these equations assume that the gas phase mass transfer rate is very high relative to the liquid-phase rate. Levenspiel gives the equations for cases where the gas phase mass transfer rates could affect the value of k_L^*. A very general analysis of the interactions of chemical reaction and mass transfer was presented by Astarita (1967).

Middleton indicates that for his regime I (very slow reaction), where k_L is little affected by the chemical reaction, the interface surface area per unit volume, a, is of little importance since the reaction takes place in the bulk liquid phase, so a bubble column is the typical reactor of choice. For Middleton's regimes II, IV, and V—diffusional control, very fast reaction, and instantaneous reaction, respectively—both high a and k_L^* are needed, so a stirred tank is the typical reactor recommended. In regime III—reaction in the mass transfer film—the most important variable is the interface area, so a packed column yielding much liquid surface area may be appropriate.

If a detailed simulation of the local mass transfer rates and reactions rates in the reactor is not to be done, a key question in attempting to design a gas–liquid reactor is the residence time distribution of the gas phase. In stirred reactors the liquid phase is usually well mixed because of the necessity to disperse the gas adequately, but the gas flows can range from plug flow to well mixed, depending on the gas rate and agitator design. This can have a significant effect on driving force for the mass transfer rates if the inlet and outlet concentrations of the reactant in the gas are significantly different, as shown in the introduction to Section 13-3. In many pure-gas mass transfer cases, the change in gas composition is insignificant and residence time distribution has little effect on mass transfer rates. With highly reactive systems, such as oxidizers, where almost all of the reactant is consumed leaving mostly inert gas components, the difference in residence time distributions can have a large effect. For example, if a reactor has an air feed at 21% oxygen but a gas outlet oxygen fraction of only 4%, whether the gas is well mixed in the vessel or travels through in an almost plug flow manner will affect the overall mass transfer rate. If the gas is well mixed, most of the bubbles are at 4% oxygen, which determines the driving force for the mass transfer. It the gas is in plug flow, an average of inlet and outlet concentrations is closer to determining the overall driving force, which would give about a threefold increase in mass transfer rate for a very fast reaction in the liquid if the same interfacial surface area is produced. Of course, the well-mixed case would probably have much greater surface area for mass transfer, so the problem is not so simple.

When competitive reactions exist in gas–liquid systems, the yield can be strongly affected by the rate of mass transfer. This is an area of continuing investigation. In some cases the rate at which products are removed from the interface can affect the yield if the second reaction is fast. In oxidations and chlorinations where overreaction can lead to undesirable by-products, the rate of mixing of the products with the bulk fluid can help reduce the overreaction effect. In such cases the placement of the sparger for the gas might not noticeably affect the rate of mass transfer from the gas, but could affect the level of by-product

formation. In this case the liquid mixing is used to remove products from the bubble surface, not to achieve the micromixing, which is important for single-phase reactions. A case study of a chlorination reaction is given in Example 13-6.

13-3.4.1 Gas–Liquid and Gas–Liquid–Solid Reactions, Gas as Reagent. With the exception of fermentation, which is the subject of Chapter 18, one of the most common gas–liquid reactions is hydrogenation. The intrinsic reaction rates of hydrogenation reactions vary over several orders of magnitude and can fall into any of the categories discussed above. Design of a hydrogenation system is generally focused on supplying a sufficient quantity of hydrogen so that hydrogen concentrations in the bulk or adsorbed on the catalyst will not be limiting. In many cases, this can be accomplished by suitable design of a subsurface sparger to accomplish absorption during transit from the sparger discharge to the vapor space. In some cases, however, the absorptivity or reaction rate is slow enough that reabsorption from the pressurized vapor space is required. This can be accomplished with alternative mixing systems that are described in Lee and Tsui (1999).

The Editors' Introduction to this book contains a discussion of the importance of mixing configuration in hydrogenation. In this example, a reaction in a laboratory autoclave with a large H/D ratio (>2) appears to be very slow when the limitation is actually ineffective sparging and lack of surface reincorporation. If this limitation is not recognized, translation to a well-mixed vessel with surface reincorporation can result in very rapid and unexpected hydrogen uptake. Heat removal could then become critical.

Surface reincorporation can be accomplished by modifications of the standard reactor configuration, including that of the Praxair AGR system, which is shown in Chapter 6. Other systems employing high recycle in loops with gas induction are also effective, as discussed in Chapter 11. Another alternative using surface reincorporation follows.

Example 13-5: Hydrogen Uptake as a Function of Vessel Mixing Configuration

- *Goal:* determination of the cause of greatly reduced hydrogen uptake rate in a manufacturing scale hydrogenator compared to a laboratory autoclave and pilot plant reactor
- *Issue:* initial manufacturing scale reaction rate unacceptably slow

Scale-up of a Raney nickel-catalyzed reduction of a phenylazo-substituted pyrimidine to a triaminopyrimidine in a 6 m^3 (6000 L) vessel required careful configuration of the hydrogen sparger, turbine agitator, and baffles. The reaction is run in water at 130°C and 8 bar hydrogen pressure. The first batch run in the 6000 L vessel during startup of production facilities had an extremely slow hydrogen uptake rate compared with expected uptake based on pilot plant experience. The fully baffled single-turbine impeller and sparger configuration is shown in Figure 13-15*a*.

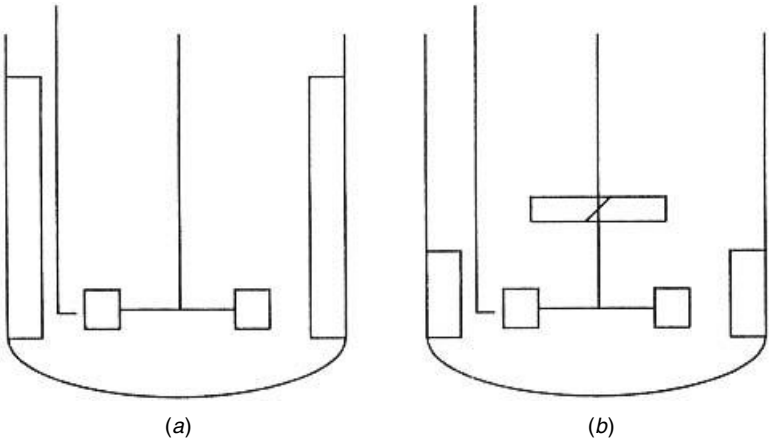

Figure 13-15 Hydrogenation internal configurations for gas dispersion: (*a*) an ineffective sparger configuration compared to (*b*) a design for increasing surface reincorporation.

Modification of sparger location, baffles, and upper axial flow turbine size and location, as shown in Figure 13-15*b*, was successful in achieving (and exceeding) the expected hydrogen uptake rate. These modifications were based on the recommendations by Oldshue (1980), where vortexing at the upper surface is used to incorporate hydrogen from the vapor space to augment that injected by sparging. These recommendations include shorter baffles and an axial flow turbine near the top surface in addition to a flat-blade lower turbine near the sparger for efficient gas dispersion.

Message: The modified configuration achieved efficient vortexing, and effective surface re-incorporation and rapid hydrogenation was established. It is apparent from the dramatic improvement accomplished with surface reincorporation of hydrogen that very little hydrogen uptake was accomplished with the initial ineffective sparger placement and the fully baffled single turbine. Unreacted hydrogen broke through to the vapor space, which became pressurized. The vapor space pressure then increased to the feed pressure, effectively shutting off the flow of hydrogen that was being fed from an on-demand system.

Many gas–liquid reactions other than hydrogenations are run in the chemical industry. Reaction system design depends primarily on the solubility of the gas in the reaction mixture and on its rate of reaction. Soluble gases can often be added without sparging by vortexing. Pitched blade turbines with partial baffles are effective in this regard. However, care must be taken, as discussed in Chapters 6 and 11, to avoid impeller balance and vibration problems.

For complex reactions, the product distribution can be affected by mixing in direct analogy to the homogeneous case discussed earlier. Some of the first experiments in this area were conducted on chlorination of *n*-decane by van de

Vusse (1966), in which mixing was shown to affect the distribution of chlorinated products. The chlorination of acetone is also a mixing-sensitive gas–liquid reaction as described in Example 13-6.

Example 13-6: Chlorination of Acetone: Mixing-Sensitive Gas–Liquid Reaction (Paul et al., 1981)

- *Goal:* determination of the cause of reduced selectivity in a manufacturing scale gas–liquid competitive-consecutive reaction and modification of the reactor to achieve target selectivity
- *Issue:* decrease in selectivity experienced on scale-up

This example presents reactor design problems experienced in the scale-up of a classical competitive-consecutive reaction from bench to manufacturing scale. Expected selectivity was not achieved initially, and a revised reactor was required.

The chlorination of acetone is a very fast reaction that produces both monochloroacetone and dichloroacetones as well as polychlorinated species. The product desired is monochloroacetone. The reactions are shown in Figure 13-16 and the product distribution in Figure 13-17. Elevated local concentrations will increase the local reaction rates.

As is often the case, the di- and polychlorinated species not only reduce yield but cause ongoing yield and purity problems in subsequent steps of a multistep synthesis because of their reactivity. The rate constant ratio between mono- and dichlorinated species is very unfavorable for making high-purity monochlorinated species, thereby requiring excellent mixing, a very high molar ratio of acetone to chlorine ($>10:1$), and subsequent acetone recovery.

Laboratory results: Semibatch addition of chlorine gas to liquid acetone in a 5 L flask; 98% monochloro, 2% overchlorinated products.

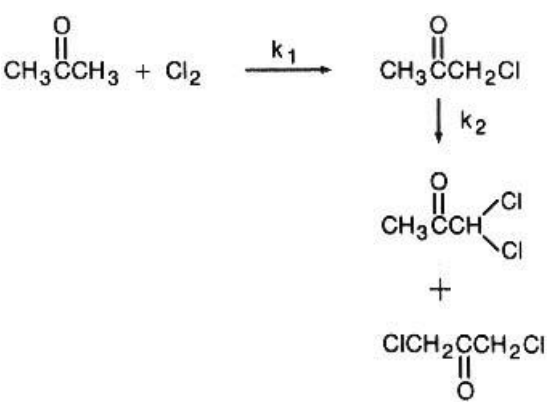

Figure 13-16 Chemistry of the classical consecutive-competitive chlorination of acetone.

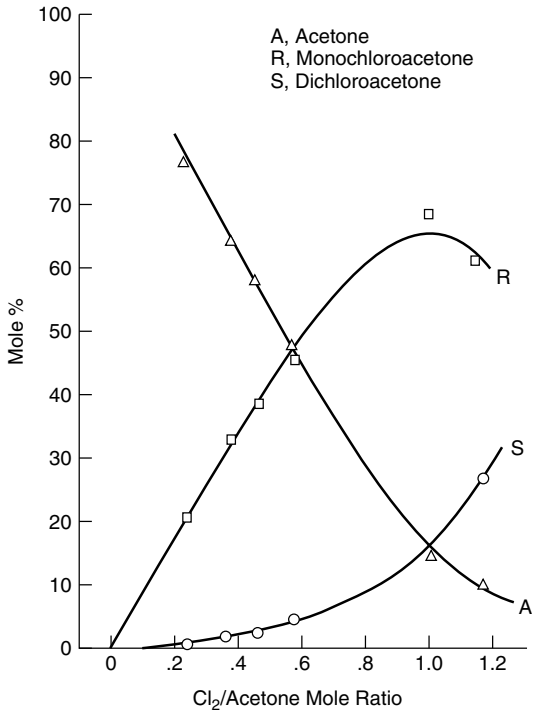

Figure 13-17 Product distribution in the chlorination of acetone as a function of the chlorine/acetone mole ratio. The formation of overchlorinated products increases with increasing mole ratio.

Manufacturing results: The ratio of products achieved in the manufacturing scale continuous vapor-phase reactor was 92% monochloro, 8% overchlorinated products. The initial configuration is shown in Figure 13-18.

Troubleshooting analysis: Laboratory results are in agreement with expected selectivity based on measured k_{R1}/k_{R2} ratio and chlorine/acetone molar charge ratio as calculated by eq. (13-5).

Manufacturing results indicate that monochloroacetone once formed is overreacting to a greater extent than indicated by the laboratory results. Figure 13-18 shows the gas phase reactor chosen for manufacturing. Both reactants are vaporized before entering the tubular reactor. Since there is no mass transfer resistance or reacting film in the gas phase, the expected selectivity should be achieved. (*Note:* Gas phase reactions are not subject to the mixing issues being discussed in this chapter because of the order-of-magnitude increase in molecular diffusivity compared to homogeneous liquid-phase or gas–liquid mixing.)

Possible problem: The reaction may not be going to completion (not consuming all of the chlorine) in the gas phase tubular reactor, thereby allowing gas phase chlorine to enter the fractionating column and react with refluxing acetone, as shown schematically in Figure 13-19.

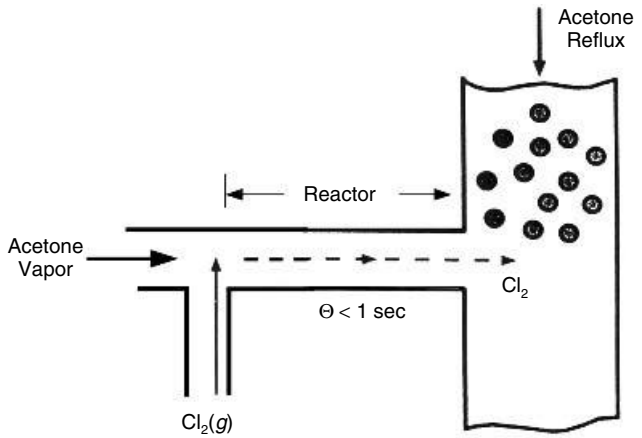

Figure 13-18 Schematic drawing of the manufacturing scale gas phase tubular chlorination reactor and downstream (connected) fractionator for the recovery of unreacted acetone (molar feed ratio 10 : 1 acetone/chlorine).

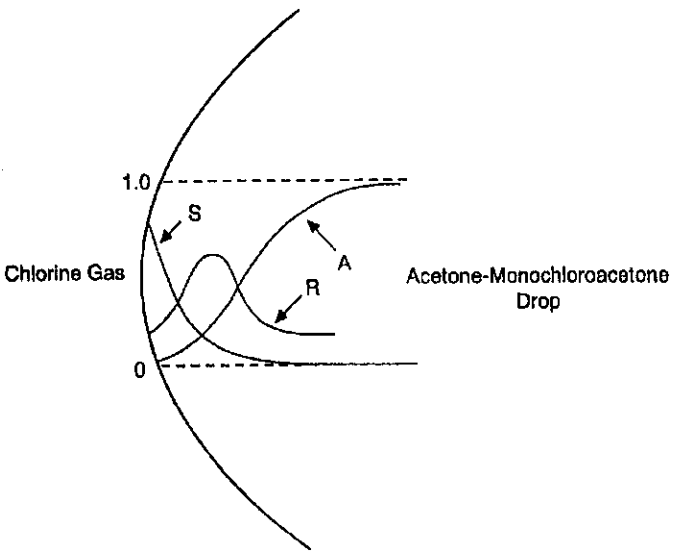

Figure 13-19 Qualitative model for consecutive reaction in the film around a liquid drop of acetone surrounded by gas phase chlorine (see Figure 13-12).

Possible solutions: Extend the length of the tubular reactor or redesign the reactor as a gas–liquid contactor.

Evaluation of alternative solutions: Temperature rise measurements in the existing gas phase reactor indicated that the conversion of chlorine was very low, thereby indicating that the length of the reactor would have to be increased

considerably. In addition, residence time distribution issues could allow unreacted chlorine to reach the fractionator.

A gas-liquid reactor with liquid acetone as the continuous phase could achieve the required conversion in a much smaller reactor.

Resolution: The solution to the problem was to mix liquid acetone and gaseous chlorine in an in-line reactor in which the reaction was completed before reaching the fractionator. The configuration is shown in Figure 13-20. The system was piloted to determine the design conditions that would allow complete reaction of chlorine. Successful scale-up was achieved in a turbulent 0.05 m (5 cm) mixer with very short residence time.

Message: As in Examples 13-3 and 13-4, the key to realization of a potential mixing issue was the knowledge of (and analytical confirmation of) consecutive reactions combined with the qualitative observation that the reactions are very fast. Large production quantities required that manufacturing operations be run in a continuous reactor, thereby ruling out a stirred vessel (which would not have been a good choice in any case because of mixing limitations). A single-point injection-line mixer was chosen. The high energy dissipation rate and gas–liquid dispersion capabilities of a static mixer would have been preferable, but these devices were not available at the time the work was done. The same conversion and product distribution were achieved as in a semibatch laboratory flask.

13-3.5 Liquid–Liquid Reactions

In liquid–liquid reactors both interphase mass transfer from the continuous phase to the dispersed phase (or vice versa) and dispersed phase mixing through coalescence and dispersion (CD) can occur. The reader is referred to the comprehensive discussion of liquid–liquid systems in Chapter 12.

As pointed out in the Editors' Introduction to this book, liquid–liquid reactions may present the most difficult scale-up challenge in heterogeneous reactions. They are very common and occur in all the regimes discussed in the classification of hetrogeneous reactivity. In regimes 1 and 2 (see Section 13-3.1), slow reactions combined with low solubility of the reactants in their respective phases,

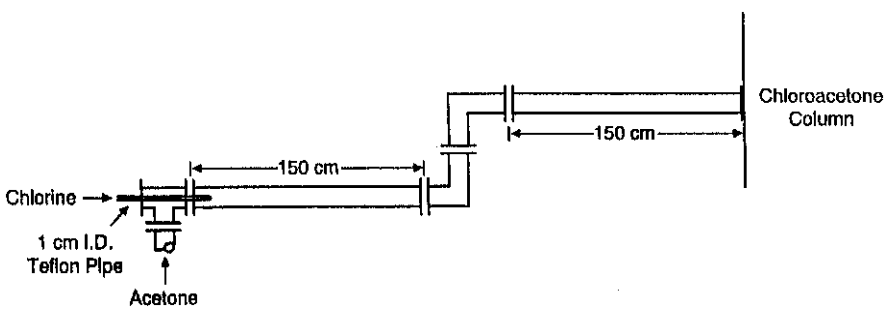

Figure 13-20 In-line reactor for mixing gas phase chlorine with liquid-phase acetone to achieve complete consumption of chlorine before fractionation.

the actual conversion rate for even very well-mixed systems may be negligible. In these cases, a third solvent may be added to improve mutual solubility or a phase transfer catalyst may be added to transfer one reagent, usually ionic, from aqueous to solvent phase. Both types of additions add downstream separation operations, however, so their use is avoided if possible.

Other strategies to promote reactivity include (1) generation of large interfacial area by intense mixing and (2) removal of one of the phases by distillation of the more volatile solvent, thereby combining the reactants in the remaining phase. The last method may be complicated by the appearance of a solid phase (reagent or product becoming insoluble) but may still be preferable to an additive.

Two examples of liquid–liquid reactions are provided below to illustrate that selectivity can be a significant issue on scale-up.

Example 13-7: Agitated Thin-Film Reactors and Tubular Reactors with Static Mixers for a Rapid Exothermic Multiple Reaction (Schutz, 1988)

- *Goal:* design of a scalable reaction system for a very fast, highly exothermic complex reaction.
- *Issue:* choice of a suitable reactor for manufacturing scale operation. This reaction scheme is:

$$A + B \rightarrow R$$

$$R + B \rightarrow S$$

with an enthalpy of reaction of -440 kJ/mol. The reactants are single-phase liquids, but the reaction mixture is two liquid phases. Optimum temperature is -20 to -30°C, and the adiabatic temperature rise at the operating concentrations is 80°C. Significantly lower yields were obtained in a 0.25 m^3 (250 L) stirred tank under semibatch conditions (30 min addition) than in the laboratory using a stirred tank.

Two alternative reactor configurations were then investigated in the laboratory; (l) agitated thin-film reactor and (2) tubular reactor with static mixers. The reaction time was found to be at most a few tenths of a second and yield increased with increasing agitator speed in the thin-film reactor and increasing flow rate in the tubular reactor. Semicommercial scale reactors of both types were assembled and tested.

The agitated thin-film reactor was an 0.08 m diameter wiped-film evaporator and was cooled by either convection or evaporation. Because of vacuum requirements for evaporation of the solvent, only convective cooling was utilized. Yields were found to be 10 to 15% higher than in the 250 L stirred tank. The increase in temperature affected the results far less than that which occurred in the stirred tank. Although no exact data on local energy dissipation rates in wiped-film evaporators was available for the unit, higher local energy dissipation rates occurred than in stirred tanks.

The tubular reactor with static mixers was chosen for the documented capability of static mixers to accomplish the following important functions for fast multiple reactions in turbulent flow: (1) homogeneity down to the molecular level can be achieved in a few tube diameters; (2) very short mixing time and narrow residence time distributions are required; and (3) high rates of energy dissipation are achievable (average energy dissipation rates can be calculated from pressure drop and local rates can be estimated).

The cooling capability of static mixers under conditions of extremely rapid heat generation is very low, leading to solvent evaporation in the mixing elements. This two-phase flow reduced the residence time further. The tubular reactor with static mixing elements discharged into a stirred tank, where evaporation and condensation removed the heat.

Yields in the tubular reactor were 15 to 25% better than in the stirred tank, depending on flow rate. This reactor configuration was also superior to the wiped-film evaporator, possibly for two reasons: (1) higher rates of turbulence energy dissipation achieved more rapid micromixing, and (2) superior mixing at the entrance to the static mixers compared to the entrance of the wiped-film evaporator, where some backmixing took place. The possible significance of backmixing in fast multiple reactors is underscored by this example and is also discussed by Bourne et al. (1981) and by Bourne and Garcia-Rosas (1984).

If the heat rise in the tubular reactor (unspecified) could not have been tolerated, the wiped-film evaporator with more effective convective heat removal (since more surface area to volume is achieved) would have been required.

Resolution: A static mixer reactor was superior to a wiped-film evaporator in yield. Heat removal was accomplished in a subsequent flash vessel.

Message: This example is illustrative of the necessity to meet multiple criteria, including liquid–liquid dispersion, short contact time, minimum backmixing, and high heat transfer rates, in a single reactor configuration. The heat transfer rate, however, was not achievable in an on-line mixer that could achieve the mixing criteria because of the extremely short contact time. Use of flash evaporative cooling at the reactor discharge is an excellent example of effective process integration.

13-3.5.1 Reactive Extraction. Enhancement of selectivity because of the presence of an immiscible phase is an important aspect of liquid–liquid systems. The improvement in selectivity is achieved by protection of the reactant(s) or product in a separate phase from an active reagent to reduce consecutive or competitive reaction to undesired by-products. Sharma (1988) discusses this subject and presents examples of very large increases in selectivity. An example from Wang (1984) is presented by Sharma in which isocyanates were prepared from amides or *N*-bromoamides by Hofmann rearrangement under phase catalysis conditions. Without a second phase the isocyanate overreacted under alkaline conditions in the aqueous phase. Addition of a carefully selected solvent achieves reaction and rapid extraction of the isocyanate, which can then be obtained in high yield. This route to isocyanates obviates the use of phosgene.

Another example of reactive extraction is provided by King et al. (1985). In this case, an acid hydrolysis could be replaced by a highly advantageous change to alkaline hydrolysis to achieve improved selectivity, productivity, quality, and waste minimization. However, the decomposition rates of reagent and reaction product under aqueous alkaline conditions are prohibitive. By running under reactive-extractive conditions, the objectives were achieved. Conventional mixing in a vessel was not feasible because of the rapid decomposition. In-line mixing followed by rapid phase separation proved to be an extremely effective method to carry out this complex reaction, which is discussed further in Example 13-8a.

Example 13-8a: Reactive Extraction (King et al., 1985)

- *Goal:* determination of the feasibility of process improvements requiring a reaction to be run under conditions of rapid simultaneous decomposition of substrate and product
- *Issue:* design of scalable reaction system for a classical parallel and consecutive reaction system

The chemistry of the hydrolysis of an intermediate in the synthesis of an antibiotic is shown in Figure 13-21. Although the chemistry for liquid–liquid acid catalyzed hydrolysis was satisfactory, several process advantages could result from a change to base hydrolysis. However, base hydrolysis was known to be unsatisfactory because of the simultaneous decomposition.

Laboratory results: Running the reaction in a standard laboratory semibatch mode adding aqueous NaOH to a solution of A at the pH required for hydrolysis (<10) resulted, as predicted by the chemists, in an unacceptable degree of decomposition of A before the hydrolysis was complete and the base could be neutralized.

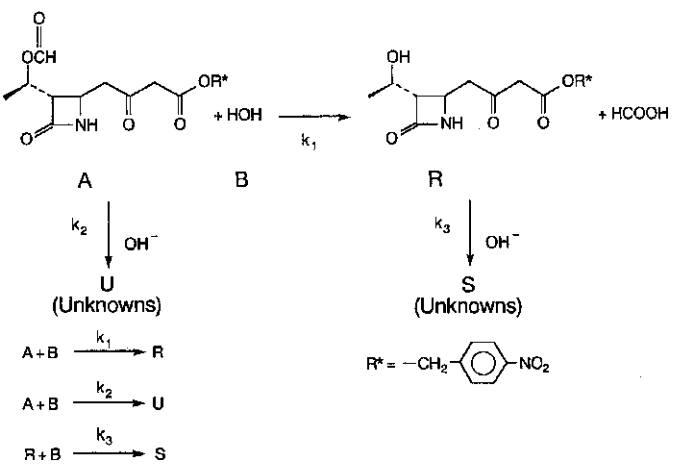

Figure 13-21 Chemistry of hydrolysis reaction in the synthesis of an antibiotic.

Challenge: Is there a reaction system that could accomplish the hydrolysis and neutralization fast enough to achieve acceptable yields of R without decomposition of A and R to unknowns? (Decomposition to unknowns occurs rapidly after the unstable four-membered ring is opened.)

Possibility: A is soluble in the organic phase (methylene chloride). It hydrolyzes to the enolate salt in the aqueous-phase film at the liquid–liquid interface, as shown in Figure 13-22, and then becomes soluble in the aqueous phase as the enolate salt. A reaction system with simultaneous contacting of the two phases and extraction of the product could be feasible. The relative rates of hydrolysis and base decomposition would determine the feasibility of the system proposed. These rates were measured independently and the ratio was found to be sufficiently favorable ($k_{R1}/k_{R2} > 100$) to proceed with design.

Reaction system: The reaction system with a static mixer followed by a centrifugal separator was assembled in the laboratory and was able to produce acceptable yields of R. A plant design was then developed as shown in Figure 13-23.

Key components:

1. Static mixer to achieve liquid–liquid contact and residence time sufficient to transfer A to the aqueous phase
2. Static mixer and extractor to provide residence time to complete the hydrolysis of A to R (~15 s)
3. Limited residence time in extractor to minimize base decomposition to U
4. Separate phases to allow continuous transfer of the aqueous phase to a vessel containing aqueous acid for neutralization and crystallization of R

Results:

1. The final plant design is as shown in Figure 13-23. The static mixer achieved the required reaction conversion and subsequent separation was completed in a suitable time frame to minimize base-catalyzed decomposition.
2. The reactor–extractor chosen was a Podbielniak centrifugal extractor. These units are normally run with countercurrent feed for extraction and are capable of having two- or three-stage efficiency. The operation, including the

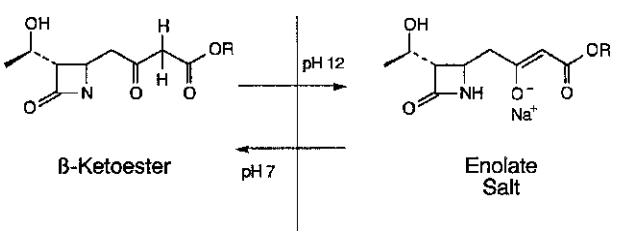

Figure 13-22 Conceptual procedure of enolization for hydrolysis under basic conditions.

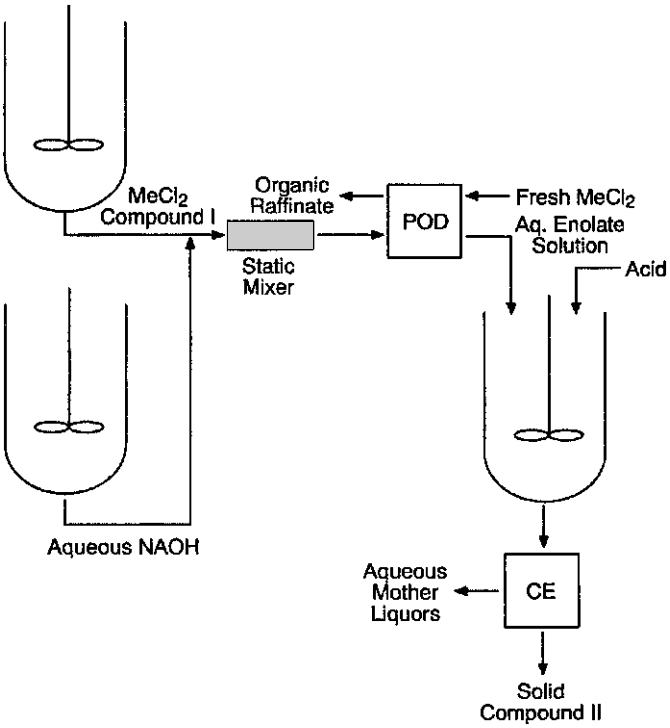

Figure 13-23 Schematic diagram of static mixer for in-line reaction, centrifugal extractor, and crystallization train.

reaction zone, is shown in Figure 13-24 in a cutaway side view of the centrifugal rotor. The mixed phases leaving the static mixer are fed to the extractor as shown. The mixing–contacting zone between the organic phase and the aqueous base provided enough interfacial area and residence time to complete the reaction and extraction. By maintaining the principal interface, the two phases are separated as exit streams and the aqueous phase transferred directly into aqueous acid to stop formation of U and to crystallize R. Although successful operation could be achieved without premixing the feeds, the improvement with a backwash with solvent was chosen as shown. This utilized the counterflow capability of the extractor to remove impurities from the organic stream. The improvements realized by base hydrolysis compared to acid hydrolysis are as follows:

- *Yield:* 95% versus 81%
- *Impurity removal:* 20% versus 0%

Message: In this example, laboratory development was actually more difficult to characterize than plant operation because a small scale extractor to simulate Podbielniak performance was not available. This case is illustrative,

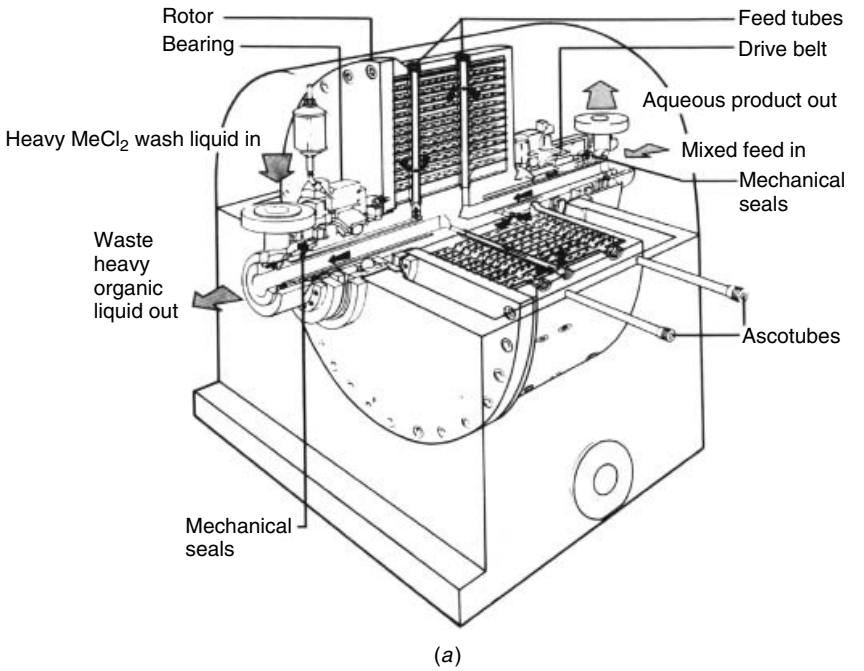

Figure 13-24 (*a*) Continuous flow countercurrent extractor. (Modified from Thornton, 1992.) (*b*) Cutaway drawing of Podbielniak extractor with mixed feeds. The feed and backwash liquids enter at the principal interface. Centrifugal force separates the heavy phase from the light phase. The direction of rotation is out of the page.

therefore, of the need to conceptualize full scale performance and equipment design in the absence of an integrated laboratory model and to utilize separate laboratory reaction rate data on the various reactions to design the overall reaction system.

The final plant design illustrates a semicontinuous operation in which the run starts with the feed streams in separate vessels and ends with the reaction/extraction product in a third vessel, in this case a crystallizer. This system allows the reaction to be carried out under the same local conditions throughout the run and at a residence time consistent with the stability of the reactants and product. This reaction could not be carried out successfully in a semibatch mode in which the product would accumulate at high pH. The overall run time is, therefore, not a function of product stability but only of production requirements and equipment sizes. In this example, an overall run time of about 2 h was satisfactory.

This example illustrates the effectiveness of two liquid-phase reactions in protecting unstable reactants and/or products from a reactive aqueous phase. In this case the protecting solvent was present in the feed stream from a previous step. In some cases, the protecting solvent is added for that purpose.

A second example of a parallel reaction involving the starting material, A, is illustrative of how mixing sensitivity during neutralization with a strong acid or base can result in unwanted reaction and/or decomposition, as discussed in Section 13-1.2. This problem is highlighted in Example 13-8b.

Example 13-8b: Neutralization Involving Parallel Decomposition (Paul et al., 1992)

- *Goal:* determination of cause of unexpected decomposition of an intermediate during pH adjustment
- *Issue:* manufacturing scale operation that resulted in 4 to 5% unexpected decomposition

This example outlines a case in which a simple pH adjustment with a strong base, sodium hydroxide, of a two-liquid-phase mixture resulted in some unexpected decomposition of the compound R (structure same as in Figure 13-21). This pH adjustment is in preparation for the hydrolysis reaction described in Example 13-8a. A is dissolved in a solvent, methylene chloride (SG = 1.4), and the pH adjusted from 2 to 7 with aqueous sodium hydroxide. No change in the concentration of A is expected, but a decrease is observed in manufacturing.

The reaction system is the classic parallel type:

$$\text{A (acid)} + \text{B (base)} \rightarrow \text{P (water)}$$

$$\text{B (base)} + \text{C (formate)} \rightarrow \text{Q (in this case R of Figure 13-21)}$$

where the base B is added to neutralize acid A in the presence of C (in Example 13-8a, C was A in a competitive-consecutive high-pH scheme). In this analysis, P is the water formed in the neutralization reaction and Q is the phenol R from Figure 13-21. Q is symbolic of a reaction by-product of the base B reacting with substrate C while neutralizing the acid.

In most cases, the rate of the neutralization reaction will be so much faster than the parallel decomposition reaction C to Q that no Q would be formed. However, as seen in Example 13-8a, C is sensitive to high pH, and in this case the local high concentration of sodium hydroxide during neutralization was the possible cause of the loss of C.

Laboratory results: A laboratory study was made of the neutralization step to determine whether A could be reacting because of insufficient mixing. The laboratory reactor was a 0.006 m^3 (6 L) fully baffled vessel with a 0.072 m (7.2 cm) six-bladed Rushton turbine. The results are shown in Figure 13-25, where the amount of Q formed is shown to depend on turbine speed. The effect of changing feed position is shown in Figure 13-26, where the expected best results from feeding near the turbine were not observed. The cause is the differences in composition of the two-liquid phases within the vessel. When the base is added in a zone that is primarily aqueous, the base strength is reduced rapidly, whereas when added in a region of high solvent composition, the decomposition is accelerated because the base strength is not reduced as readily. The laboratory reactor was run at a low turbine speed, where phase dispersion varied with depth, to exaggerate the possible effects of poor mixing that could be experienced in the manufacturing vessel (12 m^3).

Power comparisons: The local energy dissipation rates (as power per volume, $\rho\varepsilon$) at the impeller discharge in the laboratory compared to the manufacturing vessel are as follows:

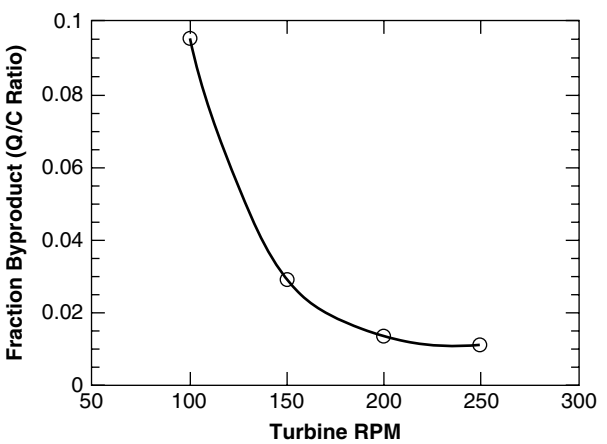

Figure 13-25 By-product formation as a function of impeller speed for a pH adjustment with competitive decomposition of substrate at the laboratory scale.

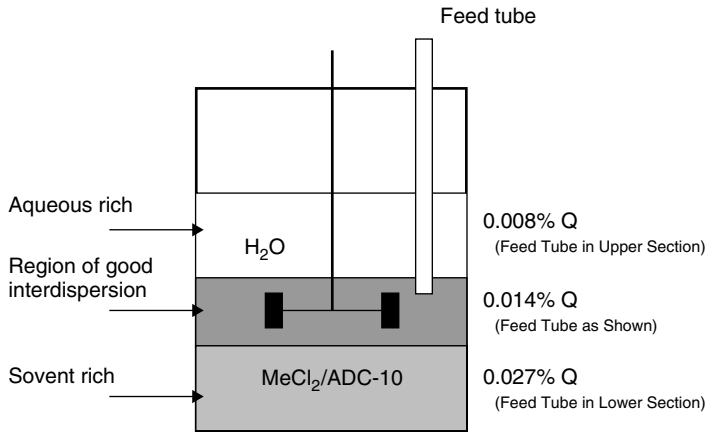

Figure 13-26 Effect of feed tube location on decomposition during the pH adjustment at the laboratory scale. The caustic (feed) is quickly diluted in the aqueous-rich zone but is more concentrated for a longer time in the lower two zones.

Lab at 4 rps	185 W/m^3
Lab at 3 rps	78 W/m^3
Plant at 1.5 rps	340 W/m^3

Manufacturing modification options:

1. Increase impeller speed and/or change type.
2. Use sodium bicarbonate ($NaHCO_{3)}$ in place of sodium hydroxide (NaOH) as the base, thereby reducing the maximum pH that could be experienced even by poor mixing from >12 to ~ 8.

Solution: Option 2 was chosen as a far less costly and less time-consuming solution.

Message: Local extremes of pH can occur in a pH adjustment because of imperfect mixing in homogeneous or heterogeneous systems, and these extremes can be expected to be more severe on scale-up. Care must be taken that possible parallel reactions are recognized and minimized by adequate mixing or reactor design. In some cases, the sensitivity may be sufficiently severe to require a high intensity line mixer for the addition point of the acid or base, possibly in a recycle system around the primary vessel.

13-3.6 Liquid–Solid Reactions

Solids in reacting systems can be either heterogeneous catalysts, dissolving reagents, precipitating products, or other reaction components, such as adsorption agents or ion-exchange resins. Reaction rates can fall in all regimes of the

kinetic spectrum, as described at the beginning of this section. A discussion of solid–liquid mixing without reaction may be found in Chapter 10.

As with all other types of heterogeneous reactions, very slow reactions in the liquid phase (regime 1) are unaffected by mass transfer in the film surrounding dissolving reagents or adsorption agents, and mixing is required only to maintain solids suspension. However, in the case of precipitating or crystallizing products, mixing can affect the particle size of the product just as it would in a precipitation without chemical reaction. Therefore, an effect of mixing in regime l must be considered. Reactions in regimes 2, 3, and 4 are all sensitive to local conditions and the films around solids and are therefore subject to mixing effects.

13-3.6.1 Solids as Dissolving Reagents. Organic and inorganic reagents are often incompletely soluble in reaction solvents for a variety of reaction types. The particle size of these reagents can be a major factor in reaction rate and/or selectivity. One objective of a laboratory development program is to determine the effect of particle size and to separate dissolution kinetics from chemical kinetics. An effective method of studying these reactions is to run the reaction under homogeneous conditions to measure true reaction kinetics. This can be accomplished by preparing a saturated solution of the reagent, even if the maximum concentration is very low, and determining the reaction rate as discussed in Section 13-4.3. Once the true chemical kinetics are established, the overall reaction rate can be evaluated for dissolution limitations.

A second effective but less quantitative method is to run the reaction with different particle size distributions of the insoluble reactant to determine effect on overall reaction rate. If no effect is measured, it could be concluded that regime l applies and chemical kinetics—not dissolution—controls. This method must be used with care, however, since other factors, such as surface coatings and incompletely characterized particle size distribution, can mask mixing effects and lead to erroneous conclusions.

An example of a reaction with dissolving solids was presented in Example 13-4 in which a direct comparison can be made with the same reaction run in the same pilot scale vessel under homogeneous and heterogeneous conditions. The selectivity is significantly lower for the heterogeneous conditions.

13-3.6.2 Solids as Precipitating/Crystallizing Products.[1] Several studies have shown the effect of mixing on the precipitation of inorganic salts. Mixing intensity was shown to affect particle size for the instantaneous reaction to form $BaSO_4$ by Pohorecki and Baldyga (1988). Particle size was found to increase with increasing impeller speed in a segregated feed CSTR. Barthole et al. (1982) used a modification of the precipitation of $BaSO_4$ (modified to indicate the degree of micromixing) by characterizing product distribution of a $BaSO_4$ EDTA complex in alkaline medium under the influence of an acid.

[1] The distinction between precipitation and crystallization is not always clear. For purposes of this discussion, precipitation is the formation of a solid phase from solution by chemical reaction. Reactive crystallization applies to cases in which the solid is crystalline and not amorphous.

Garside and Tavare (1985) modeled the effect of micromixing limits on elementary chemical reaction and subsequent crystallization. Two limiting cases are analyzed, and although the conversions of the chemical reactions are the same, the crystal size distributions can be very different. These differences are caused by the nonuniformity of supersaturation profiles that can be experienced by different fluid elements within a tank, owing to micromixing as well as macromixing effects. This modeling work also explores the sensitivity of two mixing models to reaction rate constant and nucleation kinetic parameters.

Literature references to experimental work on the crystallization or precipitation of products of organic reaction are rare, even though this is a common reaction type. The difference between crystallization and precipitation is not well defined and is interpreted differently by different investigators. The interpretation that is used here is that crystallization generates a crystalline product, whereas precipitates form rapidly and can be crystalline or amorphous. The differences are often blurred, however, because many organics actually appear first as amorphous noncrystalline solids which later turn truly crystalline. In these cases nucleation is difficult to separate from precipitation of an amorphous solid. Mersmann and Kind (1988) present an excellent discussion on precipitation as it is affected by micromixing. Additional discussion of mixing effects in crystallization may be found in Chapter 17.

An experimental study by Marcant et al. (1991) of the crystallization of calcium oxalate concluded that the particle size distribution was significantly affected by impeller speed and other mixing variables. The particle size distribution increased, passed through a maximum, and then decreased as the impeller speed was increased. This result is interpreted as changes in the key factors controlling nucleation and growth as well as reaction. Other mixing variables, including reagent addition point, were also significant and affected particle size distribution in different ways. Another observation by these authors is that measurement of particle size distribution as a function of addition on the surface compared with at the turbine can indicate whether or not micromixing effects have any influence on crystallization or whether other factors, such as nucleation and/or growth rate, dominate. This work is also summarized by Baldyga and Bourne (1999), including pictorial representation of the importance of the addition point in determination of particle size distribution for this system.

The initial appearance of a solid that results from generation of supersaturation by a chemical reaction is a very complex series of events. The conditions affecting crystallization can be critical to the overall process result, for several possible reasons. Yield from a complex reaction can be a function of the rate of crystallization and degree of supersaturation since these factors determine the concentration of that reaction product in solution at any given time. When in solution, all of the factors affecting selectivity can be significant, as discussed above in Section 13-2.5. Delayed nucleation because of improper seeding, mixing conditions, or excessive impurity levels can result in significantly reduced selectivity.

The purity of the crystallization product can be affected by the parameters that control any crystallization as well as the presence of other chemical species, including the starting materials, that can be occluded from the reaction mixture. The particle size distribution can be affected by supersaturation, reaction rate, mixing, and other factors that affect crystallization in general. The degree to which control of the crystallization must be of concern obviously depends on downstream processing. In some cases, physical attributes may not be significant and the reaction can be optimized on the basis of chemical kinetics alone. In other cases, however, the requirements for maximum selectivity may be different than those for physical attributes, requiring a trade-off in actual system design.

An example of reaction-induced crystallization where the particle size and purity must be controlled is discussed in Chapter 17 (Example 17-3; Larson et al., 1995). In this case, mixing played a key role by balancing circulation with shear to achieve micromixing for the reaction but avoiding overmixing. This configuration achieves growth without shedding and/or crystal fracture. A key factor is the time of addition—a mesomixing issue as well as a means of regulating supersaturation.

Mixing can also play a key role in affecting the morphology of a crystalline product. This effect results from the complex interaction between the impeller and nucleation and growth. The reader is referred to the discussion on mixing and crystallization in Chapter 17.

13-4 SCALE-UP AND SCALE-DOWN OF MIXING-SENSITIVE SYSTEMS

When perfect mixing or plug flow cannot be assumed but it is not feasible to perform complete simulations of the flow for mixing and chemical reactions in the vessel, scale-up based on local mixing conditions is essential. For stirred reactors with multiple reactions and mixing effects on yield, the simplest approach is to hold constant the power per unit volume. This will work only if the feed locations are in the most turbulent location and geometric similarity is maintained. A more precise scale-up criterion is to hold the rate of turbulent energy dissipation per unit mass in the region of most intense mixing constant. This is particularly useful when the feed is into the impeller stream of a stirred vessel where the mixing is at the fastest rate. Indeed, when yield is an issue, the region of most intense turbulence is almost always the best location for the feed. For geometrically similar mixing vessels, the local turbulence energy dissipation rate per unit mass is generally proportional to the overall power per unit volume, so the two criteria are essentially the same. In some cases, as shown in Example 13-3, equal selectivity on scale-up, even to a pilot scale vessel, cannot be achieved, and an in-line mixer is required. Results such as this are controlled by the local intensity of turbulence.

Scale-down for development and scale-up to manufacturing will benefit from consideration of the key points related to reactions and mixing. The idea of a local

mixing rate, as described above, is the central point, but it is only one of several issues. Interactions between reactions are always of concern. The way in which the feed is added is also critical: Concentrations should be held constant, the addition time must be slow enough to allow mixing to proceed before reaction, and the possibility of feed pipe backmixing must be avoided. Finally, the heat transfer surface area per unit volume will decrease on scale-up, possibly leading to hot spots in the vessel. These issues apply for all reactions but may be fully understood in the context of a simple single-phase (i.e., homogeneous) reaction. Additional issues must be considered for heterogeneous reactions. Experimental protocols for scaled-down development of all cases are provided in Section 13-4.3.

13-4.1 General Mixing Considerations

When it is suspected that a reacting system is subject to mixing effects, scale-up can be particularly critical since most organic reactions have multiple by-products. Success or failure on scale-up could be determined not only by the selectivity of the desired product, as it affects costs, but also by the ability to maintain the ratio of other by-products constant to minimize effects on product quality and downstream processing. Increases in by-products as little as 0.1% can be a significant problem.

13-4.1.1 Effect of Concentration on Yield for Competitive Consecutive Reactions. The molecular rates of the chemical reactions taking place in a mixed reactor are determined by rate constants, concentrations of reactants, and temperature. At a given temperature the rate of a second-order reaction in moles per unit volume per unit time depends on the product of the rate constant and the concentrations of the reactants. A characteristic time of reaction is the reciprocal of the product of the rate constant and a representative concentration (the geometric average or the resident reactant concentration in a semibatch reactor). As discussed in Section 13-1.3, the concentration at which the chemical reaction becomes faster than the mixing is the critical concentration at which conversion and yield will be affected by mixing. The correlation presented in Figures 13-2 and 13-3 illustrates the local concentration effect. Again, it is emphasized that the relative reaction rate at a point in the reactor is proportional to the product of the rate constant and the *local* concentration.

The data of Paul and Treybal (1971; see Figure 13-35), Middleton et al. (1986; see Figure 13-32), and Baldyga and Bourne (1992; see Figure 13-34), were analyzed to determine the approximate impeller rotation rate where the yield began to drop substantially: 160 rpm at 0.1 kW/m^3 for the 0.065 m^3 (65 L) Baldyga and Bourne vessel, 600 rpm at 5 kW/m^3 for the 0.03 m^3 (30 L) Middleton et al. vessel, and 400 rpm at 0.2 kW/m^3 for the 0.05 m^3 (5 L) Paul and Treybal vessel. At those rotation rates the mixing time constants were determined using the best available values of L_S and ε. The time constants for the reactions were determined as $k_{R2}C_{B0}$, where k_{R2} is the molecular rate constant of the second chemical reaction and C_{B0} is the initial concentration of the resident reactant in the vessel.

These values were combined into a mixing Damkoehler number as the ratio of mixing time constant to reaction time constant:

$$Da_M = \frac{\tau_M}{\tau_R} = \left(\frac{L_s^2}{\varepsilon}\right)^{1/3} k_{R2} C_{B0}$$

The mixing Damkoehler numbers obtained were 0.050, 0.032, and 0.023, respectively. These are reasonably close for such radically different experimental conditions: vessel size, impeller rotation rate, feed location, and concentration.

Baldyga and Bourne (1992) have used a similar Damkoehler number approach to determine the relative importance of *microscale mixing*, the time constant of which is given by eq. (13-16) and *mesoscale mixing*, the time constant of which is given by the first term in the Corrsin equation [eq. (13-13)]. For the typical case where the mesoscale mixing is controlling (see Section 13-2.1), the biggest change in yield seems to occur between mixing Damkoehler numbers as defined above of 0.01 and 0.05, which corresponds well with the analyses of the chemical reactors above.

Generally, it is recommended that bench and pilot data for mixing sensitive reactions be obtained at the same concentrations as are to be used in the commercial plant. That eliminates concentration as a concern in scale-up.

13-4.1.2 Concentration Effects in Parallel Reactions: Product Degradation Due to High pH. The effect of concentration may be very significant in the case of the use of a strong acid or base in pH adjustment. These pH adjustments actually are parallel reactions if the desired components can react with the acid or base. In addition to the neutralization reaction, a parallel reaction between the acid or base and the desired components (possible decomposition) may occur that is mixing dependent (see Example 13-8b). A common practice is the use of concentrated acid or base in production to minimize semibatch volume changes and to avoid the use of dilution equipment. An increase in unwanted decomposition could result on scale-up if the mixing effectiveness is not provided to overcome the increased feed concentration. In cases with a higher sensitivity to pH extremes, mixing intensity alone may be insufficient and dilution of the acid or base may be required to avoid yield loss and impurity generation. When appropriate, a weaker acid or base may be substituted as utilized by Paul et al. (1992) and Example 13-8b.

13-4.1.3 Effect of Feed Rate or Addition Time on Yield. The importance of feed rate on yield for a mixing-sensitive reaction has been well demonstrated by Baldyga and Bourne (1992). The time of addition of a reagent in a semibatch reaction is often increased on scale-up to production equipment because of heat transfer limitations (Chapter 14). In the case of a reaction that is sensitive to mixing, the time of addition often is increased on scale-up to account for the increase in blend time of the reagent (A) in the vessel with the added reagent (B) to maintain expected molar ratio at the feed point. The minimum feed time

to achieve expected yield is, therefore, scale dependent. Shorter feed times will result in reduced yield. At feed times greater than the minimum for that scale, the yield becomes independent of feed time, assuming that there is no parallel decomposition reaction that continues to produce unwanted by-product with time, as discussed in Section 13-3.3. The minimum feed time for expected yield is a function primarily of the rate constant of the primary reaction and the mixing intensity at the point of feed introduction and is, therefore, a mesomixing issue.

13-4.1.4 Feed Pipe Backmixing. Backmixing into reactor feed pipes can also lower yield by causing a slower overall mixing rate of the reactants. Jo et al. (1994) have shown that feed pipe backmixing can have a significant effect on yield, and they developed recommendations for v_f/v_t, the feed pipe exit velocity divided by impeller blade tip velocity. For turbulent flow in the feedpipe, Table 13-11 gives minimum values of v_f/v_t. For feedpipe laminar flow, $v_f/v_{t,min}$ was always lower than for turbulent flow. A good rule of thumb for turbulent flow is to design for $v_f/v_t > 0.5$ except for case 1, where $v_f/v_t > 2$ is necessary.

13-4.1.5 Hot Spots. For exothermic reactions, yields may be substantially lower in a large vessel than in bench or pilot scale vessels, particularly if the activation energy for the reaction producing the unwanted product is very high. This effect can result from hot spots (high localized temperatures) in a reactor that can develop because the rate of heat removal by mixing is insufficient for the rate of addition (e.g., adding water to sulfuric acid). The high local temperatures overcome activation energies that are a barrier to reaction on the small scale. This mesomixing effect has been illustrated using the simulations by Randick (2000) [see also Patterson and Randick (2000) and Section 13-5]. Design for heat transfer requirements is discussed in Chapter 14.

13-4.2 Scale-up of Two-Phase Reactions

13-4.2.1 Scale-up of Gas–Liquid Reactions. The many types of gas–liquid reactions require different considerations on scale-up. In addition to the discussions

Table 13-11 Recommended Minimum v_f/v_t For Selected Geometries for Turbulent Feed Pipe Flow Conditions

Case	Impeller	Feed Position	D/T	G/D	$v_f/v_{t,min}$
1	6BD[a]	Radial/midplane[b]	0.53	0.1	1.9
2	6BD[a]	Above/near shaft[c]	0.53	0.55	0.25
3	HE-3[d]	Radial/midplane[b]	0.53	0.1	0.1
4	HE-3[d]	Above/near shaft[c]	0.53	0.55	0.15

Source: Jo et al. (1994), Table 5.

[a] Six-blade disk turbine.

[b] Injection radially inward toward the impeller at its midplane at a distance G/D.

[c] Injection downward into the impeller at about D/4 from the centerline of the impeller shaft and G/D above the impeller midplane.

[d] High efficiency three-blade down-pumping turbine.

in Section 13-3, the reader is referred to Chapters 7, 11, and 18 and to Examples 13-5 and 13-6.

13-4.2.2 Scale-up of Liquid–Liquid Reactions. Despite the frequent need to run reactions in immiscible liquid systems, the reliability and applicability of correlations to predict drop size distribution and surface area of the dispersed phase, especially in the presence of reactions, is limited. The reader is referred to Chapter 12 and Section 13-3.5. This problem is due in part to effects that small changes in physical aspects such as small agitator blade width can have on dispersed phase drop size as well as on surfactant effects resulting from reacting substrates. It is sometimes even difficult to predict which phase will be continuous and which dispersed. Although this factor is normally a property of a given system, it can sometimes be reversed by the manner in which the phases are contacted (i.e., by mixing during addition as opposed to starting with both phases present).

Extreme care must be taken during laboratory and piloting studies to determine the extent to which interfacial differences are significant so that the impact of changes in dispersion that are very likely to occur on scale-up can be evaluated. In many cases these changes may not be significant because other aspects of the reacting system are controlling. However, phase dispersion can be critical to selectivity in some cases because of complex interfacial interactions. Selection of impellers and speeds to achieve the desired drop size distribution (which has a direct effect on settling rate) can also be critical to reactions that require subsequent phase separation.

The uncertainties inherent in scale-up of liquid–liquid systems, especially if selectivity is affected, require testing over a wide range of operating conditions in the laboratory and possibly the pilot plant to determine the sensitivity of each system to changes in dispersion characteristics. These studies should include mixing configurations and impeller speeds as well as system compositions. Despite these qualifications, much can be gained from applying scale-up correlations to specific problems to establish guidelines and limits for performance. As in the case of gas–liquid systems, the reader is referred to the texts of Oldshue (1983), Tatterson (1991), and Harnby et al. (1992).

Scale-up from laboratory data on the same system can be predicted to some extent. Constant power per unit volume is a good guide, but care must be taken with large tanks and density differences, as mentioned above. Two-phase mixing effects on chemical reactions generally result when the mass transfer rate required to bring the reactants together is much slower than the chemical reactions. This can occur for gas–liquid systems, where the chemical reaction occurs in the liquid phase or in solid–liquid systems, where reactants must diffuse to the solid surface to react. In liquid–liquid systems an interphase mass transfer effect, a droplet coalescence and dispersion effect, and an intraphase mixing effect can be present: for instance, in the case where internal circulation in droplets accounts for the mixing of the diffusing reactant with the droplet-resident reactant. (See Chapter 12 for mass transfer rates in these cases, and Example 13-8a.)

13-4.2.3 Scale-up of Liquid–Solid Reactors. Fluid dynamic scale-up of liquid–solid suspensions has been well characterized by many studies. The reader is referred to Chapter 10 for a comprehensive discussion. For reacting systems, power and speed should in some cases be above the minimum for homogeneous suspension since energy consumption is generally a smaller contributor to cost than other aspects of scale-up uncertainty (conversion and selectivity). Even this recommendation must be qualified by the potentially negative aspects of overmixing, as discussed in Section 13-3.6.2. Reacting solids can also agglomerate and thereby require large increases in energy to maintain adequate dispersion.

These system-dependent properties are extremely difficult to characterize quantitatively and require specific scaling studies at extremes of possible operating ranges to determine sensitivity. Such systems are primary contributors to the case for built-in versatility. The more important consideration in reacting systems than solid suspension may be mass transfer rate since considerably more power and speed may be required to achieve expected reaction rate for reacting solids than that required for homogeneous suspension. As discussed in Section 13-3, selectivity can also be affected in complex reactions because of the potential overreaction in the diffusive film around the dissolving or precipitating particles. An excellent discussion of mass transfer and reaction is presented by Fogler (1999).

Another critical aspect determining the effectiveness of mass transfer correlations for prediction of coefficients in reacting systems is the very troublesome but all-too-common tendency for the surface of a reacting solid, catalyst, or precipitating product to become covered by another solid or second phase liquid, or by a gas in a three-phase mixture. The gas or vapor can also come from entrainment from the headspace. Such a heterogeneous film would obviously have a profound effect on the expected mass transfer coefficient and in many cases can cause a reaction to stop before the expected conversion is achieved. These films are obviously unique to each reacting system, thereby preventing any generalizations as to whether they are susceptible to chemical or physical manipulation. Chemical manipulation could be achieved by addition of a surfactant that would be able to modify surface properties to prevent or modify formation of the film.

Physical manipulation of such films may be possible through variation in mixing intensity, primarily by local shear. Such interactions would be very scale dependent and could readily be masked in smaller scale operations. The extent to which reactions can be affected by coating of particles is illustrated in an excellent example by Wiederkehr (1988). This study also includes other aspects of reaction system design, such as the choice of continuous smaller volume reactors over batch reactors to reduce the size (and potential energy) of the reacting mass as well as the criticality of residence time distribution in complex reactions.

13-4.3 Scale-up Protocols

The concepts embodied in the mixing Damkoehler number (Da_M) are extremely useful for initial evaluation of reaction conditions in which mixing effects must

be considered:

$$\mathrm{Da_M} = \text{mixing time/reaction time} = \frac{\tau_M}{\tau_R}$$

These interactions are shown in Figure 13-2, in which Y/Y_{exp} is plotted against an expression of Da_M using k_{R1} as a measure of reaction rate and in Figure 13-3, in which X_S, a measure of overreaction product, $2S/(2S + R)$, is plotted against an expression of Da_M that uses k_{R2} as a measure of the overreaction rate.

The reaction rate constant of the consecutive reaction, k_{R2}, can vary over several orders of magnitude and for a particular reaction, the magnitude of k_{R2} can be estimated within two orders of magnitude or less. The mixing rate in vessels should not vary by more than two orders of magnitude. With these bracketed values, upper and lower limits on Da_M can readily be estimated and used as a first measure of mixing sensitivity by using the estimates of Bourne (Sharratt, 1997) for three regions of mixing sensitivity as follows:

$Da_M < 0.001$	when reaction rate is much slower than mixing rate and chemical kinetics only determine selectivity
$Da_M > 1000$	when reaction rate is much faster than mixing rate and the selectivity could approach asymptotic limit in the instantaneous reaction
$0.001 < Da_M < 1000$	when reaction and mixing rates compete and both micromixing and chemical kinetics must be considered

These concepts can be further utilized in a developmental program for a new chemical reaction as summarized in the following brief outline of an experimental protocol for a homogeneous reaction. Similar protocols for heterogeneous reactions are outlined in Sections 13-4.3.2, 13-4.3.3, and 13-4.3.4.

13-4.3.1 Scale-up Protocol for Homogeneous Reactions. Chemists report a yield of R of 68% for a reaction in which they added reagent B to A in the ratio 1.05 A/B in a round-bottomed flask with paddle impeller over a 1 h period with cooling to control the temperature at 50°C. A and B are both dissolved in solvents that are miscible in all proportions. B is consumed completely. The amounts of unreacted A and by-product S in the final reaction mixture were determined analytically to be 19% and 14%, respectively. Evaluation of the effectiveness of mixing in the round-bottomed flask can be useful but is difficult to characterize, as the types of impellers often used provide good circulation but low shear. The small scales involved may mask mixing effects.

The development and scale-up of this reaction is now taken on by the chemical engineering group, who need to answer the following questions:

1. Is this the maximum yield that can be obtained in this reaction?
2. Was there an effect of mixing in the laboratory?

3. Could there be an effect of mixing on scale-up?
4. What reactor design is most suitable for a large production requirement?

Experimental work and modeling/simulation are both to be utilized. A few key experiments are required at the outset that require setup of a scalable laboratory reactor (preferred minimum volume 0.004 m^3 (4 L) and materials that are compatible with the reacting materials—assuming in this case stainless steel, fully baffled flat or pitched blade impellers in standard configuration (see Chapter 6).

The apparent rate constant ratio can be calculated from the reported yield of 68% using eq. (13-5), resulting in $k_{R2}/k_{R1} = 0.14$. The question is whether or not the chemists' yield is less than the maximum for this reaction because the flask was not sufficiently mixed to achieve the conditions for perfect mixing and the maximum yield. This question can be answered by running the reaction with increasing mixing intensity to determine whether the yield is sensitive to mixing. Addition of B on the surface when compared to the optimum position at the impeller should be compared. The mixing rates at these two extremes of addition points can vary by a factor of 10 or more.

For this reaction system, at each increased mixing intensity, even with feed into the impeller, the yield continued to increase. This information can be used to evaluate a range for Da_M in Figure 13-2 and/or 13-3 that would indicate mixing sensitivity by noting that concentration and k_{R2} are constant but mixing rate is increasing, giving lower values of Da_M. By not reaching a constant minimum value of Da_M, it can also be concluded that mixing effects are still preventing achievement of the maximum yield, Y_{exp}. To determine the true Y_{exp} value for this reaction system, the rate constants can be determined separately and their ratio used to calculate the true Y_{exp} from eq. (13-5):

$$Y_{exp} = \frac{R}{C_{A_o}} = \frac{1}{1-\kappa}\left[\left(\frac{C_A}{C_{A_o}}\right)^{\kappa} - \frac{C_A}{C_{A_o}}\right]$$

Note: If this yield is still not being achieved, further work is necessary to determine the cause since further increases in mixing would not appear to be effective. A very high shear device such as a rotor-stator or Waring blender could be tested to determine if the reaction is still too fast (Da_M too large) to realize the maximum possible yield (minimum X_S).

Da_M can be further reduced by dilution. Experiments at 10× dilution of B and A were run at increasing mixing rates. The yield leveled off at $Y = 0.75$, beyond which further increases in mixing rate had no effect. From this result, the actual rate constant ratio can be calculated as $k_{R2}/k_{R1} = 0.11$. Using this value, the amount of residual A and by-product S can be calculated by material balance and checked against the experimental results to determine that the original chemists' results did not achieve the maximum yield possible and that there is an effect of mixing on all scales. These results answer questions 1 through 3.

The absolute value of the primary rate constant should be estimated to help in design of a manufacturing scale reactor. The one hour addition time used by

the chemists to control the reaction exotherm does not provide any information on the magnitude of k_{R1} since this addition time was actually controlled by heat transfer, not by reaction kinetics. Methods for the evaluation of k_{R1} are available, including use of stopped-flow reaction techniques.

The mixing sensitivity found in the experiments above indicates that (1) the primary reaction can be described qualitatively as being very fast, and (2) the mixing rate achievable in a stirred vessel will not be sufficient to achieve Y_{exp}. This result indicates that an in-line mixer is a good choice since these devices can maximize the required local energy dissipation at the point of feed injection and achieve complete reaction in a short residence time. (Dilution of A and/or B is usually not feasible for productivity reasons even if a stirred vessel could then achieve the maximum yield, as determined above.) The absolute value of k_{R1} can be used to predict the contact time required after in-line mixing to complete the reaction. The use of an in-line mixer would require provision for heat removal for this exothermic system and would limit choices to designs that would address both heat exchange requirements and complete initial mixing. Injection of B along the mixer length with heat exchange between injection points may be feasible. An impinging jet mixer could also be considered for manufacturing assuming that the heat generated can be adequately removed or tolerated from the adiabatic temperature rise.

If an in-line mixer is not feasible and a stirred vessel is to be used, the design shown in Figure 13-11 is recommended to provide (1) high shear and micromixing at the lower turbine with proper placement of the feed line in the impeller discharge at the point of maximum energy dissipation rate, and (2) good circulation from the upper pitched blade. Prediction of applicable feed pipe diameter and feed velocity must be evaluated by methods described in Section 13-4.1.4 and in Jo et al. (1994).

The addition time on scale-up may have to be increased to account for the slower bulk mixing time and mesomixing effects, as discussed by Bourne and Thoma (1991). A critical minimum addition time can be determined experimentally above which X_S remains constant but below which X_S can increase. Note that the local mixing rate discussed above may be held constant on scale-up, but the addition time may have to be increased because the bulk mixing time will increase and affect the rate at which reagent A is circulated throughout the reactor. This can change the local A/B mole ratio, giving rise to mesomixing effects.

During or after this experimental program, the reaction system can be modeled and the results used to check experimental results and/or predict performance. For example, the engulfment model developed by Baldyga and Bourne (1999) and described further in Sharratt (1997) can be used to calculate the Da_M relationship to X_S (as in Figure 13-3) for this reaction, thereby establishing the appropriate region of Da_M and indicating the degree of mixing sensitivity. Full reaction simulation, discussed in Section 13-5 and summarized in Table 13-10, could be used for similar purposes, giving a more complete picture of scale-up requirements.

The actual value of Da_M for this reaction system may also be determined by measurement of the absolute value of k_{R2}, from which k_{R1} can be calculated

from the estimate of k_{R2}/k_{R1} that had been determined previously from Y_{exp} using eq. (13-5). Using the calculated mixing rate for a particular reacting condition, a value of Da_M can be calculated, a point on Figure 13-2 or 13-3 as they apply for the reaction of interest determined from this, and thus the Y_{exp} or X_S measured at this mixing condition. This point can be compared with the result from modeling and thereby provide excellent insight into the reactor design issues for the system.

The effects of higher and lower values of Da_M on reactor design are as follows:

- If X_S has reached a minimum value at a mixing rate that can be achieved on scale-up, a stirred vessel can be used to achieve Y_{exp}. At values of $Da_M < 0.001$, mixing is only necessary for blending and heat exchange, and the concerns about feed pipe placement and addition rate are not applicable. Caution must be used in reaching this conclusion, as even small increases in X_S can cause downstream problems in separation.
- If the lowest value of X_S that could be achieved was much larger than that predicted by k_{R2}/k_{R1} [independently measured using eq. (13-5) and a material balance to calculate X_S from R and S], a possibly severe yield loss can be expected, and new conditions for this step are required.

Note: This protocol is focused on mixing effects for the classic competitive-consecutive reaction system. Reaction systems may also include parallel reactions in which A, B, or R are reacting to form unwanted products that are not represented by the consecutive-competitive system as used to derive eq. (13-5). To keep these reactions from making more unwanted products on scale-up, the overall reaction (addition) time may have to be held constant. In this case, the mesomixing issue for the primary reactions, $A + B \rightarrow R$ and $R + B \rightarrow S$, would predict that more S would be formed. These issues may require selection of an alternative reactor, such as an in-line mixer, for successful scale-up.

13-4.3.2 Scale-up Protocol for Solid–Liquid Reactions. Refer to Section 13-4.3.1 and change reagent B from being dissolved in a miscible solvent to being added as a fine powder, all other factors remaining unchanged.

A fifth question must be added to the four questions in the developmental strategy for homogeneous reactions:

5. Does the particle size and/or addition time of B affect yield (mesomixing)?

In addition to running the reaction with increased mixing intensity, the effect of particle size and addition time can be evaluated by running at two or three different particle sizes and addition times. If the yield continues to increase with decreasing particle size, increasing addition time, and increased mixing rate, mixing conditions are clearly demonstrated to be critical. The maximum possible yield may not have been achieved because these three factors can all affect overall reaction time, the degree to which by-products can form in the films, and the continuous phases in consecutive and parallel reactions. All experiments must be

run at impeller speeds at or above N_{js}, as defined and discussed in Chapter 10, to be valid representations of solid–liquid mixing.

Unlike homogeneous reactions, even in the laboratory, overall reaction time can have an effect on yield that is caused by the effect of mixing on mass transfer rate if there are parallel reactions in the continuous phase or in the films between phases. With slower mass transfer, these reactions have longer to generate by-products—often decomposition products—so that time of reaction is important on all scales. Determination of this possibility must be included in the experimental plan. Increased amounts of S and other by-products for longer overall reaction times would indicate this sensitivity to mass transfer rate.

For a heterogeneous system, a possible method of determining the maximum possible yield is to find a solvent system in which the reactants and products are soluble and miscible, thereby creating a homogeneous environment. As in the previous outline, high dilution may be required. Again, assuming that these changes can be tested and a yield plateau can be reached, this may be the maximum yield possible. This conclusion can be verified by separate determinations of k_{R1} and k_{R2} and calculation of the maximum yield from eq. (13-5), as before. If the k_{R1} and k_{R2} predict a still higher maximum yield, the mixing effect has reached its asymptotic value, and other factors may be the cause; in this case the reactions are not a classic consecutive-competitive system.

The scale-up recommendations for in-line mixers with very fast homogeneous reactions must be modified for many cases for heterogeneous reactions because in-line reactors may not be feasible with, for example, high solids content from dissolving reactants or crystallizing products. Achievement of the required mass transfer rates in all types of heterogeneous systems may also be an issue, and the reader is referred to the appropriate chapters and examples for discussions of these factors. As cautioned above and discussed in Example 13-7, heat exchange requirements for fast reactions in in-line mixers may be limiting.

13-4.3.3 Scale-up Protocol for Gas–Liquid Reactions. Refer to Section 13-4.3.1 and change reagent B from being dissolved in a miscible solvent to being added as a gas, all other factors remaining unchanged.

A fifth question must be added to the four questions in the developmental strategy for homogeneous reactions:

5. Does the gas–liquid mass transfer rate and its influence on addition time of the gas, reagent B, affect yield?

The reaction can be run under differing mass transfer rates by changes in impeller speed and system pressure. These changes can also affect the addition time necessary for completion of gas uptake. If the yield increases with increased mass transfer (higher impeller speed and/or higher system pressure), mixing conditions are clearly demonstrated to be critical. The maximum possible yield may not have been achieved because these factors can all affect overall reaction time and the degree to which by-products can form in the films and the continuous phases in consecutive and parallel reactions.

An additional influence on mass transfer rate can be the type and location of the gas sparger. In the case of ineffective sparging, the reaction may be very slow because the reagent gas is passing through the liquid before it can react, either because of small gas–liquid surface area or because of poor sparger location. Alternative gas–liquid contacting methods are discussed in Chapter 11 and Section 13-3.4. For exothermic reactions, caution must be taken when increasing mass transfer rate because of increased heat transfer requirements.

Unlike homogeneous reactions, even in the laboratory, overall reaction time can have an effect on yield that is caused by the effect of mixing on mass transfer rate if there are parallel reactions in the continuous phase or in the films between phases. With slower mass transfer, these reactions have longer to generate by-products—often decomposition products—so that time of reaction is important on all scales. Determination of this possibility must be included in the experimental plan. Increased amounts of S and other by-products for longer overall reaction times would indicate this sensitivity to mass transfer rate.

The scale-up recommendation on in-line mixers for very fast homogeneous reactions must be modified in many cases for heterogeneous reactions because in-line reactors may not be feasible with, for example, high gas–liquid ratios (see discussion in Chapter 7). As cautioned above and discussed in Example 13-7, heat exchange requirements for fast reactions in in-line mixers may be limiting.

13-4.3.4 Scale-up Protocol for Heterogeneous Liquid–Liquid Reactions. Refer to Section 13-4.3.1 and change reagent B from being dissolved in a miscible solvent to being added in a solvent that is immiscible with the solvent containing dissolved A. All other factors remain unchanged.

A fifth question must be added to the four questions in the developmental strategy for homogeneous reactions:

5. Does the drop size distribution and/or addition time of the solution containing B affect yield?

To determine the effect of mixing on the reaction rate, the reaction should be run with increasing mixing intensity. If the reaction rate continues to increase, the effectiveness of mixing on drop size dispersion is clearly demonstrated to affect mass transfer rate. If there is no increase in reaction rate, the chemical kinetics may be controlling.

The addition time of B may not be an important variable since the reaction time may be determined by the mass transfer rate and it would be advantageous to add all of the B solution early to maximize this rate. One exception would be a fast reaction with high mass transfer rate, which could cause heat removal to be the limiting factor.

If it is shown that shorter reaction times result in improved selectivity, a parallel or consecutive reaction in the bulk or in the liquid–liquid films around the reacting drops could result in significant yield loss if the reaction time (mass transfer) is not duplicated on scale-up. In this case, scale-up of drop size distribution is critical. The reader is referred to Chapter 12 for a comprehensive

discussion of this issue. As indicated in the Editors' Introduction, this is one of the more difficult reaction scale-up problems because drop size distributions in a large vessel with broader dispersion–coalescence rates than in small vessels can be very difficult to duplicate.

If reaction time is found to be critical, in-line mixers can be considered for liquid–liquid reactions because of their effectiveness in creating scalable drop size distributions and mass transfer rates (see Chapter 7 and Example 13-8a).

13-5 SIMULATION OF MIXING AND CHEMICAL REACTION

The methods for reactor design and scale-up described above are the usual approach to achieving a workable and economic reactor system when mixing and reaction interact. A better understanding of this interaction is needed than is available from scaling concepts alone: mixing and reaction may interact over a wide range of scales, particularly in the realm of mesomixing effects. Without the more detailed results available from simulations, these issues cannot be fully addressed. Detailed spatial simulation of the reactor using computational fluid mechanics (CFD; see Chapter 5) as the starting point is useful and can often be enlightening for some design and scale-up problems, where, for example, local concentrations and temperature are critical to the success of the process.

Efforts to link mixing and reaction rates to local flow and turbulence characteristics in combustion applications have proceeded independent of mixed reactor work in fine chemical applications. In combustion, the relationships between the degree of conversion and the degree of mixing usually depend on either a chemical equilibrium approximation or an instantaneous local mixing assumption [see the review by Patterson (1985)]. The rate of local mixing for the first approximation is almost always based on some variation of eq. (13-14), the Corrsin (1964) equation for gases, which makes use of the local rate of turbulence energy dissipation and the local concentration length scale.

Most early work on mixing effects in chemical reactors treated the reactor as a uniform field (box) with various processes (such as coalescence, reaction, and dispersion, called *C-D models*) occurring simultaneously or as a collection of environments, linked by flows, each of which had different mixing effects. Most of these models did not link the modeled effects directly to the local turbulence characteristics of the reactor, making them highly empirical. More recent models divide the reactor into zones, where accurate experimental data are available for the velocities and turbulence quantities. Although these models have provided some very useful results, significant process insight is required to develop them, and this is their main weakness. General models incorporated into CFD packages have the potential to overcome this limitation.

Models that couple the local reaction and mixing processes allow simulation of the spatial variations of concentrations due to mixing and diffusion, and thus the rates of chemical reaction. These coupled models usually use some type of computational fluid dynamics (CFD) computer program as a basis for the calculations, as discussed in Chapter 5. Simulation methods may be divided into those

using the Lagrangian (fluid element following) coordinate frame and those using the Eulerian (fixed in space) coordinate frame for computation. The Lagrangian coordinate frame is easiest to implement in one dimensional flows but becomes quite complex in three dimensions, so Eulerian simulations are the most common. The main exception is particle or fluid element tracking simulations which use the C-D model to simulate local mixing and chemical reaction.

Table 13-12 summarizes the main simulation methods that have been or are in use. In the discussion that follows, Eulerian methods based on time-averaged (or Reynolds-averaged) balance equations for the component concentrations and segregation will be emphasized, but the Lagrangian-oriented engulfment model and Monte Carlo coalescence–dispersion models are also presented.

13-5.1 General Balance Equations

Simulation of turbulent fluid mechanics, mass transfer, mixing, and chemical reaction requires the use of one (typically differential) balance equation for each

Table 13-12 Some of the Current Models Used for Determining Chemical Reaction Conversion and Yield in the Presence of Mixing

Model Name[a]	Authors and Refs.	Model Type	Frame	Implementation
Turbulent plug flow*	Vassilatos and Toor (1965); Patterson (1973)	Simplified closure	Eulerian or Lagrangian	1D flow
Blending controlled*	Middleton et al. (1986)	Null closure	Eulerian	CFD
Four-environment	Mehta and Tarbell (1983)	Mechanistic	Eulerian	Box or CFD
Spectral relaxation	Fox (1995)	Large eddy	Eulerian	CFD
Engulfment*	Baldyga and Bourne (1984, 1989); Baldyga et al. (1997)	Lamellar	Lagrangian	1D flow
Random walk mixing	Heeb and Brodkey (1990)	C-D	Lagrangian	1D flow
Mixing rate vs. reaction rate	Magnussen and Hjertager (1976)	Null closure	Eulerian	3D flow
Monte Carlo mixing*	Canon et al. (1977); van den Akker (2001)	C-D	Lagrangian	3D
Paired-interaction*	Patterson (1973, 1975, 1985)	Spiked PFD	Eulerian	CFD or 1D
β-PFD*	Baldyga (1994)	Continuous PFD	Eulerian	CFD
Direct numerical	Leonard et al. (1995)	No closure	Eulerian	CFD

[a] Those with an asterisk are discussed in some detail in this chapter.

variable to be solved. Commercial CFD codes generally use Reynolds-averaged variables, although work is progressing on large eddy simulations, where time-varying solutions are obtained for all but the smallest scales of motion. In the case of a chemical reactor, transport equations must be solved simultaneously for each velocity component (momentum per unit mass) and for the concentration of each chemical component. If Reynolds-averaged transport equations are used, differential balance equations for turbulence energies (k, averaged velocity fluctuations squared), some variable to relate turbulence energies to eddy viscosity (usually, the turbulence energy dissipation rate per unit mass, ε, leading to the famous $k-\varepsilon$ model), and segregations (s_i) for each chemical component must also be solved. Closure equations are required to relate Reynolds stresses in the momentum equations to the turbulence energy and energy dissipation rate and segregation in the concentration equations to averaged-concentration fluctuation correlations. The Reynolds stresses and segregation terms arise from the Reynolds averaging process. The reader is referred to the book by Bird et al. (1960) for a full explanation of Reynolds averaging and formation of the differential balance equations. The basic equations for the $k-\varepsilon$ model are not presented here [refer to Chapter 5 for the basics and to the book by Launder and Spalding (1972)].

The equations for component mass (concentration) and segregation used in the modeling of a second-order chemical reaction are as follows: For component mass,

$$\frac{D\overline{C_i}}{Dt} = \underbrace{\frac{\partial}{\partial x_j}\left(\frac{\nu_t \partial \overline{C_i}}{\sigma_c \partial x_j}\right)}_{\text{I}} \underbrace{-k_R(\overline{C_i}\,\overline{C_k} + \overline{c_i c_k})}_{\text{II}} \tag{13-27}$$

and for segregation ($\overline{s_i} = \overline{c_i^2}$),

$$\frac{D\overline{s_i}}{Dt} = \underbrace{\frac{\partial}{\partial x_j}\left(\frac{\nu_t \partial \overline{s_i}}{\sigma_s \partial x_j}\right)}_{\text{I}} \underbrace{+C_{g1}\nu_t\left(\frac{\partial \overline{C_i}}{\partial x_j}\right)^2}_{\text{III}} \underbrace{-\frac{2\overline{s_i}}{C_C(k/\varepsilon)}}_{\text{IV}} \underbrace{-k_R(\overline{C_i}\,\overline{c_i c_k} + \overline{C_k}\,\overline{s_i} + \overline{s_i c_k})}_{\text{II}} \tag{13-28}$$

A note on index notation is in order for those unfamiliar with its use. Index notation is used to shorten the transport equations that are presented above. Each index (shown as a subscript) can represent one of the three Cartesian directions or one of the chemical components. The index that appears on both sides of the equation in all or most terms is the *equation index*. If it is x, the equation is a balance for quantities in the x-direction; if it is 1, the equation is for chemical component 1. The indices that appear only on one side of the equation in occasional terms are running indices and take on each of the three values x, y, and z or each of the component values $1, 2, 3, \ldots$ such that the term in which they appear will have several forms that are additive. In the case of component values, indices of product components may not be equal. To illustrate use of the

index notation, the first component of eq. (13-27) is written out in full:

$$\frac{D\overline{C_1}}{Dt} = \frac{\partial}{\partial x_x}\left(\frac{\nu_t \partial \overline{C_1}}{\sigma_c \partial x_x}\right) + \frac{\partial}{\partial x_y}\left(\frac{\nu_t \partial \overline{C_1}}{\sigma_c \partial x_y}\right) + \frac{\partial}{\partial x_z}\left(\frac{\nu_t \partial \overline{C_1}}{\sigma_c \partial x_z}\right) - k_R[\overline{C}_1(\overline{C}_2 + \overline{C}_3) + \overline{c_1 c_2} + \overline{c_1 c_3}]$$

We now turn our attention to the physical meaning of each of the terms in eq. (13-27) and (13-28), as a discussion of the solution of the full differential equations is best treated elsewhere.

The left-hand sides of these equations are the substantial derivatives describing convective transport, or transport by bulk motion. Terms I are turbulent diffusion; terms II are the rates of decrease due to chemical reaction; term III is the Spalding (1971) rate of segregation production, where concentration fluctuations may increase with time as bulk mixing penetrates into previously uniform (but unmixed) portions of the vessel; term IV is the Corrsin (1964) rate of segregation decay or mixing without the Schmidt number term, which is usually small. The complete form of the Corrsin term is given in eq. (13-13), with the substitution of k/ε for $(L_S^2/\varepsilon)^{1/3}$.

A number of values have been proposed for the constant C_C. The value used here, $C_C = 2.2$, is based on a best fit to the data of Vassilatos and Toor (1965) for turbulent mixing in a tubular reactor (Zipp and Patterson, 1998). Corrsin predicted a value of C_C of about 4.0, but he used the term $(L_s^2/\varepsilon)^{1/3}$ instead of k/ε. Where the scales of the mixing lamellae are determined by the turbulent flow, that is, away from the influence of the feed jets, the term k/ε is considered to be about twice as large as $(L_s^2/\varepsilon)^{1/3}$ (Pope, 1985), which probably leads to the smaller constant. A value of 4.0, instead of the 2.7 recommended by Spalding (1971) and the 2.8 recommended later by Elghobashi et al. (1977), was used by Zipp and Patterson for C_{g1} because $C_{g1} = 4.0$ gave closer results for segregation production without reaction. This larger value does not correspond to Spalding's prescription of $C_{g1} = 2/\sigma_C$.

In following sections some methods for modeling the transport and reactions described by eqs. (13-27) and (13-28) are discussed and demonstrated. Particular attention is directed to terms containing the fluctuating concentration, c. All of these terms require modeling. This is the closure problem discussed at the beginning of the section. The objective is to determine the effect of mixing on the conversion and yield of competing chemical reactions.

13-5.2 Closure Equations for the Correlation Terms in the Balance Equations

Ever since Toor and co-workers (Vassilatos and Toor, 1965; Toor, 1969; Mao and Toor, 1971; Li and Toor, 1986) defined methods for relating reaction conversion for non-premixed reactants to their degree of mixing, workers in the field of mixed chemical reactors have attempted to build upon and refine their analysis,

which was based on the use of an assumed probability density function (PDF) for reactant concentration (see Donaldson 1975; Brodkey and Lewalle, 1985; Kosaly, 1987; Baldyga, 1994; Baldyga and Henczka, 1995). Pope (1985) presented an extensive review of concentration PDF closure methods for mixed chemical reactions, but only the spiked and β-PDFs are presented here.

The *paired-interaction closure* (Patterson, 1975, 1985) is one of the simplest closures and depends on a spiked PDF shown in Figure 13-27, which represents the probabilities of zero, maximum, and mean concentrations for each chemical component. The paired-interaction closures for $\overline{c_i c_k}$ for the reaction terms in both equations and for $\overline{s_i c_k}$ in the segregation equation are as follows:

$$c_i c_k = \frac{-\overline{s_i s_k}}{\overline{C_i C_k}} \tag{13-29}$$

$$\overline{s_i c_k} \simeq 0 \tag{13-30}$$

The assumption of $\overline{s_i c_k}$ equal to zero is based on the idea that since s_i is always positive, its correlation with c_k should be much smaller in magnitude than the correlation of c_i with c_k.

A more representative PDF for the mixing process is the beta-probability density distribution (β-PDF), which has been used by Baldyga (1994) and Baldyga

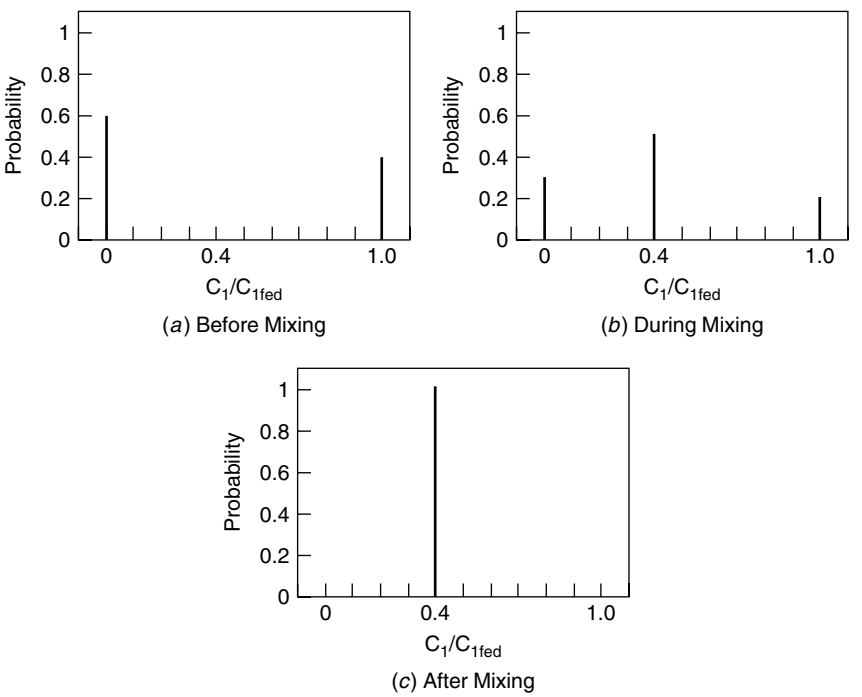

Figure 13-27 Spiked PDF for paired-interaction closure.

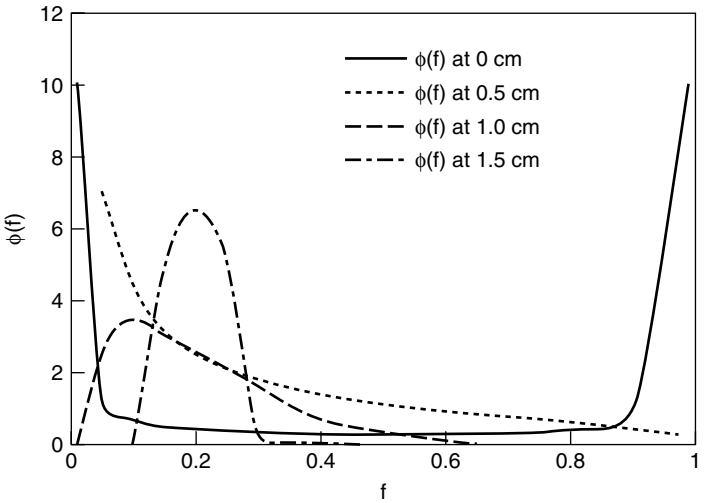

Figure 13-28 β-PFD versus distance downstream in a mixing pipe. (Based on the data of Vassilatos and Toor, 1965 and Baldyga, 1994.)

and Henczka (1995, 1997) to simulate chemical reactions with turbulent mixing. The β-PDF is gradually transformed from a heterogeneous mixture of pure components to a homogeneous solution with a peak at the average concentration as shown in Figure 13-28. The equations that describe the β-PDF are as follows:

$$\phi(f) = \frac{f^{v-1}(1-f)^{w-1}}{\int_0^1 u^{v-1}(1-u)^{w-1}\,du} \tag{13-31}$$

where

$$v = f\left[\frac{f(1-f)}{s-1}\right] \quad \text{and} \quad w = (1-f)\left[\frac{f(1-f)}{s-1}\right]$$

The product of the β-PDF with the reactant concentrations is integrated at all points to obtain the mean of the product of instantaneous concentrations. When this is multiplied by the reaction rate constant, the last term of eq. (13-27) becomes

$$k_R(\overline{C_i C_k}) = k_R(\overline{C_i}\,\overline{C_k} + \overline{c_i c_k}) = k_R \int_0^1 C_i(f) C_k(f) \phi(f)\,df \tag{13-32}$$

In this set of equations f represents the concentration of a nonreacting (passive) scalar, which is depicted by the following equation:

$$f = \frac{C_i - C_k + C_{ko}}{C_{io} + C_{ko}} \tag{13-33}$$

In the application of this closure it is assumed that the rate of chemical reaction has no effect on the rate of mixing, which is, however, inherent in eq. (13-28). The current value of segregation, s, is computed with the Corrsin equation, eq. (13-13), modified as in eq. (13-28). Therefore, eqs. (13-13), (13-27), and (13-28) (omitting the last term) and eqs. (13-31) through (13-33) constitute the β-PDF closure. Typically, the closure is applied to the first reaction of a competitive-consecutive reaction scheme ($A + B \rightarrow R$; $R + B \rightarrow S$) and to both reactions of a competitive-parallel reaction scheme ($A + B \rightarrow R$; $A + C \rightarrow S$). Baldyga (1994) and Baldyga and Henczka (1995, 1997) demonstrated the use of this β-PDF closure for the plug flow pipe reactor [data by Vassilatos and Toor (1965)], an opposed jet reactor, and a concentric jet flow into a pipe reactor. Good results were shown for all geometries.

13-5.3 Assumed Turbulent Plug Flow with Simplified Closure

If the mixing of two fluids flowing downstream in a pipe mixer can be assumed to be occurring in a plug flow at a given turbulence energy and energy dissipation rate, the mixing rate and rate of chemical reaction can be computed. This approach is particularly applicable to the multiple-jet header issuing reactants into a pipe and the static mixer geometries. The following equations then apply for the concentration and segregation of each reacting component with the paired-interaction closure (see Section 13-5.2) used for the c_i and s_i terms. Other closures may be substituted.

$$\frac{d\overline{C_i}}{dx} = -\frac{k_R(\overline{C_iC_j} + \overline{c_ic_j})}{U_x} \tag{13-34}$$

$$\frac{d\overline{c^2}}{dx} = -\frac{k_R(\overline{c_i^2}\,\overline{C_j} + \overline{C_i}\,\overline{c_ic_j})}{U_x} - \frac{\overline{c_i^2}}{\tau_M U_x} \tag{13-35}$$

$$\overline{c_ic_j} = -\frac{\overline{c_i^2c_j^2}}{\overline{C_iC_j}} \tag{13-36}$$

Equation (13-13) is used to compute τ_M with $L_S = 0.39k^{3/2}/\varepsilon$ if the turbulence energy k instead of segregation scale L_S is used. Initial values of $\overline{c_ic_j}$ should be set equal to the products of the initial concentrations of the reactants as if they were completely mixed. If the mixing time constant is very small, $\overline{c_ic_j}$ will quickly become zero and $d\overline{C_i}/dx = -k_R(\overline{C_iC_j})$, making the molecular kinetic rate equation valid. Note that no segregation production term is used, since no segregation production is expected beyond the maximum assumed at the injection point. This is because the scale of segregation is already comparable to the size of the grid at injection.

Use of this one dimensional method leads to results that compare well with experimental data taken in the pipe reactor of Vassilatos and Toor (1965), shown in Figure 13-29. The value of U_x was 0.75 m/s. The chemical reaction was

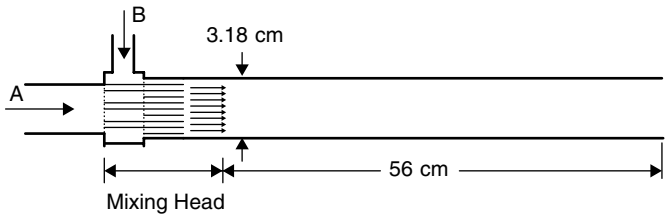

Figure 13-29 Schematic of tubular reactor with multiple injector header used by Toor and co-workers and by Brodkey and co-workers.

an acid–base neutralization ($H_2CO_3 + NaOH$) with $k_R = 12\ 400\ m^3/kmol \cdot s$. Injection concentrations were 0.025 and 0.031 $kmol/m^3$, giving a reactant ratio of 1.26. Values of L_S and ε, as determined from experimental data obtained in the same geometry by McKelvey et al. (1975), varied from the injection point to the pipe outlet; L_S increased from a low of 0.0005 m to level out at 0.0050 m, and ε decreased from a high of 7 m^2/s^3 to level out at 0.2 m^2/s^3, all in a distance of 0.065 m. Beyond 0.065 m these values were nearly constant at the center of the pipe. Comparison of the simulation results with the experimental results for the pipe reactor is shown in Figure 13-30.

Data for a Kenics twisted-ribbon static mixer geometry obtained by Baldyga et al. (1997) is shown in Figure 13-31. In this case only final yields for a complex reaction were measured. The static mixer used by Baldyga et al. (1997) was 0.04 m in diameter. The method developed above was used to simulate the reactions in the static mixer. Even though it is not true in individual elements of the static mixer, plug flow overall was assumed. Also, in contrast with the

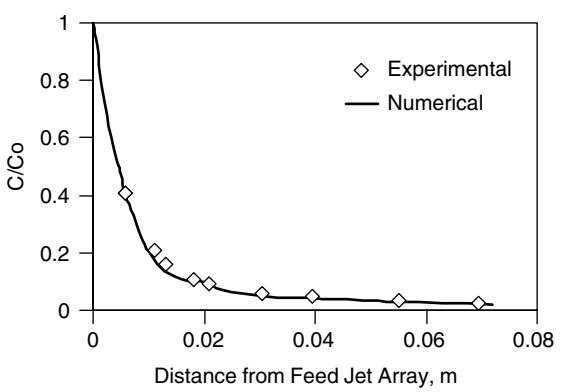

Figure 13-30 Normalized concentration downstream of the feed jet array in the Toor tubular reactor for $k_r = 12\ 400$ L/mol · s; reactant feed ratio of 1.26 and an average velocity of 0.75 m/s. The experimental values of Vassilatos and Toor (1965) are compared to simulation values using paired-interaction closure. The reaction was a single second-order acid–base neutralization.

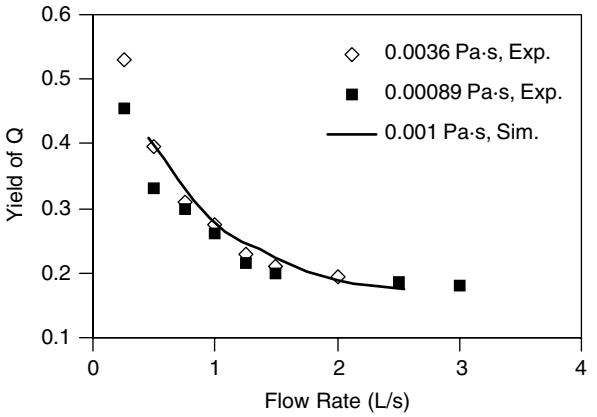

Figure 13-31 Comparison of the Baldyga et al. data for mixed reaction in a static mixer with results of paired-interaction closure for the reaction $A + B \rightarrow$ p-R + o-R; p-R + o-R + $B \rightarrow S$; $AA + B \rightarrow Q$. (See Baldyga et al., 1997, for details.)

mixing-head pipe mixer discussed above, the values of L_S and ε were assumed constant since they were generated by the mixing elements throughout the static mixer. Details of this one dimensional simulation are given in Example 13-9. If significant radial blending must be accounted for in such a simulation, a two or three dimensional simulation using CFD may be necessary.

Example 13-9: Yields from a Static Mixer Reactor Assumed to Be Plug Flow. The approach given in eqs. (13-34) to (13-36) may be used to compute the yield values for a static mixer reactor. Following Baldyga et al. (1997), the pipe radius divided by 2 was assumed as an approximation of the mixing scale, L_S. The method may easily be modified to compute conversions and yields as a function of distance downstream for any turbulent plug flow reactor and set of chemical reactions if realistic feed conditions can be given.

The chemical reactions with their respective rate constants in the Baldyga et al. case may be depicted as follows:

$$\begin{aligned}
A + B &\rightarrow \text{p-R} \qquad k_{R1} = 12\ 238\ \text{m}^3/\text{kmol} \cdot \text{s} \\
A + B &\rightarrow \text{o-R} \qquad k_{R2} = 921\ \text{m}^3/\text{kmol} \cdot \text{s} \\
\text{p-R} + B &\rightarrow S \qquad k_{R3} = 1.835\ \text{m}^3/\text{kmol} \cdot \text{s} \\
\text{o-R} + B &\rightarrow S \qquad k_{R4} = 22.25\ \text{m}^3/\text{kmol} \cdot \text{s} \\
AA + B &\rightarrow Q \qquad k_{R5} = 125\ \text{m}^3/\text{kmol} \cdot \text{s}
\end{aligned}$$

Since the static mixer has a diameter of 0.04 m, the value of L_S is given as 0.01 m, one-half the radius, and is assumed to be constant, although that is a strong approximation. Normalized values of the reactants and products were

computed for comparison with the experimental results as A/A_0, B/B_0, $p\text{-}R/B_0$, S/B_0, Q/B_0, and AA/AA_0. The values of ε at various flow rates were calculated from pressure drop data given by the authors and were as follows:

Q (m^3/s)	ε (m^2/s^3)
0.0005	1.38
0.0010	11.0
0.0015	37.1
0.0020	88.0
0.0025	171.9

The values of Sc and ν were taken to be 2000 and 0.89×10^{-6} m^2/s. The resulting yields for flow rates ranging from 0.0005 to 0.0025 m^3/s are shown in Figure 13-31, where they are compared with the experimental data. The experimental data showed that the viscosity had some effect on the yield of Q at low flow rate, and therefore at low mixing rate, but little effect at the higher flow rates. The simulations focused on the effect of geometry, so viscosity was held constant.

The equations that were solved to obtain the simulated yields are as follows:

$$\frac{dC_A}{dt} = -k_{R1}(C_A C_B + c_A c_B) - k_{R2}(C_A C_B + c_A c_B) \qquad C_{A0} = 0.02 \text{ kmol/m}^3$$

$$\frac{dC_B}{dt} = -k_{R1}(C_A C_B + c_A c_B) - k_{R2}(C_A C_B + c_A c_B) - k_{R3}(C_{p-R} C_B + c_{p-R} c_B) - k_{R4}(C_{o-R} C_B + c_{o-R} c_B) - k_{R5}(C_{AA} C_B + c_{AA} c_B) \qquad C_{B0} = 0.0166 \text{ kmol/m}^3$$

$$\frac{dC_{p-R}}{dt} = k_{R1}(C_A C_B + c_A c_B) - k_{R3}(C_{p-R} C_B + c_{p-R} c_B) \qquad C_{p-R,0} = 10^{-6} \text{ kmol/m}^3$$

$$\frac{dC_{o-R}}{dt} = k_{R1}(C_A C_B + c_A c_B) - k_{R4}(C_{o-R} C_B + c_{o-R} c_B) \qquad C_{o-R,0} = 10^{-6} \text{ kmol/m}^3$$

$$\frac{dC_{AA}}{dt} = -k_{R5}(C_{AA} C_B + c_{AA} c_B) \qquad C_{AA,0} = 0.08 \text{ kmol/m}^3$$

$$\frac{dC_S}{dt} = k_{R3}(C_{p-R} C_B + c_{p-R} c_B) + k_{R4}(C_{o-R} C_B + c_{o-R} c_B) \qquad C_{S0} = 0 \text{ kmol/m}^3$$

$$\frac{dC_Q}{dt} = k_{R5}(C_{AA}C_B + c_{AA}c_B) \qquad C_{Q0} = 0 \text{ kmol/m}^3$$

$$c_A c_B = -\frac{s_A s_B}{C_A C_B}$$

$$c_{p-R} c_B = -\frac{s_{p-R} s_B}{C_{p-R} C_B}$$

$$c_{o-R} c_B = -\frac{s_{o-R} s_B}{C_{o-R} C_B}$$

$$c_{AA} c_B = -\frac{s_{AA} s_B}{C_{AA} C_B}$$

$$\frac{ds_A}{dt} = -\frac{s_A}{\tau_M} \qquad s_A = 0.000332 \text{ (kmol/m}^3)^2$$

$$\frac{ds_B}{dt} = -\frac{s_B}{\tau_M} \qquad s_B = 0.000332 \text{ (kmol/m}^3)^2$$

$$\frac{ds_{p-R}}{dt} = -\frac{s_{p-R}}{\tau_M} \qquad s_{p-R0} = 0$$

$$\frac{ds_{AA}}{dt} = -\frac{s_{AA}}{\tau_M} \qquad s_{AA} = 0.00531 \text{ (kmol/m}^3)^2$$

$$\frac{ds_{o-R}}{dt} = -\frac{s_{o-R}}{\tau_M} \qquad s_{o-R0} = 0$$

$$\tau_M = 2.05\left(\frac{L_S^2}{\varepsilon}\right)^{1/3} + 0.5\left(\frac{\nu}{\varepsilon}\right)^{0.5} \ln(Sc)$$

Computations for this example were done using the program Polymath (distributed by the Cache Corp., an affiliate of AIChE), but any program that integrates sets of stiff differential equations (e.g., those using Gear methods) may be used. For this problem steady state was attained in the reactor after 0.5 s of integration for all flow rates used. This corresponds to reactor lengths which depend on the velocity of the feed stream(s).

13-5.4 Blending or Mesomixing Control of Turbulently Mixed Chemical Reactions

Middleton et al. (1986) measured yields of a competitive-consecutive chemical reaction under various stirred vessel conditions (size, impeller rotation rate) for semibatch reactors in which the added reactant was injected rapidly. They used the *Bourne reaction*, which is the reaction of 1-naphthol (component A) with diazotized sulfanilic acid (component B) to produce two products according to

the scheme $A + B \rightarrow R$; $R + B \rightarrow S$ (see Section 13-2.5). The reaction rate constants of these reactions are 7.3×10^3 and 3.5 L/mol · s, respectively. Reactant B at a concentration of 0.016 mol/L was added very rapidly at the top of the reactor vessel to reactant A at 0.0058 mol/L. This rapid feed injection produced a large unmixed cloud of reactant B. From this we would expect blending or mesomixing effects to dominate (see Section 13-2.1.3) and the resulting mixing to scale with N.

Middleton et al. (1986) compared their experimental results with the results of a simulation which assumed no effect of local concentration fluctuations. Local average concentrations were used with the kinetic rate equations, and it was assumed that segregation on the small scale was zero everywhere. There were concentration variations throughout the vessel which gradually diminished as blending and chemical reaction occurred. This is the assumption of large scale mesomixing control as opposed to small scale mesomixing or micromixing control.

Figure 13-32 shows the results of Middleton et al. (1986) plotted as yield versus power per unit volume, which would be consistent with micromixing control. It is clear that the results for the two reactor sizes do not coincide on such a plot. This work shows that constant power per unit volume (which corresponds to micromixing rate control) is inadequate for scale-up under mesomixing conditions. Yields for the large vessel were considerably lower than for the small vessel at equal power per unit volume.

If Figure 13-32 is replotted as yield versus N (impeller rotation rate), which is based on the assumption that mesomixing controls, the result is as shown in

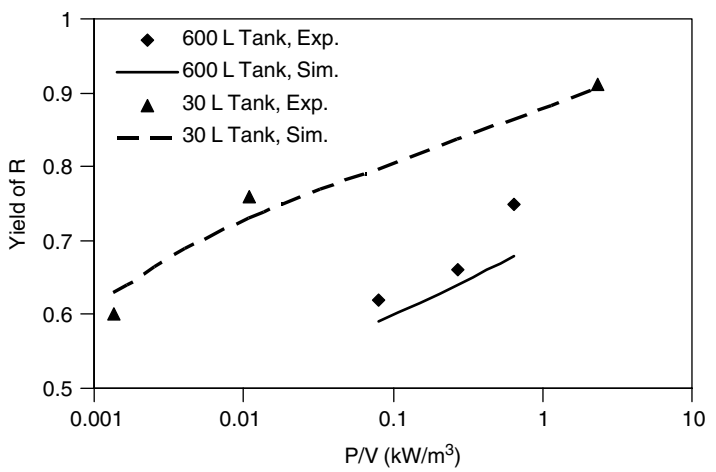

Figure 13-32 Yield of R in the reaction $A + B \rightarrow R$; $R + B \rightarrow S$ from experimental data of Middleton et al. (1986) and from their simulations, which assume no local mixing rate effect. Simulations using paired-interaction closure agree with the Middleton et al. simulations, showing that the controlling mixing rate is not micromixing.

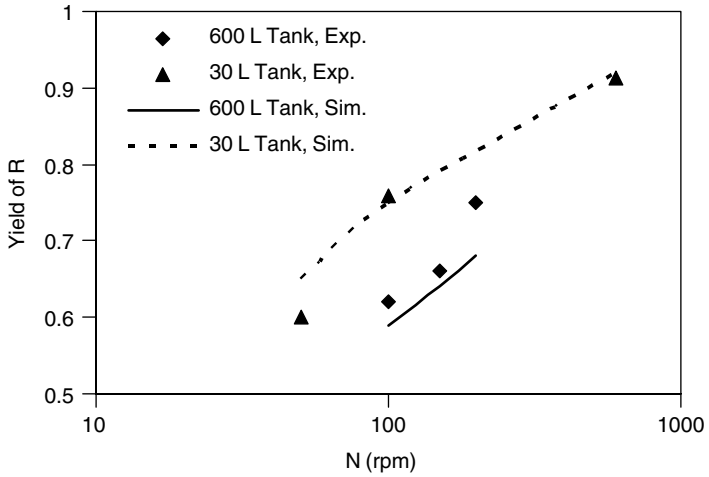

Figure 13-33 Yield versus N for Middleton et al. (1986) data shown in Figure 13-32. The results are close to mesomixing control, as shown by the closer agreement between small and large scale results when scaling is based on N.

Figure 13-33. The yields for the two scales are closer together for equal N, but there is still significant deviation, suggesting that for this chemical reaction there is an effect of flow pattern on yield.

Example 13-10: Use of Fluent to Simulate Blending Rate Control in a Stirred Reactor. Simulation of mesomixing controlled chemical reactions can be accomplished using any of the common commercial CFD codes. The experiments resulting in Figure 13-32 were simulated using the commercial code Fluent. The simulation was set up in the usual way to compute the flow patterns in the vessel with some attention given to the flow or flows of feed into the vessel. The reactor is semibatch, and since Fluent does not accommodate changing volume, an outflow far from the feed point(s) was specified. The volume fraction of feed was small compared to the volume of the resident liquid in the reactor, so the errors incurred in this strategy were small. The mixing of the reactants and products was accounted for by the mass balance capabilities of the program. To account for the very rapid feed injection of the Middleton et al. experiments, a starting condition with a cloud of unmixed component B was established. For the chemical reaction equations the kinetic rate constant option without any mixing effect was chosen. This means that at any point in the reactor, the reaction rate is determined by local average concentrations at the scale of the grid, as if all components are perfectly mixed at that point. The model then consists of eq. (13-27) with the term $\overline{c_i c_k}$ equal to zero. The results of the simulation are essentially the same as those obtained by Middleton et al. using their own computer code.

A somewhat related simulation method is the one proposed by Magnussen and Hjertager (1976) for combustion, which has been incorporated into the code

Fluent. That method computes reaction rate using the intrinsic kinetics if the mixing rate is fast and using the mixing rate if the intrinsic reaction rates are fast. The Magnussen–Hjertager method has found success for combustion simulations where diffusion is fast and mesomixing rate effects dominate. No account of the degree of mixing (segregation) is kept in either of these methods, in contrast with PDF-based methods (paired-interaction, β-PDF, etc.). A complete description with examples of the use of the Magnussen–Hjertager method in Fluent was given by Bakker et al. (2001).

13-5.5 Lamellar Mixing Simulation Using the Engulfment Model

Bourne (1983) realized the important effect of the mixing process on the yield and product distribution of series–parallel chemical reactions. He and co-workers used the first Bourne reaction, described in Section 13-2.5, to do experimental studies of the effects of mixing on yield. They made extensive use of this reaction system (Bourne et al., 1981; Bourne and Rohani, 1983; Angst et al., 1984; Bourne and Dell'Ava, 1987) and used the results to determine parameters in their models.

Alkaline hydrolysis of nitromethane was used by Klein et al. (1980). These results were used to determine the parameters in the interaction and exchange with mean (IEM) model of Villermaux and Zoulalian (1969), which uses the balance equation for component j in the injection region for component i:

$$\frac{dC_j}{dt} = I(\overline{C_j} - C_j) + r_j \tag{13-37}$$

where I is the interaction rate, $\overline{C_j}$ the concentration of component j in the region surrounding the injection region (mixing-reaction zone), and r_j the rate of appearance or disappearance in the injection region of component j based on molecular kinetics. This model is basically a Lagrangian model in which the progress of the chemical reaction is followed in time as reacting fluids flow downstream. The flowing stream can be the feed jet in a plug flow reactor or stirred tank. The surrounding fluid is drawn into the flowing jet by turbulent diffusion, causing expansion of the jet. The interaction parameter may be assumed constant or changing as the fluid flows downstream.

More recently, Baldyga and Bourne (1988, 1992) and Baldyga et al. (1993) have shown experimentally and through use of simulation the effects of mixing intensity, feed location, order of reactant addition, and relative molecular kinetics on yields in stirred vessels of competitive-consecutive and parallel-competitive reactions. The data of Baldyga and Bourne using the Bourne reaction are plotted in Figure 13-34 as the yield of R as a function of power per volume for long feed times at various feed points relative to disk turbine impellers. Under these conditions, scaling based on a micromixing mechanism was expected. The chemical reactions were carried out using semibatch addition of reactant B at a concentration of 11.8 mol/L into reactant A at 0.128 mol/L. They did simulations using

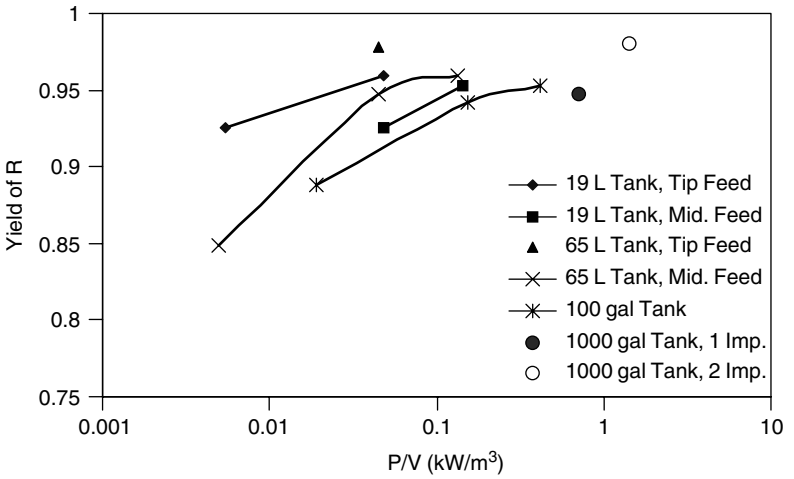

Figure 13-34 Yields in four stirred vessel sizes. The 19 and 65 L tanks were studied by Baldyga and Bourne (1992): feed points were at the impeller tip and midway between the tip and the tank wall. In the 100 and 1000 gal (378 and 3780 L, respectively) tanks studied by Paul (1988), the feed points were all at the impeller blade tips. In both cases a Bourne reaction of the form $A + B \rightarrow R$; $R + B \rightarrow S$ was used.

the engulfment model for micromixing, which is a Lagrangian simulation of the expanding jet (zone) of mixing and reaction. The model assumes that the volumetric flow rate of completely mixed, B-rich fluid through the expanding volume of the mixing-reaction zone is proportional to distance from the feed nozzle, the fraction of B-rich fluid in the zone, and the turbulent diffusivity, which is related to the engulfment rate, E. Through manipulation of the basic balance equations, the following equation is reached for the rate of change of the fraction B-rich fluid in the mixing-reaction zone:

$$\frac{dX_B}{dt} = EX_AX_B - \frac{X_B}{t} \tag{13-38}$$

where $E = 1/\tau_E$, X_B is the fraction of B-rich fluid, and X_A is the fraction of A-rich fluid. Here τ_M is computed using eq. (13-16).

Equation (13-38) was combined with the equation for the engulfment model to give the rate of change of the concentration of any of the reactants or products:

$$\frac{d\overline{C_j}}{dt} = E(1 - X_B)(\overline{C_j} - C_j) + r_j \tag{13-39}$$

The model is similar to the interaction and exchange with the mean model, but the engulfment rate and the fraction B-rich fluid in the reaction zone determine the interaction rate, that is, $I = E(1 - X_B)$.

Note that contrary to the Middleton et al. results, the yields in Figure 13-34 are greater for the larger tank in the Baldyga and Bourne results when plotted as a function of power per unit volume. This may be caused by the slow semi-batch addition of reactant B into the high-turbulence region near the impeller, causing micromixing conditions to occur, rather than the very rapid injection near the top of the tank, which has very low turbulence and causes mesomixing conditions to occur. Similar experimental conditions were considered by Paul (1988) and are shown in Figure 13-35. The decrease in yield as power per unit volume decreases seems to begin at about the same level (0.1 to 1 kW/m^3) for all cases, but data do not agree in absolute values of yield. Differences in feed pipe velocities are suspected to be the major variant. This can cause variations in the balance between mesomixing and micromixing, even when micromixing is the dominant effect. See the discussions in Section 13-2.1.3 under "Mesomixing" and in Section 13-2.4 for more details on the effects of feed pipe velocities.

Baldyga et al. (1993) simulated the 19 and 65 L yield results of Figure 13-34 using eq. (13-39) and data on the flow rates of the impeller stream and the feed stream. The results were very close to the experimental data, indicating a dependence on Batchelor scale micromixing. The method for accomplishing the simulation is straightforward and was published as a TK Solver program by Penney et al. (1997; available from Penney).

13-5.6 Monte Carlo Coalescence–Dispersion Simulation of Mixing

Generally, yield of the component R in the reaction sequence $A + B \rightarrow R$; $R + B \rightarrow S$ increases with power dissipation (increased impeller rotation rate),

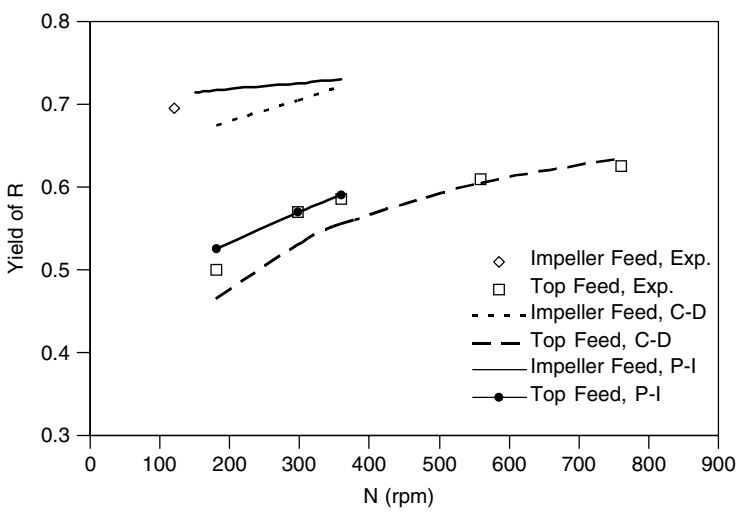

Figure 13-35 Results from Paul and Treybal (1971) experiments compared with C-D simulation (Canon et al., 1977) and paired-interaction (P-I) simulation (Patterson and Randick, 2000).

impeller size, and proximity of feed to the impeller. Feed component B is usually added to resident component A when component B participates in both reactions. Paul and Treybal (1971) made measurements of the final yield of one product of a competitive-consecutive reaction as a function of impeller speed in two small (T = 0.15 m and 0.29 m) semibatch reactors, showing how mixing rate affects yield. The data for the 0.29 m-diameter vessel are plotted in Figure 13-35. In the reaction sequence used by Paul and Treybal, A was tyrosine, B was iodine, R was monoiodated tyrosine, and S was diiodated tyrosine. Iodine was fed at a concentration of 2 mol/L into tyrosine at 0.2 mol/L.

Canon et al. (1977) simulated the flow, mixing, and reaction in the Paul and Treybal stirred reactor using a Monte Carlo coalescence and dispersion (C-D) method. In this method elements of the fluid are simulated by points that move according to the flow pattern in the vessel. These points have mass and composition representing some fraction of the fluid in the vessel. The points are caused to mix (coalesce), react, then disperse. The number of points undergoing C-D during each time increment is proportional to a C-D frequency. The local C-D frequency (coalescences/time/site) was found to be related to local turbulence as follows:

$$I_{CD} = 0.1\left(\frac{\varepsilon}{L_S^2}\right)^{1/3} \equiv 0.186\left(\frac{\varepsilon}{k}\right) \tag{13-40}$$

The choice of points to undergo C-D is done by a Monte Carlo algorithm in which each of two points for each C-D event is chosen randomly within a flow zone.

As shown in Figure 13-35, the C-D results are reasonably close to the experimental ones. Similarly good results based on Monte Carlo methods have been obtained by van den Akker (2001).

Example 13-11: Use of Monte Carlo C-D Simulation for a Mixed Chemical Reactor. The McKelvey et al. (1975) study of mixing in the Toor geometry (see Figure 13-29) gives data for the segregation of mixing water solutions as a function of distance downstream of the injection nozzles. The data, summarized in Table 13-13, also give hydrodynamic data such as velocities, turbulence intensities, length scales, and rates of turbulence energy dissipation. The data for L_S and ε were discussed in Example 13-10. If one assumes that $I_{CD} = K_{CD}(\varepsilon/L_S^2)^{1/3} = -\frac{1}{2}(ds/s\,dt)$ based on the incremental effect of each coalescence on s, then K_{CD} should be approximately 0.25 when the integral of this equation is compared with the integral of the Corrsin equation. A plot of the values of $-\frac{1}{2}(\Delta s/s\,\Delta t)$ versus $(\varepsilon/L_S^2)^{1/3}$ is shown in Figure 13-36, with the value of K_{CD} given as the slope of the straight line. The zero value at the origin is fixed. The slope is $K_{CD} = 0.0944$. A more complete analysis using many data points and the chemical results of Vassilatos and Toor (1965) gives a value of $K_{CD} = 0.1$, as given in eq. (13-40).

Table 13-13

L_x (cm)	t(s)	s/s_o	$\Delta s/s$	$-\frac{1}{2}(\Delta s/s\Delta t)$ (s^{-1})	ε_{avg} (cm^2/s^3)	$L_{S,avg}$ (cm)	$(\varepsilon/L_S^2)^{1/3}$ (s^{-1})
1.1	0.0147	0.015	0	–	0	–	0
3.0	0.040	0.0020	1.73	35.2	30 600	0.0175	378
5.0	0.067	0.00095	0.71	13.2	9675	0.025	132
8.1	0.108	0.00040	0.81	9.95	3050	0.038	96

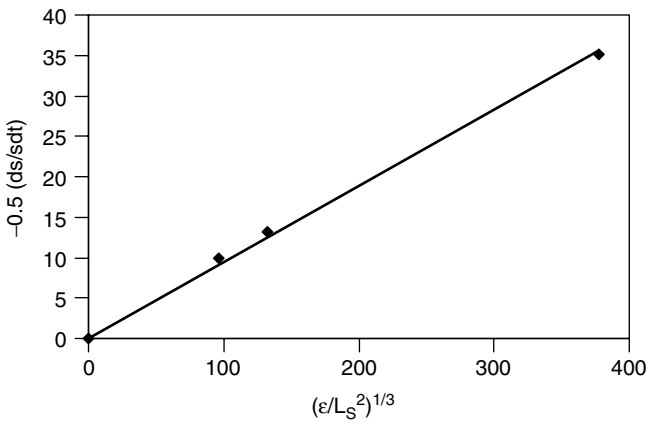

Figure 13-36 Linear fit of K_{CD} as a function of rate of segregation decay and the time constant of mixing. Best-fit line gives $K_{CD} = 0.0944$.

13-5.7 Paired-Interaction Closure for Multiple Chemical Reactions

Paired-interaction closure [eqs. (13-29) and (13-30)] may be used in three dimensional simulations of turbulent mixed reactors with multiple simultaneous chemical reactions. The assumptions of the closure are that (1) only one concentration probability need be used to capture the most important aspects of the interaction of mixing and chemical reaction, and (2) that the reactants need only be considered in pairs and that higher-order interactions of the reactants are not important. These assumptions give a closure that is very fast to compute and results very close to experimental results (see Zipp and Patterson, 1998; Randick, 2000).

The earliest attempts to simulate mixing and chemical reaction in stirred vessels were based on the use of connected zones within which mixing and reaction took place. In some of these simulations, the flow in and out, L_S and ε, were based on experimental data (Patterson, 1975; Mann and Knysh, 1984). It is now possible using standard CFD codes to numerically compute spatial distributions of Reynolds-averaged variables of the turbulent flow and mixing of miscible fluids with similar viscosities and densities in almost any geometry (see Hutchings

et al., 1989; Bakker and van den Akker, 1990; Ju et al., 1990; Bakker and Fasano, 1993; Perng and Murthy, 1993; Dilber and Rosenblat, 1995; Harvey et al., 1995; Fox, 1995; Armenante and Chou, 1996; Zipp and Patterson, 1998). Circulation patterns and distribution of turbulence intensities are generally good and predict the trends correctly, but the values of the turbulent quantities k and ε are not always correct. Turbulence energy and energy dissipation rate, which are the major parameters determining local mixing rate, can be distorted by the presence of trailing vortices (Wu and Patterson, 1989) and macroinstabilities (Roussinova et al., 2000). The usual problem is that the k and ε values are too low in regions where the vortices feed energy into the turbulence. Interestingly, in the case of the radial flow impeller, the ratio of k to ε, the important quantity for mesomixing rate computation, is still nearly correct (Zipp and Patterson, 1998). This has not been tested for pitched blade impellers or other axial flow impellers. Great care must therefore be exercised when simulating mixing and chemical reaction in stirred vessels. Ways to achieve an acceptable simulation are discussed in Example 13-12. Use of sliding mesh methods solves these problems only partially, as the vortices are very small and energetic, requiring a very fine mesh for simulation. Further improvement could be obtained by using large eddy simulation (LES), in which the large eddies are simulated on a time-dependent basis. Derksen and van den Akker (1999) have done pioneering work in using LES for stirred vessel simulations.

Simulation of single and multiple chemical reactions in stirred vessels may be done using a CFD computer code with added subroutines for mixing rates and chemical reaction rates. Validation of this simulation method has been done by simulation of the semibatch vessel and chemical reaction used by Paul and Treybal (1971), shown in Figure 13-35, and by comparisons of semi-batch measurements made by Doshi (2001) with corresponding simulations by Randick (2000) and Gross (2002) as discussed in Example 13-12.

Example 13-12: Use of Paired-Interaction Closure for Multiple Chemical Reactions—Isothermal Case. An example of recent more detailed simulations are those made by Randick (2000) and Gross (2002) to determine the effects of impeller rotation rate, impeller type, feed location, chemical reaction rate constants, heat of reaction and activation energy, and vessel size on yield of a consecutive-competitive chemical reaction. The fluid dynamics code Fluent was used to simulate the flow patterns and turbulence in the vessel in the usual way. The outflow from the impellers was simulated by fixing the velocity of the fluid at the locus of points swept by the impeller edge at the fluid outflow. This is more efficient than using sliding mesh to simulate the impeller flows, but is not always feasible (see Chapter 5). When detailed impeller outflow and turbulence data are not available, a sliding mesh (or similar) method must be used. Complete experimental impeller flow data are necessary for the best accuracy, but for the Rushton turbine fixing only the angular velocity at the impeller tip gave good results. The resulting radial velocities, turbulence energy, and dissipation rates were close to those determined by fixing all the values at the blade tips.

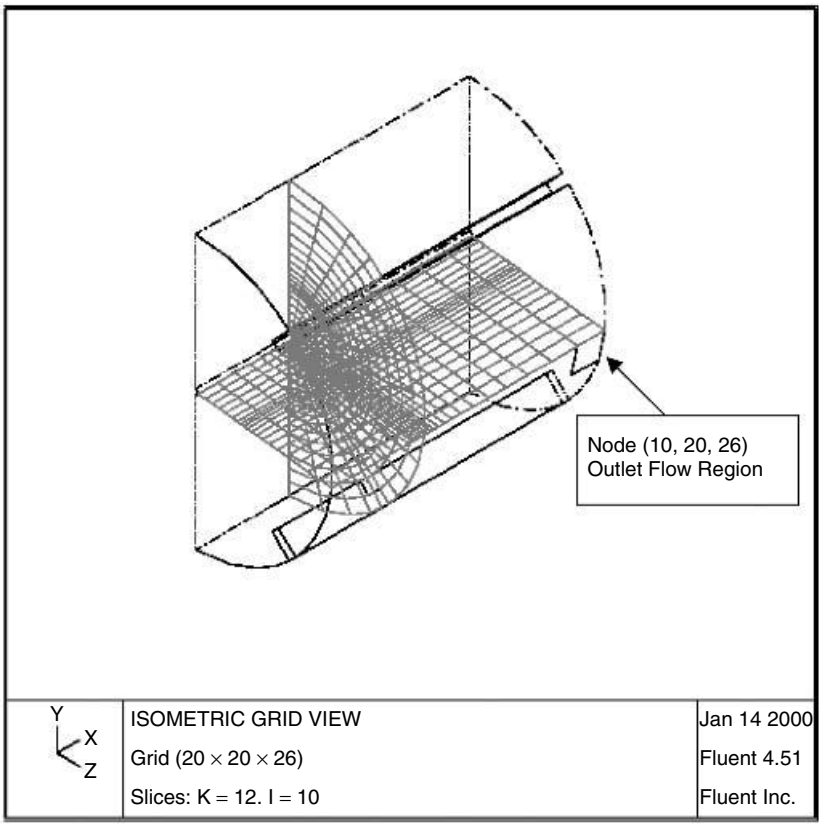

Figure 13-37 Isometric view of grid used in simulations in a mixing tank.

The grid used in the simulations is shown in Figure 13-37. It consisted of 20 r-z grids unevenly spaced in the angular direction. They were closer together near the baffles. Each r-z grid was 20×26 nodes with node compression near the impeller tips in both directions. Grid refinement experiments showed that this grid spacing was adequate for the mixing effects being modeled. Grid refinement should always be done to determine whether any grid-size effects are influencing the results of the simulation.

In this example eqs. (13-27) to (13-30) (the paired-interaction closure) were incorporated into a subroutine called by Fluent to compute the rates of segregation growth and decay and the rates of the chemical reactions. The subroutine, called Pairin, is available from author Patterson. Pairin may easily be adapted to other fluid dynamics simulators if desired. Pairin may also be used as an example for development of new subroutines using more or less sophisticated closures. In addition, the subroutine developed by Baldyga and co-workers (see Sections 13-5.2 and 13-5.8) for use of the β-PDF may be used instead of the Pairin subroutine.

Two impeller types were simulated: the standard six-blade disk turbine and a 45° pitched blade turbine. The outflow from the disk turbine was simulated by fixing the tangential velocities at the blade tip locus (the FIX option in Fluent). The radial velocities and k/ε ratios generated were close to the values that have been measured by Wu and Patterson (1989). The outflow velocities and turbulence energy from the pitched blade turbine were fixed at the bottom locus of the impeller blades using the data of Fort et al. (1999). The resulting flow patterns were close to the data measured.

Doshi (2001) made measurements of the final yields for the tyrosine–iodine reaction used by Paul and Treybal (1971), but in vessels (0.785 and 19.1 L) with standard geometry (T = H = 3 D), using both Rushton or disk and pitched blade impellers. Four feed locations were used: the top surface of the liquid in the vessel, the center of the impeller (disk turbine only), into the impeller discharge very near the blade tips, and the inside edge of the baffles at the height of the impeller directed toward the shaft. A range of feed times were examined, showing a threshold of minimum feed time for micromixing similar to that obtained by Baldyga and Bourne (1992). These experimental data for feed into the impeller discharge very near the blade tips are compared in Figure 13-38 with the simulation results obtained by the method described above by Randick and Gross.

It is clear that for the conditions of these experiments the larger vessel gives slightly higher yields at the same power per volume. This is consistent with the data of Baldyga and Bourne (1992) for feed into the high-turbulence region near the impeller. The absolute volume of this region is larger in the larger vessel.

13-5.8 Closure Using β-PFD Simulation of Mixing

Baldyga (1994) gives several examples of conversion and yield calculations using the β-PFD closure for various reactor geometries where mixing is a factor. One

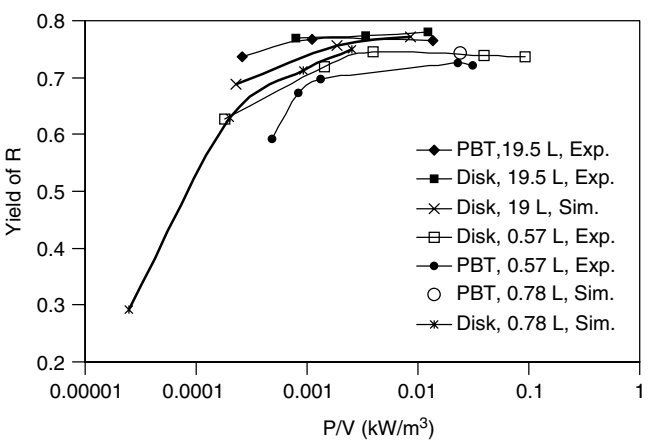

Figure 13-38 Comparisons for the Doshi (2001) experimental data for fed-batch reaction (impeller feed) with the Randick (2000) and Gross (2002) simulations.

of these examples is the simulation of the yield results obtained experimentally by Li and Toor (1986). They measured yields at various flow rates (Reynolds numbers) in the multijet reactor illustrated in Figure 13-29 using the Bourne reaction of 1-naphthol with diazotized sulfanilic acid. Details of the calculation method were given in the Baldyga (1994) article. Their results show very good correspondence with the experiments, as shown in Figure 13-39. The volume feed ratio and reactant concentration ratio were both near 1.

13-5.9 Simulation of Stirred Reactors with Highly Exothermic Reactions

Of great importance because of the prevalence of semibatch reactors are the effects of temperature rise in semibatch reactors with exothermic chemical reactions. Several semibatch cases with exothermic reaction were simulated by Randick (2000) using Fluent with Pairin. The method used for the simulations was the same as that described in Example 13-12. The simulations frequently required 2 or more days on a fast computer. The reactions were $A + B \rightarrow C$ (k_{R1}) and $A + C \rightarrow D$ (k_{R2}). The conditions for the semibatch simulations were $k_{R1} = 36$ L/kmol · s, $k_{R2} = 3.6$ L/kmol · s, $\Delta H_{R1} = 0$, $\Delta H_{R2} = -1.0 \times 10^8$ J/kmol, $E_{R1} = 0$, $E_{R2} = 1.0 \times 10^7$ to 3.0×10^7 J/kmol, where k_{Ri} are rate constants, ΔH_{Ri} are heats of reaction, and E_{Ri} are activation energies. Figure 13-39 shows the results of simulations that were done in the semibatch mode.

The effect of activation energy on yield is clearly shown by Figure 13-40, where yield is plotted as a function of stirring power per unit volume for the various determining variables. Power per unit volume and tank size have a much stronger effect for the exothermic reactions than for the isothermal reactions, as shown. In both cases direct comparison of results in the 0.785 L tank with the 3785 L tank indicates a yield difference of about 25%. Figures 13-41 and 13-42 show how concentration and temperature change with time as the semibatch

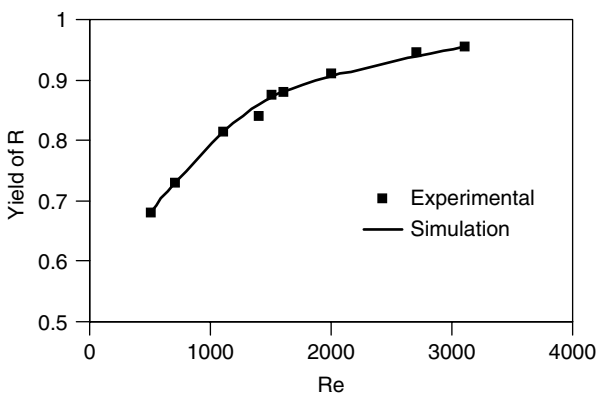

Figure 13-39 Comparison of β-PDF simulation of yield from Baldyga (1994) as a function of Reynolds number with the data of Li and Toor (1986).

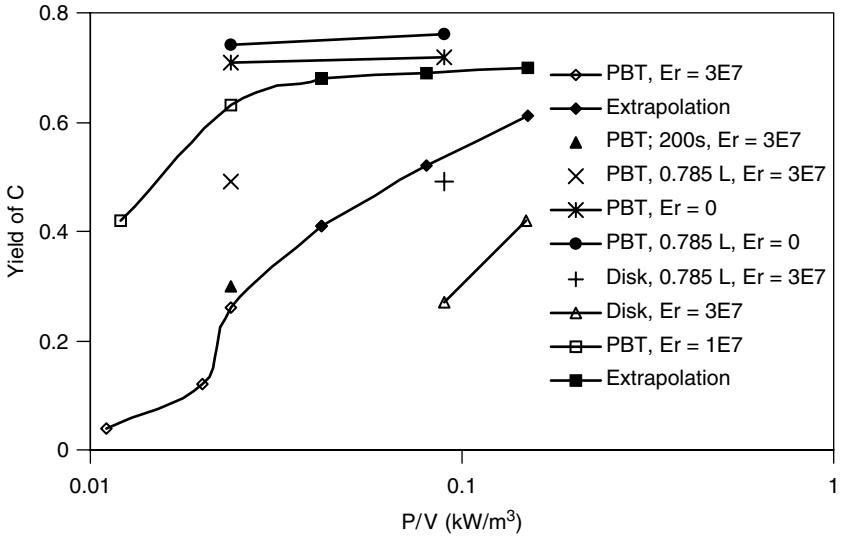

Figure 13-40 Comparisons of yields for exothermic semibatch cases; $k_{R1}/k_{R2} = 10$, volume = 3785 L, and addition time = 50 s except where noted.

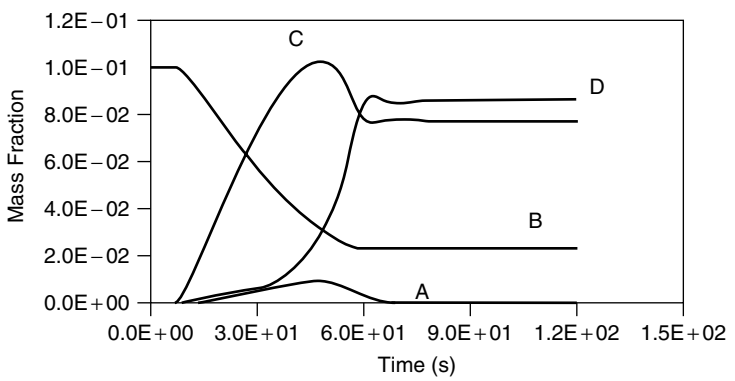

Figure 13-41 Mole fraction versus time at a position near the top of the vessel for a fed-batch reaction (Randick's trial 10): A + B → C; A + C → D (see Randick, 2000). The conditions in the reactor are: volume = 3785 L; pitched blade impeller; N = 100 rpm; $V_{feed} = 1.045$ m/s; $t_f = 50$ s; $\Delta H_{R1} = 0$; $\Delta H_{R2} = -10^8$ J/kmol; $E_{R1} = 0$; $E_{R2} = 3 \times 10^7$ J/kmol. Yield of C was 41.3%.

reactions proceed. Wall cooling with a heat transfer coefficient of 283 J/s · m^2 · K and a temperature of 323 K were assumed.

This preliminary research shows that prediction of yield on scale-up of a highly exothermic chemical reaction series can be particularly difficult. The heats of reaction and activation energies of each reaction must be well known. The

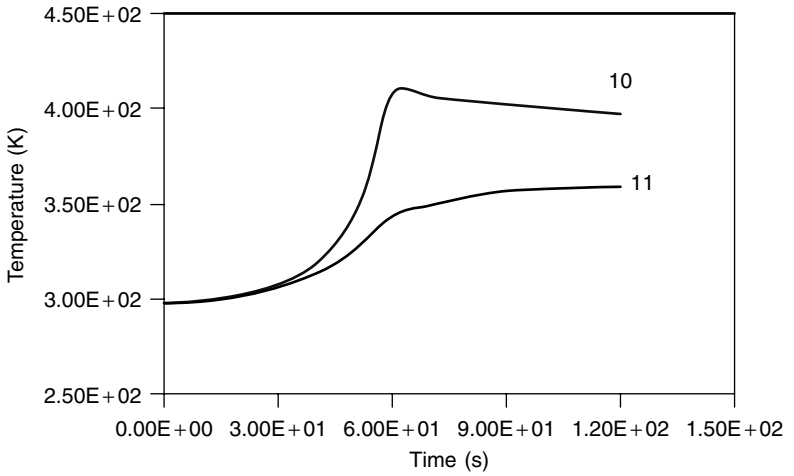

Figure 13-42 Temperature response for two exothermic reactions measured at the same location as the concentrations in Figure 13-24. One plot is for Randick's trial 10 (see Figure 13-41) and the other is for a reaction with a lower reaction activation energy.

power per unit volume, feed point, and impeller type must also be carefully specified. Only a full simulation of the reaction system using CFD is capable of incorporating all these determining variables.

It must be emphasized that even though these results seem reasonable and that extensive validation of stirred-tank simulations has been done for various continuous flow and semibatch cases, only isothermal validation has been done, and no large ratio scale-up validations have been done. The feed time of 50 s for a 3.8 m^3 vessel is very short and exaggerates the heat effects. These aspects of the problem need to be studied before complete confidence may be placed on the CFD simulation of highly exothermic reactions.

13-5.10 Comments on the Use of Simulation for Scale-up and Reactor Performance Studies

Simulation has not yet reached the point that it is a replacement for experimental results. However, simulation has several very useful aspects:

1. Many results may be obtained in a relatively short time using simulation once the users become highly conversant with the methods.
2. Simulations may be cheaper per result than experiments if personnel are available who have expertise in the simulation methods equivalent to the expertise of the experimenters.
3. Simulations may be used profitably to study details of flow, turbulence, or mixing rate that cannot conveniently be done experimentally or possibly cannot be done at all. This is particularly true where simulations at the

same conditions as the experiments give results close to the experimental results. Significant design insights can sometimes come from such studies.

4. Simulation is based on the fundamental physics of the process and therefore always has the potential of giving more realistic information on the performance of the process than that of methods based on dimensional analysis, mechanistic approximations, or space-averaged (one-point) theories or correlations, *provided that the model equations are well defined.* The directional changes shown by the simulations should in general be the same as the experimental ones, and the magnitudes of those changes should also be similar.
5. Simulation of mixing effects in reactors requires good data for reaction kinetics; physical constants such as viscosity, density, and diffusivity; and knowledge of the exact geometrical configuration of the vessel, including feed locations.
6. The approximations involved in simulation are constantly improving, the main ones being spatial and time averaging (Reynolds averaging), the numerical methods used to reach convergence, and the closures needed to link the averages to provide a closed set of equations. Large-eddy simulation (LES) methods may well provide a way to reduce the severity of these approximations and lead to more realistic simulations. At this writing, objective comparison of LES results with time-resolved experimental results is extremely difficult, so validation is reduced to time averaging the LES results for comparison with time-averaged experimental results.

Simulations should always be used in conjunction with some experiments, the balance between the two being dictated by the level of uncertainty in the simulations being done. Uncertainty increases as reactors progress from homogeneous stirred tanks and pipes to the much more difficult two- and three-phase reactors where in addition to the chemical reactions, the following must be addressed: gas bubble and/or dispersed-liquid droplet sizes; gas, liquid, or solids distributions in the vessel; coupling of momentum between the phases; rates of breakup, agglomeration, and coalescence; surface effects; and mass transfer coefficients. Progress over the last 10 years has been significant, but many challenges remain to be resolved.

13-6 CONCLUSIONS

In this chapter we have shown that the mechanism and kinetics of a chemical reaction scheme can be combined with a rather detailed fine scale picture of the fluid dynamics in a simple reactor to predict yield and selectivity for fast homogeneous reactions. With a lot more information we can predict some of the reaction effects when another phase is present and interphase mass transfer becomes important. Heterogeneous analysis is severely limited because our

knowledge of the phenomena and the descriptive equations dictating surface area creation and disappearance are only now being developed.

Industrially, the information needed about chemical mechanisms and intrinsic chemical kinetics is difficult to obtain. An experimental program to measure fast kinetics under industrial conditions (often, high temperatures and pressures) is very expensive. Frequently, the industrialist must deal with lumped rate expressions for a multistep reaction which are obtained from a poorly characterized lab reactor. Many industrialists and consultants have developed experimental protocols to determine mixing effects in laboratory scale chemical reactors. When combined with the concepts in this chapter, this allows us to scale up to full scale without all of the details of the kinetics, phase behavior, and full mathematical models. We emphasize for a final time that laboratory equipment tends to have shorter mixing times because of scale effects and higher turbulence levels. This can obscure rate-controlling kinetic steps in several important classes of reaction. The reader will note that there is no general summary table for reaction scale-up rules, there is no unique definition of Da_M, no unique correlation for critical feed time. This is because there are many things which are still not understood or are poorly quantified. The first of these is the wide spectrum of reaction mechanisms and kinetics. The second is the entire area of inertial scale or mesoscale mixing, combined with the infinite possible variations of industrial reactor geometries, leading to an equally wide range of local turbulence conditions.

The fluid flow and turbulence in many plant reactors is more complex than in vessels modeled by academics. CFD is useful for understanding the flow patterns in such reactors; however, at the time of writing CFD still does a poor job of predicting the local turbulence quantities vital to micromixing and mesomixing analysis. This is another area where greater understanding is needed.

There is an entire class of problems where the particle size and particle size distribution are critical characterization parameters in addition to yield or purity. Another set of equations describing nucleation and growth along with population balances must then be added to the models. Success in predicting these effects has so far been limited, possibly due to inaccurate or unrealistic kinetics. When the question of morphology is added to the mix, the problem becomes daunting. Again, experimental protocols based on an understanding of micromixing can help the engineer determine good and bad strategies for scale-up, but more understanding is needed.

There is a final class of phenomena associated with two-phase surface energy systems, such as liquid–liquid dispersions and emulsions, in which rapid physiochemical kinetics can be observed. The rate of mixing can have a profound effect on the properties of such systems. One example is the shocking of a stabilized dispersion where the addition of more continuous phase upsets the local surface-active-agent balance and can cause agglomeration or coagulation. Rapid addition with rapid dilution (mixing) can avoid such affects.

As this is written, there are undoubtedly more examples of complex reactions being developed in laboratories around the world. An understanding of how fluid motion and particularly, turbulence can affect the path of reactions is extremely

useful for understanding many of the problems encountered in developing these reactions, and more important, in determining ways to avoid mixing problems on scale-up.

NOMENCLATURE

a	mass transfer area per unit volume of the total fluid (m^2/m^3)
a'	mass transfer area per unit bubble volume (m^2/m^3)
A	reactant or moles of reactant
A	cross-sectional area (m^2)
A_0	initial moles of reactant A
B	baffle width (m)
B	moles of reactant B
$\overline{c_0^2} = \overline{s_0}$	initial or maximum segregation (usually, $\overline{C_{10}} < \overline{C_{20}}$) $(mol/m^3)^2$
c_i	fluctuation of component i concentration about average (mol/m^3)
C_{i0}	initial concentration of reactant i as if already mixed (mol/m^3)
C_i	concentration of component i at any location (mol/m^3)
C_i^*	saturated or equilibrium concentration of component i in liquid (mol/m^3)
C_C	constant in Corrsin term for energy dissipation
C_{g1}	constant in Spalding term for segregation production
d_{jo}	initial jet diameter (m)
D	impeller diameter or pipe diameter (m)
D_{AB}	molecular diffusivity of A in B (m^2/s)
Da_M	mixing Damkoehler number
D_t	turbulent diffusivity (m^2/s)
E	engulfment rate constant (s^{-1})
E_{Ri}	activation energy for reaction i
f	mixture fraction
G	ratio of distance from impeller to impeller diameter (−)
G	molar gas flow rate (mol/s)
H	vessel height (m)
H_{Ri}	heat of reaction for reaction i (kJ/mol)
I	interaction rate in the IEM model
I_{CD}	rate of coalescence and dispersion in CD simulation of mixing rate
k	turbulence energy (m^2/s^2)
k_L	liquid-side mass transfer coefficient
k_L^*	liquid-side mass transfer coefficient corrected for reaction rate effect
k_R	reaction rate constant (depends on reaction order)
K	constant in the C-D equation
K_H	Henry's law constant
L	pipe or static mixer length (m)
L_S	concentration macroscale (m)

L_f	scale of the feed (m)
n	number of feed points ()
n	reaction order ()
N	impeller rotation rate (rps)
N_p	power number for stirred vessels ()
p	probability of a given concentration ()
P	fluid mixing power (W)
q	lumped parameter (see Section 11-6.3)
Q_B	volumetric feed rate of component B (m^3/s)
Q_L	volumetric liquid flow rate (m^3/s)
Q_G	gas feed rate (m^3/s)
r	radial distance from vessel axis (m)
r_i	rate of production of component i by reaction (mol/s)
R	vessel radius, T/2 (m)
R	moles of product R (mol)
Re	Reynolds number (ND^2/ν for a stirred tank; DV/ν for a pipe)
s_i	square of concentration fluctuation; its mean square is segregation (mol/m^3)
S	moles of product S (mol)
Sc	Schmidt number for molecular diffusion, ν/D_{AB} ()
t	time (s)
t_f	feed time (s)
$t_{1/2}$	half-life (s)
T	vessel diameter (m)
u'	root-mean-square fluctuating velocity (m/s)
U	bulk-mean velocity in a pipe or ambient velocity near a feed location (m/s)
U_{jo}	bulk-mean jet velocity (m/s)
U_{tip}	impeller blade tip velocity (m/s)
U_x	velocity in a plug flow reactor (m/s)
V	total volume of fluid in vessel (m^3)
V_L	liquid-phase volume (m^3)
v_f	feed pipe velocity (m/s)
v_r	rise velocity of bubbles in vessel (m/s)
v_s	superficial gas velocity (m/s)
v_t	impeller blade tip velocity (m/s)
x	distance downstream (m)
x	mole fraction in liquid phase ()
x_i	Cartesian coordinate (m)
X_A, X_B	fraction A- and B-rich fluids
X_S	selectivity to product S
Y_{exp}	ideal yield with perfect mixing
Y_{Ao}, Y_{Ai}	outlet and inlet mole fractions of A in gas
Y_R, Y_S	yield of R or S product
z	axial distance from impeller disk plane (m)

Greek Symbols

ε	turbulence energy dissipation rate (m^2/s^3)
θ	tangential coordinate
λ_B	Batchelor length scale (m)
μ	fluid viscosity (kg/ms)
ν	kinematic viscosity (m^2/s)
ν_t	turbulent momentum diffusivity (m^2/s)
ρ	fluid density (kg/m^3)
σ_c	Schmidt number for mass diffusion
σ_s	Schmidt number for segregation diffusion
τ_B	blending time (s)
τ_{crit}	feed time beyond which there are no yield effects of feed rate (s)
τ_D	mesomixing time based on feed rate, ambient velocity, and turbulent diffusivity (s)
τ_M	Corrsin mixing time (s)
τ_R	reaction time constant ($1/k_RC$) for second-order reaction (s)
τ_S	mesomixing time based on the Corrsin formulation (s)
Φ	volume fraction gas or dispersed phase holdup

REFERENCES

Angst, W., J. R. Bourne, and P. Dell'Ava (1984). Mixing and fast chemical reaction: IX. Comparison between models and experiments, *Chem. Eng. Sci.*, **39**, 335–342.

Armenante, P. M., and C.-C. Chou (1996). Velocity profiles in a baffled vessel with single or double pitched-blade impellers, *AIChE J.*, **42**, 42–54.

Astarita, G. (1967). *Mass Transfer with Chemical Reaction*, Elsevier, New York.

Bakker, R. A., and J. B. Fasano (1993). Time dependent turbulent mixing and chemical reactions in stirred tanks, *Paper 70c*, presented at the AIChE Annual Meeting, St. Louis, MO.

Bakker, R. A., and H. E. van den Akker (1990). *A Computational Study on Dispersing Gas in a Stirred Reactor*, Kramers Laboratory, Delft University of Technology, Delft, The Netherlands.

Bakker, A., A. H. Haidari, and L. M. Marshall (2001). Design reactors via CFD, *Chem. Eng. Prog.*, **97**, Dec., pp. 31–39.

Baldyga, J. (1994). A closure model for homogeneous chemical reactions, *Chem. Eng. Sci.*, **49**, 1985–2003.

Baldyga, J., and J. R. Bourne (1984). A fluid mechanical approach to turbulent mixing and chemical reaction, *Chem. Eng. Commun.*, **28**, 231–278.

Baldyga, J., and J. R. Bourne (1988). Calculation of micromixing in inhomogeneous stirred tank reactors, *Chem. Eng. Res. Des.*, **66**, 33–38.

Baldyga, J., and J. R. Bourne (1989). Simplification of micromixing calculations: I. Derivation and application of new model, *Chem. Eng. Sci.*, **42**, 83–92.

Baldyga, J., and J. R. Bourne (1990). The effect of micromixing on parallel reactions, *Chem. Eng. Sci.*, **45**, 907–916.

Baldyga, J., and J. R. Bourne (1992). Interactions between mixing on various scales in stirred tank reactors, *Chem. Eng. Sci.*, **47**, 1839–1848.

Baldyga, J., and J. R. Bourne (1999). *Turbulent Mixing and Chemical Reactions*, Wiley, Chichester, West Sussex, England.

Baldyga, J., and M. Henczka (1995). Closure problem for parallel chemical reactions, *Chem. Eng. J.*, **58**, 161–173.

Baldyga, J., and M. Henczka (1997). Turbulent mixing and parallel chemical reactions in a pipe: application of a closure model, *Recent. Prog. Genie Precedes*, **11**, 341–348.

Baldyga, J., J. R. Bourne, and Y. Yang (1993). Influence of feed pipe diameter on meso-mixing in stirred tank reactors, *Chem. Eng. Sci.*, **48**, 3383–3390.

Baldyga, J., W. Podgorska, and R. Pohorecki (1995). Mixing-precipitation model with application to double feed semibatch precipitation, *Chem. Eng. Sci.*, **50**, 1281–1300.

Baldyga, J., J. R. Bourne, and S. J. Hearn (1997). Interaction between chemical reactions and mixing on various scales, *Chem. Eng. Sci.*, **52**, 457–466.

Baldyga, J., J. R. Bourne, and B. Walker (1998). Non-isothermal micromixing in turbulent liquids: theory and experiment, *Can. J. Chem. Eng.*, **76**, 641–649.

Barthole, J., R. David, and J. Villermaux (1982). *A New Chemical Method for the Study of Local Micromixing Conditions in Industrial Stirred Tanks*, ISCRE, Boston.

Batchelor, G. K. (1959). Small scale variation of convected quantities like temperature in turbulent fluid: I. Discussion and the case of small conductivity, *J. Fluid Mech.*, **5**, 113–133.

Bird, R. B., W. Stewart, and E. N. Lightfoot (1960). *Transport Phenomena*, Wiley, New York.

Bourne, J. R. (1983). Mixing on the molecular scale, *Chem. Eng. Sci.*, **38**, 5–8.

Bourne, J. R., and P. Dell'Ava (1987). Micro- and macro-mixing in stirred tank reactors of different sizes, *Chem. Eng. Res. Des.*, **65**, 180–186.

Bourne, J. R., and J. Garcia-Rosas (1984). Rapid mixing and reaction in a Ystral in-line dynamic mixer, *Paper 52c*, presented at the AIChE Annual Meeting, San Francisco.

Bourne, J. R., and C. P. Hilber (1990). The productivity of micro-mixing-controlled reactions: effect of feed distribution in stirred tanks, *Chem. Eng. Res. Des.*, **68**, 51–56.

Bourne, J. R., and S. Rohani (1983). Mixing and fast chemical reaction: VII. Determining reaction zone model for the CSTR, *Chem. Eng. Sci.*, **38**, 911–916.

Bourne, J. R., and S. Thoma (1991). Some factors determining the critical feed time of a semi-batch reactor, *Chem. Eng. Res. Des.*, **69**, 321–323.

Bourne, J. R., and S. Yu (1994). Investigation of micromixing in stirred tank reactors using parallel reactions, *Ind. Eng. Chem. Res.*, **33**, 41–55.

Bourne, J. R., F. Kozicki, U. Moergeli, and P. Rys (1981). Mixing and fast chemical reaction: III. Model–experiment comparisons, *Chem. Eng. Sci.*, **36**, 1655–1663.

Bourne, J. R., O. M. Kut, J. Lenzner, and H. Maire (1990). Kinetics of the diazo coupling between 1-naphthol and diazotized sulfanilic acid, *Ind. Eng. Chem. Res.*, **29**, 1761–1765.

Bourne, J. R., O. M. Kut, and J. Lenzner (1992). An improved reaction system to investigate micromixing in high-intensity mixers, *Ind. Eng. Chem. Res.*, **31**, 949–958.

Boussinesq, J. (1903). *Théorie analytique de la chaleur*, Vol. 2, Gauthier-Villars, Paris.

Brodkey, R. S., and J. Lewalle (1985). Reactor selectivity based on first-order closures of the turbulent concentration equations, *AIChE J.*, **31**, 111–118.

Canon, R. M., A. W. Smith, K. W. Wall, and G. K. Patterson (1977). Turbulence level significance of the coalescence–dispersion rate parameter, *Chem. Eng. Sci.*, **32**, 1349–1352.

Cichy, P. T., and T. W. F. Russell (1969). Two-phase reactor design tubular reactors: reactor model parameters, *Ind. Eng. Chem. Res.*, **61**, 15.

Corrsin, S. (1964). The isotropic turbulent mixer: II. Arbitrary Schmidt number, *AIChE J.*, **10**, 870–877.

Danckwerts, P. V. (1958). The effect of incomplete mixing on homogeneous reactions, *Chem. Eng. Sci.*, **8**, 93–99.

Derksen, J., and H. E. A. van den Akker (1999). Large eddy simulations of the flow driven by a Rushton turbine, *AIChE J.*, **45**, 209–221.

Dilber, I., and S. Rosenblat (1995). Anisotropic turbulence models for simulation of mixing processes, Paper 122f, presented at the AIChE Annual Meeting, Miami Beach, FL, Nov.

Donaldson, C. (1975). On the modeling of the scalar correlations necessary to construct a second-order closure description of turbulent reacting flows, in *Turbulent Mixing in Nonreactive and Reactive Flows*, S. N. B. Murthy, ed., Plenum Press, New York, pp. 131–162.

Doraiswamy, L. K., and M. M. Sharma (1984). *Heterogeneous Reactions: Analysis, Examples, and Reactor Design*, Wiley, New York.

Doshi, J. (2001). Effect of mixing on multiple chemical reactions, M.S. thesis, University of Missouri–Rolla.

Elghobashi, S. E., W. W. Pun, and D. B. Spalding (1977). Concentration fluctuations in isothermal, turbulent confined jets, *Chem. Eng. Sci.*, **32**, 161–166.

Fasano, J. B., and W. R. Penney (1991). Avoid blending mix-ups, *Chem. Eng. Prog.*, **87**(10), 56–63.

Fogler, H. S. (1999). *Elements of Chemical Reaction Engineering*, 3rd ed., Prentice Hall, Upper Saddle River, NJ.

Forney, L. J., N. Nafia, and H. X. Vo (1996). Optimum jet mixing in a tubular reactor, *AIChE J.*, **42**, 3113–3122.

Fort, I., P. Vortuba, and J. Medek (1999). Turbulent flow of liquid in mechanically agitated closed vessel, manuscript from I. Fort.

Fox, R. O. (1995). The spectral relaxation model of the scalar dissipation rate in homogeneous turbulence, *Phys. Fluids*, **7**, 1082–1094.

Garside, J., and N. S. Tavare (1985). Mixing, reaction and precipitation in an MSMPR crystallizer: effects of reaction kinetics on the limits of micromixing, in *Industrial Crystallization*, Vol. 84, S. Jancic and E. J. de Jong, eds., Elsevier, Amsterdam, pp. 131–136.

Grenville, R. K. (1992). Blending of viscous Newtonian and pseudo-plastic fluids, Ph.D. dissertation, Cranfield Institute of Technology, Cranfield, Bedfordshire, England.

Gross, J. (2002). Simulation of effects of impeller rotation rate, reactor size and density gradients on yield in a stirred, fed-batch reactor, M.S. thesis, University of Missouri–Rolla.

Harnby, N., M. F. Edwards, and A. W. Nienow, eds. (1992). *Mixing in the Process Industries*, Butterworth-Heinemann, Wolburn, MA.

Harvey, A. D., C. K. Lee, and S. E. Rogers (1995). Steady-state modeling and experimental measurement of a baffled impeller stirred tank, *AIChE J.*, **41**, 2177–2186.

Heeb, T. G., and R. S. Brodkey (1990). Turbulent mixing with multiple second-order chemical reactions, *AIChE J.*, **36**, 1457–1470.

Homsi, K. L., A. Thompson, and M. P. Thien (1993). A facile and selective large-scale bromination of aminotoluidine using N-bromosuccinimide/acetone solution addition, presented at the AIChE National Meeting, St. Louis, MO, Nov.

Hutchings, B. J., R. R. Patel, and R. J. Weetman (1989). Computation of flow fields in mixing tanks with experimental verification, presented at the ASME Annual Winter Meeting, San Francisco, Dec.

Jo, M. C., W. R. Penney, and J. B. Fasano (1994). Backmixing into reactor feedpipes caused by turbulence in an agitated vessel, *AIChE Symp. Ser. 299*, **90**, 41–49.

Ju, S. Y., T. M. Mulvahill, and R. W. Pike (1990). Three-dimensional turbulent flow in agitated vessels with a nonisotropic viscosity turbulence model, *Can. J. Chem. Eng.*, **68**, 3–16.

Khang, S. J., and O. Levenspiel (1976). New scale-up and design method for stirrer agitated batch mixing vessels, *Chem. Eng. Sci.*, **31**, 569–580, and *Chem. Eng.*, Oct. 11, pp. 141–148.

King, M. L., A. L. Forman, C. Orella, and S. H. Pines (1985). Extractive hydrolysis for pharmaceuticals, *Chem. Eng. Prog.*, **81**(5), 36–39.

Klein, J., R. David, and J. Villermaux (1980). Interpretation of experimental liquid phase micromixing phenomena in a continuous stirred tank reactor with short residence times, *Ind. Eng. Chem. Fundam.*, **19**, 373–379.

Kosaly, G. (1987). Premixed simple reaction in homogeneous turbulence, *AIChE J.*, **33**, 1998–2002.

Larson, K. A., M. Midler, and E. Paul (1995). Reactive crystallization: control of particle size and scale-up, presented at the Association for Crystallization Technology Meeting, Charlottesville, VA.

Launder, B. E., and D. B. Spalding (1972). *Mathematical Models of Turbulence*, Academic Press, New York.

Lee, S. Y., and Y. P. Tsui (1999). Succeed at gas/liquid contacting, *Chem. Eng. Prog.*, July, pp. 23–49.

Leonard, A. D., R. D. Hamlen, R. M. Kerr, and J. C. Hill (1995). Evaluation of closure models for turbulent reacting flows, *Ind. Eng. Chem. Res.*, **34**, 3640–3652.

Levenspiel, O. (1962). *Chemical Reaction Engineering*, Wiley, New York.

Levenspiel, O. (1972). *Chemical Reaction Engineering*, 2nd ed., Wiley, New York.

Levenspiel, O. (1999). *Chemical Reaction Engineering*, 3rd ed., Wiley, New York.

Li, K. T., and H. L. Toor (1986). Turbulent reactive mixing with a series–parallel reaction: effect of mixing on yield, *AIChE J.*, **32**, 1312–1320.

Magnussen, B. F., and B. H. Hjertager (1976). On mathematical models of turbulent combustion with special emphasis on soot formation and combustion, *Proc. 16th International Symposium on Combustion*, Combustion Institute, Pittsburgh, PA.

Mann, R., and P. Knysh (1984). Utility of networks of interconnected backmixed zones to represent mixing in a closed stirred vessel, *Inst. Chem. Eng. Symp. Ser.*, **89**, 127–145.

Mao, K. W., and H. L. Toor (1971). Second-order chemical reactions with turbulent mixing, *Ind. Eng. Chem. Fundam.*, **10**, 192–197.

Marcant, B., R. David, R. Mamourian, and J. Villermaux (1991). In *Industrial Crystallization,* Vol. 90, 205, A. Mersmann, ed., Germmish, Germany.

McKelvey, K. N., H.-C. Yieh, S. Zakanycz, and R. S. Brodkey (1975). Turbulent motion, mixing and kinetics in a chemical reactor configuration, *AIChE J.*, **21**, 1165–1176.

Medek, J. (1980). Power characteristics of agitators with flat inclined blades, *Int. Chem. Eng.*, **20**, 664–672.

Mehta, R. V., and J. M. Tarbell (1983). Four-environment model of mixing and chemical reaction, *AIChE J.*, **29**, 320–328.

Mersmann, A., and M. Kind (1988). Chemical engineering aspects of precipitation from solution, *Chem. Eng. Technol.*, **11**, 264–276.

Middleton, J. C. (1992). Gas–liquid dispersion and mixing, Chapter 15 in *Mixing in the Process Industries*, N. Harnby, M. F. Edwards, and A. W. Nienow, eds., Butterworth-Heinemann, Wolburn, MA.

Middleton, J. C., F. Pierce, and P. M. Lynch (1986). Computations of flow fields and complex reaction yield in turbulent stirred reactors and comparison with experimental data, *Chem. Eng. Res. Des.*, **64**, 20–22.

Nauman, E. B. (1982). Reactions and residence time distributions in motionless mixers, *Can. J. Chem. Eng.*, **60**, 136–140.

Nienow, A. W. (1997). On impeller circulation and mixing effectiveness in the turbulent flow regime, *Chem. Eng. Sci.*, **52**, 2557–2565.

Nienow, A. W., and K. Inoue (1993). A study of precipitation micromixing, macromixing, size distribution, and morphology, Paper 9.4, presented at CHISA, Prague, Czech Republic.

Oldshue, J. Y. (1980). Mixing in hydrogenation processes, *Chem. Eng. Prog.*, **76**(6), 60–64.

Oldshue, J. Y. (1983). *Fluid Mixing Technology*, McGraw-Hill, New York.

Ottino, J. M. (1980). Lamellar mixing models for structured chemical reactions and their relationship to statistical models, *Chem. Eng. Sci.*, **35**, 1377–1391.

Patterson, G. K. (1973). Model with no arbitrary parameters for mixing effects on second-order reaction with unmixed feed reactants, in *Fluid Mechanics of Mixing*, E. M. Uram, and V. W. Goldschmidt, eds., ASME, New York, pp. 31–38.

Patterson, G. K. (1975). Simulating turbulent-field mixers and reactors, in *Application of Turbulence Theory to Mixing Operations*, R. S. Brodkey, ed., Academic Press, New York, pp. 223–275.

Patterson, G. K. (1985). Modeling of turbulent reactors, in *Mixing of Liquids by Mechanical Agitation*, J. J. Ulbrecht, and G. K. Patterson, eds., Gordon & Breach, New York, pp. 59–91.

Patterson, G. K., and J. Randick (2000). Simulation with validation of mixing effects in fed-batch reactors, *Proc. 10th European Conference on Mixing*, H. E. A. van den Akker, and J. J. Derksen, eds., Delft, The Netherlands, July, pp. 53–60.

Paul, E. L. (1988). Design of reaction systems for specialty organic chemicals, *Chem. Eng. Sci.*, **43**, 1773–1782.

Paul, E. L., and R. E. Treybal (1971). Mixing and product distribution for a liquid-phase, second-order, competitive-consecutive reaction, *AIChE J.*, **17**, 718–731.

Paul, E. L., J. Aiena, and W. A. Sklarz (1981). Effect of mixing on the selectivity of the competitive-consecutive chlorination of acetone, presented at the AIChE National Meeting, New Orleans, LA.

Paul, E. L., H. Mahadevan, J. Foster, M. Kennedy, and M. Midler (1992). The effect of mixing on scale-up of a parallel reaction system, *Chem. Eng. Sci.*, **47**, 2837–2840.

Penney, R. W. (1971). Scale-up for mixing operations, *Chem. Eng.*, Mar., p. 22.

Penney, R. W., H. X. Vo, and G. K. Patterson (1997). Implementation of the Bourne engulfment model using TK-Solver, presented at the AIChE Annual Meeting, Los Angeles.

Perng, C. Y., and J. Y. Murthy (1993). A moving mesh technique for simulation of flow in mixing tanks, in *Process Mixing: Chemical and Biochemical Applications*, Part II, G. B. Tatterson, R. V. Calebrese, and W. R. Penney, eds., AIChE Symp. Ser.

Pohorecki, R., and J. Baldyga (1988). The effects of micromixing and the manner of reactant feeding on precipitation in stirred tank reactors, *Chem. Eng. Sci.*, **43**, 1949–1954.

Pope, S. B. (1985). PDF methods for turbulent reactive flows, *Prog. Energy Combust. Sci.*, **11**, 119–192.

Randick, J. J. (2000). Simulation of scale-up effects on stirred chemical reactors, M.S. thesis, University of Missouri–Rolla.

Roussinova, V., B. Grgic, and S. M. Kresta (2000). Study of macro-instabilities in stirred tanks using a velocity decomposition technique, *Chem. Eng. Res. Des.*, **78**, 1040–1052.

Schaftlein, R. W., and T. W. F. Russell (1968). Two-phase reactor design, tank-type reactors, *Ind. Eng. Chem.*, **60**, 12–20.

Schutz, J. (1988). Agitated thin-film reactors and tubular reactors with stator mixers for a rapid exothermic multiple reaction, *Chem. Eng. Sci.*, **43**, 1975–1980.

Sharma, M. M. (1988). Multiphase reactions in the manufacture of fine chemicals, *Chem. Eng. Sci.*, **43**, 1749–1750.

Sharratt, P. N., ed. (1997). *Handbook of Batch Process Design*, Blackie, London.

Spalding, D. B. (1971). Concentration fluctuations in a round turbulent free jet, *Chem. Eng. Sci.*, **26**, 95–108.

Tatterson, G. B. (1991). *Fluid Mixing and Gas Dispersion in Agitated Tanks*, McGraw-Hill, New York.

Thoma, S. (1989). Interactions between macro- and micro-mixing in stirred tank reactors, Dissertation 9012, ETH, Zurich.

Thoma, S., V. V. Ranade, and J. R. Bourne (1991). Interaction between macro- and micromixing during reactions in stirred tanks, *Can. J. Chem. Eng.*, **69**, 1135–1141.

Thornton, J. D. (1992). *Science and Practice of Liquid–Liquid Extraction*, Vol. 2, Oxford University Press, Oxford, pp. 290–291.

Tipnis, S. K., W. R. Penney, and J. Fasano (1994). An experimental investigation to determine a scale-up method for fast competitive-parallel reactions in agitated vessels, *AIChE Symp. Ser. 299*, **90**, 78–91.

Toor, H. L. (1969). Turbulent mixing of two species with and without chemical reaction, *Ind. Eng. Chem. Fundam.*, **8**, 655–659.

Tosun, G. (1997). A study of diffusion and reaction in unpremixed step growth copolymerization in a micro-segregated continuous stirred reactor, *Ind. Eng. Chem.*, **36**, 4075–4086.

Van de Vusse, J. G. (1966). Consecutive reactions in heterogeneous systems, *Chem. Eng. Sci.*, **21**, 631–643, 1239–1252.

Van den Akker, H. E. A. (2001). Poster presented at Mixing XVIII, Pocono Manor, PA, June.

Vassilatos, G., and H. L. Toor (1965). Second-order chemical reactions in a nonhomogeneous turbulent field, *AIChE J.*, **11**, 666–672.

Villermaux, J., and R. David (1987). Interpretation of micromixing effects on fast consecutive competitive reactions in semi-batch stirred tanks by a simple interaction model, *Chem. Eng. Commun.*, **54**, 333–352.

Villermaux, J., and J. C. Devillon (1972). Representation de coalescence de la redispersion des domaines de segregation, *Proc. 2nd International Symposium on Chemical Reaction Engineering*, Amsterdam, pp. B1–B13.

Villermaux, J., and Z. Zoulalian (1969). Etat du mélange du fluide dans in réacteur continu: a propos d'un modèle de Weinstein et Alder, *Chem. Eng. Sci.*, **24**, 1513–1518.

Wang, Y. D. (1984). Study on the Hofmann rearrangement in a two phase system, *Jilin Daxue Ziran Kexue Xuebao*, **2**, 89–93.

Wiederkehr, H. (1988). Examples of process improvements in the fine chemicals industry, *Chem. Eng. Sci.*, **43**, 1783–1791.

Wu, H., and G. K. Patterson (1989). Laser-Doppler measurements of turbulent flow parameters in a stirred mixer, *Chem. Eng. Sci.*, **44**, 2207–2221.

Zhou, G., and S. M. Kresta (1996). Impact of geometry on the maximum turbulence energy dissipation rate for various impellers, *AIChE J.*, **42**, 2476–2490.

Zipp, R. P., and G. K. Patterson (1998). Experimental measurements and simulation of mixing and chemical reaction in a stirred tank, *Can. J. Chem. Eng.*, **76**, 657–669.

CHAPTER 14

Heat Transfer

W. ROY PENNEY
University of Arkansas
VICTOR A. ATIEMO-OBENG
The Dow Chemical Company

14-1 INTRODUCTION

Heat transfer in agitated vessels, a common industrial practice, has been researched extensively. Experimental work started in the 40s with peak activity in the 50s and 60s. The 1959 paper by Brooks and Su is an excellent example of the work done in the 50s and 60s. Comprehensive coverage is beyond the scope of this work; only a summary of the most useful and general information is presented here. Books by Sterbacek and Tausk (1965), Holland and Chapman (1966), Uhl and Gray (1966), and Nagata (1975) present comprehensive coverage. Parker (1964), Jordan (1968), Edwards and Wilkinson (1972a,b), and Rase (1977) present less comprehensive coverage. Penney (1983) and Dream (1999) give summaries of the most useful correlations for heat transfer coefficients in agitated vessels. Fasano et al. (1994) give correlations for the vessel wall and for the vessel bottom head for various impellers. Haam et al. (1992, 1993) discuss an experimental technique based on surface calorimeters for measuring local heat flux.

The intent of this chapter is to provide sufficient information to enable the designer to design a heating or cooling system for the job at hand. Only the most commonly used agitator impellers and heat transfer surfaces are covered here. To determine the economic optimum system will often require going beyond the knowledge base of this chapter. The reader is advised to contact vendors and use their expertise for a more economical design than that of the "base case," which one can obtain by using the information in this chapter.

Handbook of Industrial Mixing: Science and Practice, Edited by Edward L. Paul, Victor A. Atiemo-Obeng, and Suzanne M. Kresta
ISBN 0-471-26919-0

14-2 FUNDAMENTALS

A jacketed agitated vessel may be used for heating or cooling its fluid contents. The rate of heat transfer, Q, can be expressed by Newton's law of heat transfer as follows:

$$Q = UA\ \Delta T \tag{14-1}$$

U, the overall heat transfer coefficient, depends on the fluid properties, the operating parameters of the mixer, and the system configuration. It is the key parameter that is affected by the operation of the mixer. The available area for heat transfer, A, depends on the geometry of the system. Usually, the area per volume decreases on vessel scale-up. The temperature driving force, ΔT, depends on the operating conditions of both the process and the heating or cooling fluid.

Heat transfer between the jacket fluid and the vessel contents occurs by conduction and forced convection. The resistance to heat transfer is a composite of the resistances through the various sections indicated in Figure 14-1. Using the classical film theory and heat conduction through composite layers, the overall heat transfer coefficient can be expressed as

$$\frac{1}{U_{ps}} = \frac{1}{h_{htfs\ film}}\frac{A_{ps}}{A_{htfs}} + f_{htfs}\frac{A_{ps}}{A_{htfs}} + \frac{x_{wall}}{k_{wall}}\frac{A_{ps}}{A_{wall}} + \frac{x_{lining}}{k_{lining}}\frac{A_{ps}}{A_{lining}} + f_{ps} + \frac{1}{h_{ps\ film}} \tag{14-2}$$

In a jacketed agitated vessel, mixing affects only the process-side film heat transfer coefficient, $h_{ps\ film}$. The largest resistance in the expression dominates the value of the overall heat transfer coefficient. The thermal resistance due to fouling on either the heat transfer fluid side, f_{htfs}, or the process fluid side, h_{ps}, can significantly affect heat transfer. For carbon steel vessels, the wall conductivity is normally high enough so that the conductive resistance is a minor fraction of the overall thermal resistance. The thermal conductivity is lower for stainless steel and glass lining and can affect the overall heat transfer coefficient significantly. Values of thermal conductivity for various materials are given in Table 14-1.

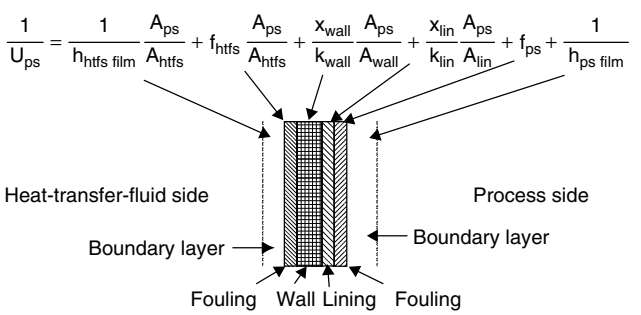

Figure 14-1 Resistances to heat transfer.

Table 14-1 Physical Properties of Vessel Materials

Material	Thermal Conductivity, k Btu/(hr ft^2 °F/ft) [W/m · K]	Specific Heat, c_p Btu/lb °F [J/kg · K]	Density, ρ lb/ft^3 [g/cm^3]
Carbon steel	30 [52]	0.11 [460]	484 [7.8]
Copper	218 [377]	0.092 [385]	559 [9.0]
Cupro-nickel 90/10	30 [52]	0.106 [444]	541 [8.7]
Cupro-nickel 70/30	20 [35]	0.106 [444]	519 [8.3]
Glass	0.67 [1.16]	0.2 [835]	155 [2.5]
Hastelloy C276	7.5 [11]	0.092 [385]	558 [8.9]
Incoloy 825	6.9 [12]		508 [8.1]
Inconel 600	9.2 [16]	0.106 [444]	520 [8.3]
Monel (400, 404, R405, 411)	15 [26]	0.102 [427]	551 [8.8]
Nickel (200, 201, 220, 225)	38 [66]	0.105 [440]	555 [8.9]
Stainless steel (304, 316, 321, 347)	9.8 [17]	0.12 [502]	481 [7.7]
Tantalum	32 [54]	0.036 [151]	1036 [16.6]
Titanium	11.5 [20]	0.139 [582]	283 [4.5]

The following steps are required to design an agitated vessel to satisfy certain heat transfer requirements:

1. Select the agitator and vessel geometry.
2. Select the vessel internals.
3. Size the agitator and heat transfer surfaces.

The most important parameters affecting the design of an agitated vessel for heat transfer are:

1. The process results, other than heat transfer, to be obtained
2. The heat duty per unit of vessel volume
3. The fluid physical properties (primarily viscosity)
4. The vessel volume

For low to moderate viscosities ($\mu < 10\,000$ cP, i.e., 100 poise), in industrial-sized vessels (volume > 1 m^3), high impeller pumping rates producing turbulent motion are possible, and nonproximity impellers (shown in Figure 14-2 and Chapter 2) are used. For fluids with higher viscosity where laminar flow patterns are likely, proximity impellers such as anchors and helical ribbons are used.

For low to moderate heat duties (in terms of heat duty per unit of vessel volume), a vessel jacket is usually adequate to provide the required heat transfer surface. As heat duty increases, internal heat transfer surfaces (helical coils,

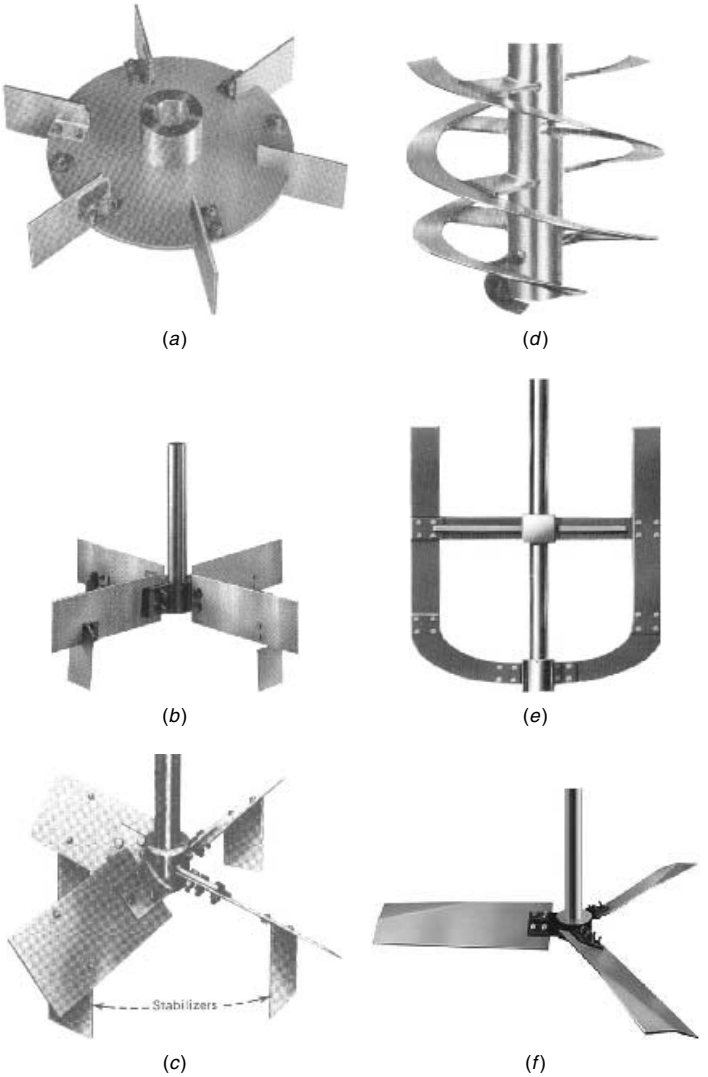

Figure 14-2 Typical impellers for mechanically agitated vessels: (*a*) six-blade disk impeller (6BD) or Rushton turbine; (*b*) four-blade flat impeller (4BF); (*c*) four-blade pitched impeller (4BP); (*d*) helical ribbon impeller; (*e*) anchor impeller; (*f*) high efficiency turbine impeller.

baffle pipes, or plate coils) may be required. For some systems, with very high heat duties, adequate heat exchange is not possible even with the installation of internal heat transfer surfaces. For such systems additional heat transfer surface can readily be provided by using an external pumped-through heat exchanger.

For systems where a volatile component can be vaporized and condensed, evaporative cooling is often the most economical means of heat removal. The

vaporized component is condensed and returned (i.e., refluxed) back to the vessel. For information on the selection and design of external heat exchangers and condensers, the reader should refer to other sources, such as Saunders (1988).

A special problem exists for heat removal applications. Because agitator power requirements (which always add heat to the vessel contents) are much more strongly dependent on agitator speed than are heat transfer coefficients, a maximum heat removal capability exists for any particular agitated vessel. This phenomenon is of particular importance for heat removal in high viscosity systems. Refer to Penney and Koopman (1971) for recommendations concerning optimum design. Penney and Koopman have given the following recommendations for the magnitude of agitator power input to obtain maximum net heat removal. For the laminar regime, the agitator power to obtain maximum net heat removal is about 20% of the net heat removed, and for the turbulent regime, the agitator power to obtain maximum net heat removal is in the range 5 to 20% of the net heat removal. A value of 20% for the turbulent regime is generally applicable where all thermal resistances other than the inside vessel fluid film are about 0.001 hr-ft^2-°F/Btu, and a value of 5% is applicable where they are about 0.01 hr-ft^2-°F/Btu for typical organic liquids in plant-sized vessels.

14-3 MOST COST-EFFECTIVE HEAT TRANSFER GEOMETRY

The first consideration regarding heat transfer needs in agitated vessels concerns which surface and which heat removal system to use. Which heat removal system is most cost-effective? In general the choices listed in order of least to most expensive are:

1. Vessel wall jacket
2. Vessel bottom head jacket
3. Internal surface (e.g., helical coils, plate coils, or vertical harp coils)
4. Reflux cooling by solvent evaporation and external condenser
5. External pumped-through heat exchangers

It is important to remember that for the most demanding heat removal requirements, one should always consider introducing a solvent that can be made to boil at the process temperature and pressure, vaporizing that solvent, condensing it, and returning (i.e., refluxing) the condensate to the vessel. This option is often overlooked when designing a heat removal system. There are myriad reflux cooling applications in industrial practice, and an excellent example is the reflux cooling used to remove the heat of polymerization from polystyrene reactors by evaporating and condensing the styrene monomer.

The geometry of internal coils needs to be selected carefully because all geometries are not equally effective. The most important geometrical considerations are summarized in Table 14-2. The vessel, vessel internals, and an agitation source are the components of the typical installation. Mechanical agitators (consisting of a drive, a drive shaft, and an impeller) are most often used to

Table 14-2 Most Effective Geometry for Heat Transfer

Geometrical Variable	Most Effective Value(s) (Best → Least)
Type of surface	+ → Helical coils (see Figure 14-3). → Harp (i.e., vertical tube baffles) coils (see Figure 14-4). → Plate coils (see Figure 14-4).
Number of coils, plates, etc.	+ For helical coils, use two maximum. + For harps and plate coils, up to 16 can be used effectively.
Position of surface in vessel	+ Helical coils are placed inside and attached to baffles. + Harp coils and plate coils act as baffles and are positioned vertically along the vessel walls as baffles.
Distance between coil banks	+ Minimum distance is twice the tube diameter.
Spacing of harps and plate coils	+ Up to 16 are used; above about 8 the harps and plate coils are normally positioned at about 45° to the vessel diameter.
Spacing between tubes in harps and helical coils	+ Minimum spacing is one tube diameter.

provide agitation; however, gas sparging and liquid jets (i.e., jet mixing) entering the vessel (primarily from circulation through a pump) are also used to provide agitation. Quantitative design methods for gas sparging are available in the literature and the source literature references are given later in this chapter, but quantitative design methods are not available for jet mixing.

14-3.1 Mechanical Agitators

Figure 14-2 presents visuals of commonly used mechanical agitator impellers. Heat transfer correlations for these impellers are presented later. The reader is referred to Chapter 6 for information on their performance characteristics and guidelines for their selection and use.

14-3.2 Gas Sparging

For bubble columns with height/diameter > 5, a simple open pipe at the bottom of the column is often adequate. For height/diameter < 5, a ring or finger-style perforated pipe sparger is desirable to obtain uniform radial distribution of the gas and to prevent excessive channeling of the gas up the center of the vessel. For heat transfer in bubble agitated columns, see Hart (1976) and Tamari and Nishikawa (1976).

14-3.3 Vessel Internals

With nonproximity agitators, baffles are almost always used to prevent swirl and subsequent vortexing and to increase top-to-bottom motion and turbulence.

Helical coils, pipe baffles, and plate coil baffles are the most common heat transfer surfaces within the vessel.

14-3.3.1 Wall Baffles. Figure 14-3 shows the recommended geometry; the baffle width is $\frac{1}{12}$ of the vessel diameter, and the baffles are most often positioned a short distance (about T/75) from the vessel wall. Sometimes vortexing is desirable (e.g., when wetting semibatch fed powders or dispersing small volumes of gas from the vessel headspace) (Deeth et al., 2000). For these applications partial baffling is recommended. The most commonly used partial baffling is half-baffles, which are normally $\frac{1}{12}$ the vessel diameter in width but extend only halfway up the liquid height up the vessel wall from the vessel bottom.

Vortex depth in nonbaffled agitated vessels has been investigated by Brennan (1976) and Rieger et al. (1979); both references present predictive methods. For

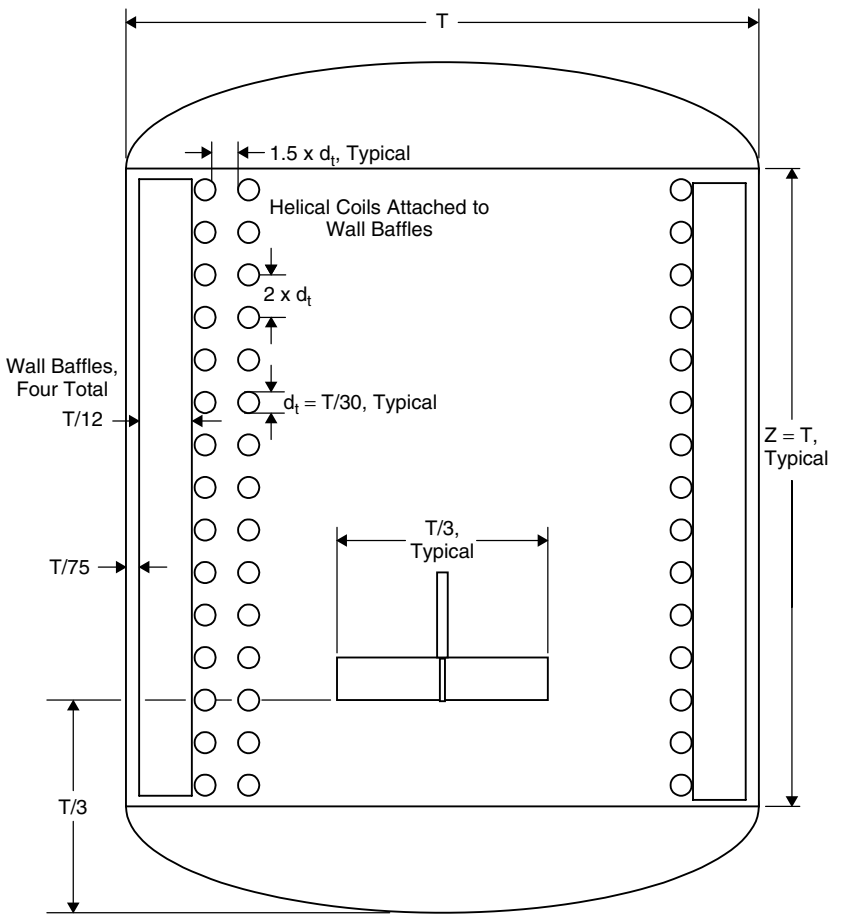

Figure 14-3 Recommended geometries for wall baffles and helical coils.

thin liquids with turbulent conditions, for quick estimating purposes $X/D \simeq 4(Fr)$ [see Table 1 in Brennan (1976) and Figure 14-3 in Rieger et al. (1979)]. Often, half-baffles (i.e., $B = T/12$ and the baffles extend only halfway up the vessel wall) are used in the lower portion of the vessel to produce a significant vortex while reducing swirl sufficiently to provide sufficient shear to be effective in dispersing solids agglomerates or to entrain and disperse small volumes of gas from the vessel headspace.

Axial flow impellers (<5 kW) are often mounted angled, off-center (Rushton, 1947; Weber, 1963; Uhl and Gray, 1966) to prevent swirl and vortexing. For clockwise rotation (looking along the shaft from the drive to the impeller), Uhl and Gray (1966, pp. 153–156) recommend that the agitator shaft be moved off-center T/6, tilted back at an angle of 10°, and then moved back so that the impeller centerline is located on the centerline of the vessel.

14-3.3.2 Helical Coils. Figure 14-3 presents the recommended geometry. Rushton (1947), Parker (1964), and Hicks and Gates (1975) give recommendations concerning coil geometry. This geometry is not the economical optimum for all cases; for example, Rushton (1947, p. 653) says, "clearance between pipes in a helix need not be great and, if $\mu < 500$ cP, the clearance between layers may be as little as one-third pipe diameter." Unfortunately, insufficient quantitative information is available to allow prediction of the heat transfer coefficient for a gap spacing of less than one pipe diameter; thus, the recommendation given in Figure 14-3 is a gap spacing of one pipe diameter. For cases where the geometry of Figure 14-3 does not provide sufficient heat duty, an equipment manufacturer should be contacted. They may be able to recommend more compact geometries which have greater heat transfer surface per unit volume than those recommended here. Manufacturers often have additional design information which allows selection of a more economical geometry. For example, for some situations a second and a third coil (Marshall and Yazdani, 1970; Hicks and Gates, 1975), may be economical, although the heat transfer coefficients will be reduced for the middle and outer coils in a three-coil band—to about 60 and 40%, respectively, of the inner coil—according to Marshall and Yazdani (1970).

14-3.3.3 Baffle Pipes and Plate Coil Baffles. The recommended geometries are presented in Figure 14-4. The baffle pipes can be placed either radially across the vessel or at an angle of 45° with the vessel radius. With radial positioning, four pipes per baffle are recommended; and with angled positioning, five pipes per baffle are recommended. The experimental work discussed later was done with four baffles. When using plate coils, more than four baffles are used; in fact, as many as 16 angled plate coils have been installed in agitated vessels. Probably six baffles would have little effect on the heat transfer coefficient; however, above some number, perhaps six, the heat transfer coefficient will be reduced as additional plate coils are added. For more than six baffles, a manufacturer of plate coils and/or a manufacturer of fluid mixing equipment should be consulted.

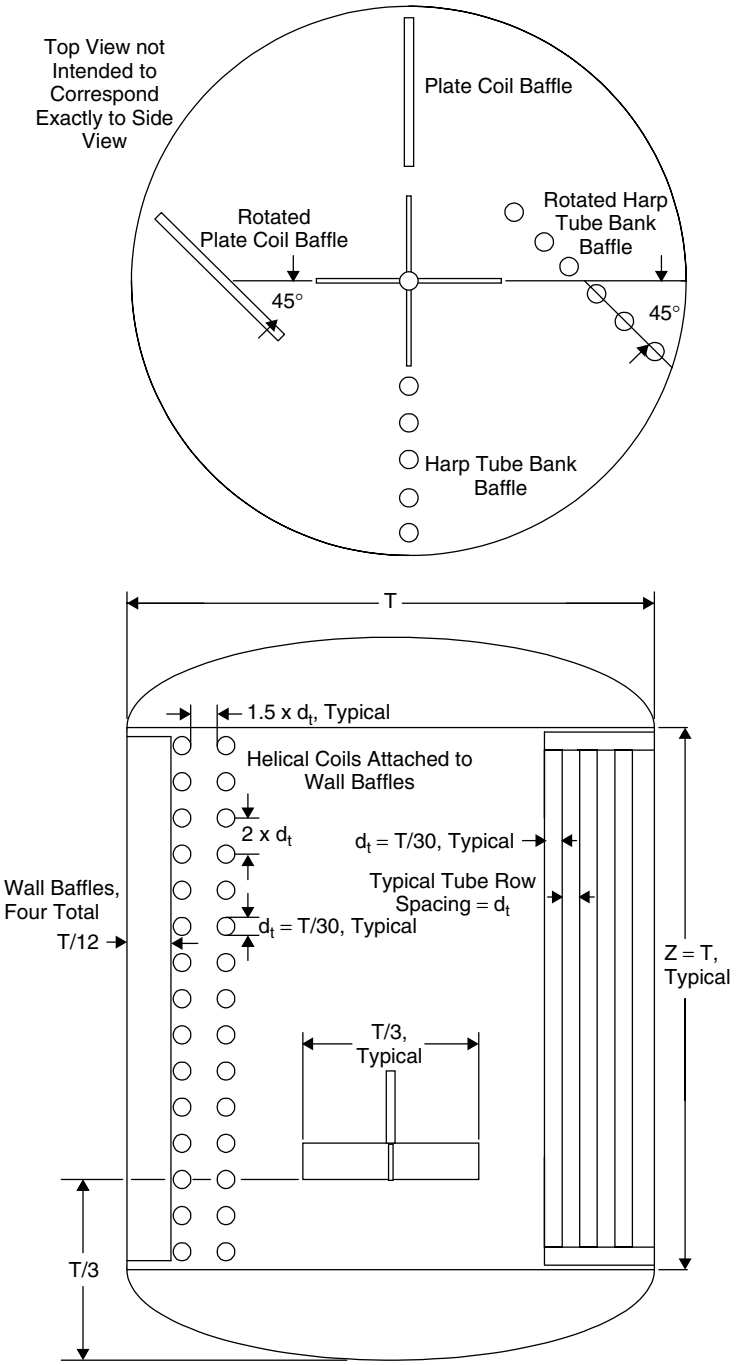

Figure 14-4 Recommended geometries for vertical tube baffles (harp coils) and plate coils.

14-4 HEAT TRANSFER COEFFICIENT CORRELATIONS

Published correlations for the process-side heat transfer coefficient are all of the form

$$Nu = K \cdot Re^a Pr^b \mu_R^c G_c \tag{14-3}$$

where G_c represents a geometry correction. Several correlations are presented in Table 14-3. The dimensionless numbers are explained below.

Nusselt Number, Nu

For heat transfer to or from the vessel wall or bottom head in a jacketed vessel

$$Nu = \frac{hT}{k} \tag{14-4a}$$

For a harp or helical coil

$$Nu = \frac{hd_t}{k} \tag{14-4b}$$

For a plate coil

$$Nu = \frac{h(W_{PC}/4)}{k} \tag{14-4c}$$

The characteristic length of $W_{PC}/4$ is recommended for a plate coil because Petree and Small (1978) used the width of the plate coil divided by the number of utility fluid passes within the utility side of the plate coil as the characteristic length in the Nusselt number. It is unlikely that the number of passes on the utility side have any significant effect on the heat transfer coefficient. Thus, the only reason to use $W_{PC}/4$ as the characteristic length in the Nusselt number is that Petree and Small (1978) used a plate coil with four passes in their experimental apparatus.

Prandtl Number, Pr

$$Pr = \frac{\mu_b C_p}{k} \tag{14-5}$$

where the subscript b refers to the bulk of fluid.

Viscosity Ratio, μ_R

$$\mu_R = \frac{\mu_b}{\mu_w} \tag{14-6}$$

where the subscript b refers to the bulk fluid and the subscript w refers to the vessel wall.

Geometrical Corrections (i.e., G_C). In some cases the exact forms of the geometric corrections have been changed from the original references, and in several

Table 14-3 Heat Transfer Coefficient Correlations for Agitated, Baffled Vessels[a]

Impeller	Surface	Re Range	K	a	B	c	Geometry Correction[a]	Reference
6BD	Wall	>100	0.74	2/3	1/3	0.14	$(1/[H/T])^{0.15}(L/L_S)^{0.2}$	Fasano et al. (1994)
4BF	Wall	>100	0.66	2/3	1/3	0.14	$(1/[H/T])^{0.15}(L/L_S)^{0.2}$	Fasano et al. (1994)
4BP	Wall	>100	0.45	2/3	1/3	0.14	$(1/[H/T])^{0.15}(L/L_S)^{0.2}$	Fasano et al. (1994)
HE3	Wall	>100	0.31	2/3	1/3	0.14	$(1/[H/T])^{0.15}$	Fasano et al. (1994)
PROP	Wall	>100	0.5	2/3	1/3	0.14	$(1/[H/T])^{0.15}(1.29[P/D])/(0.29+ [P/D])$	Strek et al. (1963)
6BD	BH[c]	>100	0.50	2/3	1/3	0.14	$(1/[H/T])^{0.15}(L/L_S)^{0.2}$	Fasano et al. (1994)
4BF	BH	>100	0.40	2/3	1/3	0.14	$(1/[H/T])^{0.15}(L/L_S)^{0.2}$	Fasano et al. (1994)
4BP	BH	>100	1.08	2/3	1/3	0.14	$(1/[H/T])^{0.15}(L/L_S)^{0.2}$	Fasano et al. (1994)
HE3	BH	>100	0.9	2/3	1/3	0.14	$(1/[H/T])^{0.15}$	Fasano et al. (1994)
RCI[d]	Wall and BH	>100	0.54	2/3	1/3	0.14	$(1/[H/T])^{0.15}$	Ackley (1960)
PROP	Helical coil		0.016	0.67	0.37	0.14	$([D/T]/[1/3])^{0.1}$ $([d/T]/0.04)^{0.5}$	Oldshue (1966)
6BD	Helical coil	>100	0.03	2/3	1/3	0.14	$(1/[H/T])^{0.15}(L/L_S)^{0.2}([D/T]/[1/3])^{0.1}([d/T]/0.04)^{0.5}(2/N_B)^{0.2}$	Oldshue and Gretton (1954)
6BD	45° harp coils	>100	0.021	0.67	0.4	0.27[e]	$(1/[H/T])^{0.15}(L/L_S)^{0.2}([D/T]/[1/3])^{0.33}([d/T]/0.04)^{0.5}$	Gentry and Small (1978)
4BF	0° harp coils	>100	0.06	0.65	0.3	0.42[e]	$(1/[H/T])^{0.15}(L/L_S)^{0.2}([D/T]/[1/3])^{0.33}([d/T]/0.04)^{0.5}$	Dunlap and Rushton (1953)
6BD	Plate coils	>100	0.031	0.66	0.33	0.5[e]	$(1/[H/T])^{0.15}(L/L_S)^{0.2}$	Petree and Small (1978)
Anchor	Wall	<1	Not recommended! In the laminar regime; the anchor fails to give top-to-bottom fluid motion					
	Wall	>12, <100	0.69	1/2	1/3	0.14		Harry and Uhl (1973)
	Wall	>100	0.32	2/3	1/3	0.14		Harry and Uhl (1973)
Helical	Wall	<13	0.94	1/3	1/3	0.14		Ishibashi et al. (1979)
ribbon	Wall	>13, <210	0.61	1/2	1/3	0.14		Ishibashi et al. (1979)
	Wall	>210	0.25	2/3	1/3	0.14		Ishibashi et al. (1979)

[a] The correlations are of the following form: $Nu = K \cdot Re^a Pr^b \mu_R^c G_c$, where Nu (vessel wall), Nu (coil), Pr, and μ_R are as defined in eq. (14-2), (14-3), and (14-4).

[b] d, tube diameter in helical coil; D, impeller diameter; L, height of the impeller blade parallel with the axis of rotation; L_s, standard height of the impeller blade parallel to the axis of rotation (for 6BD, $L_s/D = 0.2$; for 4BF, $L_s/D = \frac{1}{5}$; for 4BP, $L_s/D = 0.17$); N_B, number of blades on the Impeller; P, pitch of a propeller or a helical ribbon impeller (forward motion of the impeller blade over 360° of rotation); T, tank diameter, H, height of the batch.

[c] BH bottom head.

[d] RCI retreat curve impeller.

[e] These authors used the ratio to bulk to film viscosity. It is recommended that one use c = 0.14 and use the ratio of bulk to wall viscosity.

cases, additional geometric corrections have been included. In some cases this procedure changed the value of K from the original reference, but the final correlation remains the same. The geometrical corrections have been consistently included as a ratio of a geometrical parameter to a standard geometrical parameter. The value for the standard value is normally the experimental value (or a value in the midpoint of the experimental data) used by various investigators. This practice, where the geometrical correction is unity for the standard value of a parameter, makes it much easier to compare various correlations directly.

For turbulent conditions, typical values for the exponents in eq. (14-3) are $\frac{2}{3}$, $\frac{1}{3}$, and 0.14, respectively, for a, b, and c. With these values for the exponents, eq. (14-3) can be written in terms of the specific energy input or energy dissipation, ε, for a given impeller and physical properties as follows:

$$h \propto \varepsilon^{2/9} \left(\frac{D}{T}\right)^{2/9} T^{-1/9} \tag{14-7}$$

This form helps one appreciate the effect of energy input and impeller size on the process-side film heat transfer coefficient. To double h, ε must increase by a factor of 23! Similarly, the effect of impeller size, represented by D/T, is also weak. A change of impeller diameter from 0.33T to 0.67T improves h by only 10%.

14-4.1 Correlations for the Vessel Wall

- *Flat, disk, pitched blade turbines and HE-3*. The correlations by Fasano et al. (1994) are recommended. Corrections for dimensionless batch height and dimensionless impeller height are given.
- *Propeller*. The correlation of Strek et al. (1965) is recommended. A correction for dimensionless batch height is given. The vessel is baffled with heat transfer at the wall.
- *Glass-coated three-bladed impeller (RCI)–one finger-style baffle*. The correlation of Ackley (1960) is recommended. A correction for dimensionless batch height is given.

14-4.2 Correlations for the Bottom Head

- *Flat, disk, pitched blade turbines and HE-3*. The correlations recommended by Fasano et al. (1994) are recommended. Corrections for dimensionless batch height and dimensionless impeller height are given.
- *Propeller*. The correlation of Strek et al. (1965), which was developed for the vessel wall, is recommended.
- *Glass-coated three-bladed impeller–one finger-style baffle*. The correlation of Ackley (1960), which was developed for the vessel wall, is recommended.

14-4.3 Correlations for Helical Coils

- *Flat, disk, and pitched blade turbines*. Oldshue and Gretton's (1954) correlation is recommended for the standard geometry. Corrections for dimensionless batch height and dimensionless impeller height are given.
- *Propeller*. Oldshue's (1966) correlation is recommended for the standard geometry. Corrections for dimensionless batch height and dimensionless impeller height are given.

14-4.4 Correlations for Vertical Baffle Coils (i.e., Vertical Baffle Pipes)

- *Four-blade disk turbines–vertical baffle coil*. Dunlap and Rushton's (1953) correlation is recommended with appropriate geometric corrections added. Table 14-3 gives $K = 0.06$, which seems high based on the findings of Gentry and Small (1978) for baffle pipes oriented at 45° to the vessel diameter. It may be prudent to use $K = 0.04$ rather than $K = 0.06$.
- *Two six-blade disk turbines–vertical tube baffles*. Gentry and Small's (1978) correlation is recommended with corrections added for dimensionless batch height and dimensionless impeller height.

14-4.5 Correlations for Plate Coils

- *Two six-blade disk turbines–vertical plate coils*. Petree and Small's (1978) correlation is recommended.

14-4.6 Correlations for Anchors and Helical Ribbons

Uhl (1970), Harry and Uhl (1973), and Nishikawa et al. (1975) have summarized all previous work. Ishibashi et al. (1979) and Rautenbach and Bollenrath (1979) have published the latest works. Coyle et al. (1970) have presented very useful experimental data. Nagata et al. (1970) and Mitsuishi and Miyairi (1973) are of interest. The correlations by Harry and Uhl (1973) and Ishibashi et al. (1979) are recommended. The recommended impeller geometries (Penney, 1983) are given in Table 14-4 and the applicable correlation parameters are given at the bottom of Table 14-3.

Table 14-4 Recommended Impeller Geometries for Anchors and Helical Ribbons

Geometric Ratio	Anchor	Helical Ribbon
P/D	∞	1/2
W/D	0.082	0.082
C_w/D	0.02	0.02
D/T	0.96	0.96

14-5 EXAMPLES

Example 14-1: Turbine Impeller. Determine the process-side heat transfer coefficient for Problem 15.9, page 460, from McCabe et al. (1993). A turbine-agitated (6BD) vessel of diameter $T = 2$ m contains 6233 kg of a dilute aqueous solution at 40°C. The agitator is a standard-geometry (thus $L = L_s$) six-blade disk impeller of diameter $D = \frac{2}{3}$ m and $N = 140$ rpm. Determine the vessel wall heat transfer coefficient.

SOLUTION

Solution specific heat, C_p	4187 J/kg · K
Solution density, ρ	992 kg/m^3
Solution viscosity, μ	0.000657 kg/m · s
Solution thermal conductivity, k	0.63 W/m · K

We first need to consider the system geometry. Let's calculate the batch height (i.e., H).

$$H = \frac{m}{\rho} / \frac{\pi D^2}{4} = \frac{(6233 \text{ kg})}{(992 \text{ kg/m}^3)} / \frac{\pi(2 \text{ m})^2}{4} = 2 \text{ m}$$

Thus, the batch is what we refer to as a "square" batch (i.e., $H = T$). We need to use the correlation from Table 14-3 for a 6BD and the vessel wall.

$$Nu = \frac{hT}{k} = 0.74 Re^{2/3} Pr^{1/3} \mu_R^{0.14} \left[\frac{1}{(H/T)}\right]^{0.15} \left(\frac{L}{L_S}\right)^{0.2}$$

$$Re = \frac{ND^2\rho}{\mu} = \frac{(140/60 \text{ rps})(2/3 \text{ m})^2(992 \text{ kg/m}^3)}{0.000657 \text{ kg/m} \cdot \text{s}} = 1.57 \times 10^6$$

$$Pr = \frac{\mu C_p}{k} = \frac{(0.000657 \text{ kg/m} \cdot \text{s})(4187 \text{ J/kg} \cdot \text{K})}{0.63 \text{ J/m} \cdot \text{K}} = 4.37$$

Assume that $\mu_R \approx 1$.

$$Nu = \frac{hT}{k} = 0.74(1.57 \times 10^6)^{2/3}(4.37)^{1/3}(1)^{0.14} \left(\frac{1}{1}\right)^{0.15} (1)^{0.2}$$

$$= (0.74)(13\,500)(1.64)(1)(1)(1) = 16\,400$$

$$h = \frac{Nu \cdot k}{T} = \frac{16\,400(0.63 \text{ W/m} \cdot \text{K})}{(2 \text{ m})} = 5170 \text{ W/m}^2 \cdot \text{K}$$

Example 14.2: Helical Ribbon Impeller. Determine the process-side heat transfer coefficient for the tank blending design example for a helical ribbon impeller (Bakker and Gates, 1995):

SOLUTION

Tank diameter, T	2.5 m
Impeller diameter, D	$0.96(T) = 0.96(2.5) = 2.4$ m
D/T	0.96
H/T	1
Batch height, H	2.5 m
Fluid viscosity, μ	$25\ Pa \cdot s = 25\ kg/m \cdot s$
Fluid density, ρ	$1200\ kg/m^3$
Impeller speed, N	16.4 rpm
Fluid thermal conductivity, k	$0.25\ W/m \cdot K$
Fluid specific heat, C_p	$2500\ J/kg \cdot K$

Calculate the Reynolds number:

$$Re = \frac{ND^2\rho}{\mu} = \frac{(16.4/60\ rps)(2.4\ m)^2(1200\ kg/m^3)}{(25\ kg/m \cdot s)} = 76$$

Select the appropriate heat transfer coefficient correlation. From Table 14-3 (for the standard helix pitch/impeller diameter ratio $P/D = \frac{1}{2}$, the appropriate heat transfer correlation is

$$Nu = 0.61Re^{1/2}Pr^{1/3}(\mu_B/\mu_W)^{0.14}$$

$$Pr = \frac{\mu_B C_P}{k} = \frac{(25\ kg/m \cdot s)(2500\ J/kg \cdot K)}{(0.25\ W/m \cdot K)} = 2.5 \times 10^5$$

$$Nu = \frac{hT}{k} = (0.61)(76)^{1/2}(2.5 \times 10^5)^{1/3}(\sim 1)^{0.14} = (0.61)(8.72)(63.4) = 337$$

$$h = \frac{337(0.25\ W/m \cdot K)}{(2.5\ m)} = 34\ W/m^2 \cdot K$$

NOMENCLATURE

A	heat transfer area (m^2)
B	baffle width (m)
C_p	specific heat of the fluid ($J/kg \cdot K$)
C_w	wall clearance for close clearance impellers (m)
d	outside diameter of the tube of which a coil is made (m)
D	impeller diameter (m)
d_t	tube diameter (m)
ΔT	temperature driving force (°C or K)
f	thermal resistance due to fouling $\left(\frac{m^2K}{W}\right)$
Fr	Froude number $= N^2D/g$

G_c geometry correction factor
h process-side heat transfer coefficient ($W/m^2 \cdot K$)
h_U utility-side heat transfer coefficient ($W/m^2 \cdot K$)
H tank height (m)
k fluid thermal conductivity ($W/m \cdot K$)
K precorrelation factor for Nu
L height of the impeller blade parallel with the axis of rotation (m)
L_S standard height of the impeller blade parallel to the axis of rotation (m)
N impeller rotational speed (rps or rpm)
N_B number of blades on the impeller
Nu Nusselt number = hT/k for the vessel wall or bottom head; N_u = hd/k for a coil
P pitch of a propeller or helical ribbon impeller (i.e., the distance along the axis of rotation which the impeller would move over 360° of rotation) (m)
Pr Prandtl number = $C_p\mu/k$
Q rate of heat transfer (W)
Re impeller Reynolds number = $\dfrac{ND^2\rho}{\mu}$
t time to heat or cool the batch from T_I to T_F (s)
T tank diameter (m)
T_F final temperature after cooling or heating of the batch is complete (K)
T_I initial temperature of the batch before heating or cooling starts (K)
T_U utility fluid temperature (K)
U overall heat transfer coefficient ($W/m^2 \cdot K$)
W blade width (m)
x Wall thickness (m)
X vortex depth below surface (m)
Z height of the batch (m)

Greek Symbols

ρ density $\left(\dfrac{kg}{m^3}\right)$
θ angle of the impeller blade with the axis of rotation
μ fluid viscosity ($kg/m \cdot s$)
μ_b fluid viscosity at the bulk fluid temperature ($kg/m \cdot s$)
μ_R viscosity ratio: bulk viscosity/wall viscosity = μ_b/μ_w
μ_w fluid viscosity at the fluid wall temperature ($kg/m \cdot s$)

REFERENCES

Ackley, E. J. (1960). Film coefficients of heat transfer for agitated process vessels, *Chem. Eng.*, Aug. 22, pp. 133–140.

Bakker, A., and L. E. Gates (1995). Properly choose mechanical agitators for viscous liquids, *Chem. Eng. Prog.*, Dec., pp. 25–33.

Brennan, D. J. (1976). Vortex geometry in unbaffled vessels with impeller agitation, *Trans. Inst. Chem. Eng*., **54**, 209–217.

Brooks, G., and G. J. Su (1959). Heat transfer in agitated vessels, *Chem. Eng. Prog.*, **55**, 54–57.

Coyle, C. K., et al. (1970). Heat transfer to jackets with close clearance impellers in viscous liquids, *Can. J. Chem. Eng*., **48**, 275–278.

Deeth, B. P., W. R. Penney, and M. F. Reeder (2000). Gas dispersion from vessel headspace: experimental scale-up studies to maintain k_La constant, *Paper f*, Session 178, Winter Annual AIChE Meeting, Los Angeles, Nov.

Dream, R. F. (1999). Heat transfer in agitated jacketed vessels, *Chem. Eng. Jen.*, pp. 90–96.

Dunlap, I. R., and J. H. Rushton (1953). Heat transfer coefficients in liquid mixing using vertical-tube baffles, *Chem. Eng. Prog. Symp. Ser.* 5, **49**, 137–151.

Edwards, M. F., and M. A. Wilkinson (1972a). Heat transfer in agitated vessels: I. Newtonian fluids, *Chem. Eng.*, Aug., pp. 310–319.

Edwards, M. F., and M. A. Wilkinson (1972b). Heat transfer in agitated vessels: II. Non-Newtonian fluids, *Chem. Eng.*, Sept., pp. 328–335.

Fasano, J. B., A. Bakker, and W. R. Penney (1994). Advanced impeller geometry boosts liquid agitation, *Chem. Eng.*, Aug., pp. 110–116.

Gentry, C. L., and W. M. Small (1978). Heat transfer and power consumption for agitated vessels having bare and finned, vertical tube baffles, *Proc. 6th International Heat Transfer Conference*, **4**, 13–18.

Haam, S. J., R. S. Brodkey, and J. B. Fasano (1992). Local heat transfer in a mixing vessel using heat flux sensors, *Ind. Eng. Chem. Res*., **31**, 1384–1391.

Haam, S. J., R. S. Brodkey, and J. B. Fasano (1993). Local heat transfer in a mixing vessel using a high-efficiency impeller, *Ind. Eng. Chem. Res*., **32**, 575–576.

Harry, F. P., and V. W. Uhl (1973). Heat transfer to viscous materials in a vessel with a helical ribbon impeller, presented at the 74th National AIChE Meeting, New Orleans, LA, Mar.

Hart, W. F. (1976). Heat transfer in bubble-agitated systems: a general correlation, *Ind. Eng. Chem. Process Des. Dev*., **15**, 109–114.

Hicks, R. W., and L. E. Gates (1975). Fluid agitation in "Fluid agitation in polymer reactors", *Chem. Eng. Prog.*, **71**, Aug., pp. 74–79.

Holland, F. A., and F. S. Chapman (1966). *Liquid Mixing and Processing in Stirred Tanks*, Reinhold, New York.

Ishibashi, K., A. Yamanaka, and N. Mitsubishi (1979). Heat transfer in agitated vessels with special types of impellers, *J. Chem. Eng. Jpn.*, **12**, 230–235.

Jordan, D. G. (1968). *Chemical Process Development*, Interscience, New York, Pt. 1, Chap. 3, pp. 111–174.

Marshall, V. C., and N. Yazdani (1970). Design of agitated, coil-in-tank coolers, *Chem. Process. Eng*., Apr., pp. 89–101.

McCabe W. L., J. C. Smith, and P. Harriott (1993). *Unit Operations of Chemical Engineering*, 5th ed., McGraw-Hill.

Mitsuishi, N., and Y. Miyairi (1973). Heat transfer to non-Newtonian fluids in an agitated vessel, *J. Chem. Eng. Jpn.*, **6**, 415–420.

Nagata, N. (1975). *Mixing: Principles and Applications*, Wiley, New York.

Nagata, S., M. Nishikawa, and T. Kayama (1972). Heat transfer to vessel wall by helical ribbon impeller in highly viscous liquids, *J. Chem. Eng. Jpn.*, **5**, 83–85.

Nishikawa, M., N. Kamata, and S. Nagata (1975). Heat transfer for highly viscous liquids in mixing vessels, *Heat Transfer Jpn. Res.*, **5**, 84–92.

Oldshue, J. Y. (1966). Fluid mixing, heat transfer and scale-up, *Chem. Eng. Prog.*, Apr., pp. 183–188.

Oldshue, J. Y., and A. T. Gretton (1954). Helical coil heat transfer in mixing vessels, *Chem. Eng. Prog.*, **50**, Dec., pp. 615–621.

Parker, N. H. (1964). Mixing: modern theory and practice on the universal operation, *Chem. Eng.*, June 8, pp. 165–220.

Penney, W. R. (1983). *Agitated vessels*, Chapter 14 in *Heat Exchanger Design Handbook*, Hemisphere, New York.

Penney, W. R. and R. N. Koopman (1971). Prediction of new heat removal for agitated vessels (and pumped-through heat exchangers), *AIChE Preprint 10*, 12th National Heat Transfer Conference, AIChE-ASME, Tulsa, OK.

Petree, D. K., and W. M. Small (1978). Heat transfer and power consumption for agitated vessels with vertical plate coils, *AIChE Symp. Ser. 174*, **74**, 53–59.

Rase, H. F. (1977). *Chemical Reactor Design for Process Plants*, Vol. 1, *Principles and Techniques*, Wiley, New York, pp. 331–392.

Rautenbach, R., and F. M. Bollenrath (1979). Heat transfer in stirred vessels to high-viscosity Newtonian and non-Newtonian substances, *Ger. Chem. Eng.*, **2**, 18–24.

Rieger, F., P. Ditl, and V. Novak (1979). Vortex depth in mixed unbaffled vessels, *Chem. Eng. Sci.*, **34**, 397–401.

Rushton, J. H. (1947). Design and utilization of internal fittings for mixing vessels, *Chem. Eng. Prog.*, **43**, Dec., pp. 649–657.

Saunders, E. A. D. (1988). *Heat Exchangers: Selection, Design and Construction*, Longman, Harlow, Essex, England.

Sterbacek, Z., and P. Tausk (1965). *Mixing in the Chemical Industry*, Pergamon Press, London.

Strek, F., S. Masiuk, G. Gawor, and R. Jagiello (1965). Heat transfer in mixers for liquids (studies of propeller agitators), *Int. Chem. Eng.*, **5**, 695–710.

Tamari, M., and K. Nishikawa (1976). The stirring effect of bubbles upon heat transfer to liquids, *Heat Transfer Jpn. Res.*, **5**, 31–44.

Uhl, V. W. (1970). Mechanically aided heat transfer to viscous materials, *Proc. Symposium on Augmentation of Convective Heat and Mass Transfer*, ASME Winter Annual Meeting, New York, Dec., pp. 109–117.

Uhl, V. W., and J. B. Gray, eds. (1966). *Mixing: Theory and Practice*, Vols. I and II, Academic Press, New York.

Weber, A. P. (1963). Selecting propeller mixers, *Chem. Eng.*, Sept. 2, pp. 91–98.